WDL-TR2366
2 January 1965

GUIDANCE AND CONTROL

COMET AND CLOSE-APPROACH ASTEROID MISSION STUDY

FINAL REPORT

VOL. 5

This work was performed for the Jet Propulsion Laboratory, California Institute of Technology, sponsored by the National Aeronautics and Space Administration under Contract NAS7-100.

Prepared for

Jet Propulsion Laboratory
Pasadena, California

WDL-TR2366
2 January 1965

GUIDANCE AND CONTROL

COMET AND CLOSE-APPROACH ASTEROID MISSION STUDY

FINAL REPORT

VOLUME 5

Contract JPL 950870

Prepared by

PHILCO CORPORATION
A Subsidiary of Ford Motor Company
WDL Division
Palo Alto, California

Prepared for

Jet Propulsion Laboratory
Pasadena, California

FOREWORD

This document is the final report of work performed on Guidance and Control by the WDL Division of the Philco Corporation during the Comet and Close-Approach Asteroid Mission Study for the Jet Propulsion Laboratory under Contract JPL 950870. The report covers work performed during the period 2 July 1964 to 2 January 1965.

ACKNOWLEDGMENT

This work reported in this volume was performed by Marvin Fluck with contributions by Steven Ziegler to the Midcourse Propulsion Subsystem section and John King to the Microthruster section.

SUMMARY

18133 ABST

This study has defined system requirements for the stabilization system and for comet tracking, the salient problem being the comet tracking capability. The study has defined the required optical system weight required for a given threshold of comet brightness. A summary of the comet brightness model is included. The comet selected for this mission is Pons-Winnecke which is a periodic type comet for which the brightness is low until near encounter. As a result of the low brightness, tracking for the purpose of computing trajectory and guidance corrections is impractical with sensitive detectors of the image orthicon and image dissector class. Tracking of the comet near encounter for purposes of directing the scientific package and a TV system toward the nucleus is recommended.

The large uncertainty in the comet brightness model forms the basis for recommending that the comet be observed from threshold levels up to the high levels of brightness expected at encounter. This can be accomplished by observing the comet with a small-angle TV system (1° field) during the pre-encounter phase and with a wide-angle field (20° field) during intercept. Since the only requirement for tracking prior to intercept is to orient the TV, it is possible to track using the TV-system output and thereby eliminate the need for a separate tracking system. Acquisition of the comet is to be carried out by presetting the tracker orientation and having a preprogrammed search mode for backup.

The studies have investigated hardware components for which a potential improvement in the probability of mission success can be expected. Preliminary feasibility studies have been carried out on the use of a bipropellant midcourse engine. The use of microthrusters and bipropellant torquers for the attitude stabilization subsystem has been found attractive.

Finally, as a result of an industrial survey of inertial components, several improved inertial sensors were found to be available for this mission.

Author

TABLE OF CONTENTS

Appendix

LIST OF ILLUSTRATIONS

LIST OF TABLES

SECTION 1

OBJECTIVES AND REQUIREMENTS

1.1 OBJECTIVES

The objectives of this study have been the following:

a. Organize and define the operational requirements of the attitude control and midcourse propulsion subsystem.

b. Define preliminary system configurations to meet the operational requirements and to provide a basis for making the final selection of an attitude control system.

c. Identify critical subsystem areas and components and provide a detailed evaluation of available options for missions during 1967-1975.

d. Recommend a system and identify the areas requiring further study.

Within the scope of the study, the effort has been based on relevance to the scientific mission objectives and, consequently, on components that limit the performance. System performance is measured by reliability, precision, component weight and power requirements. The subsystem performances required for comet missions do not require any extension of the performance state-of-the-art. A system has been defined and the limiting components identified and, consequently, the options are indicated. Where standard control system components are acceptable, the use of these components is recommended.

The Mariner-C system has been adopted as the standard system. The study recommends improvements, by either the addition or the exchange of components to the Mariner-C attitude control and propulsion systems. The principal study areas reported are the following:

a. Comet tracking prior to encounter and during the encounter phase.
b. Propulsion system tradeoffs.
c. Improved inertial components.

1.2 SUBSYSTEM REQUIREMENTS

1.2.1 Attitude Control

The attitude control and stabilization system (A/C) is required to acquire and maintain three-axis control over the entire mission beginning with an acquisition mode following separation from the third-stage booster. The detailed consideration of requirements for pointing intercept experiments, for pointing the high-gain antenna, and for maintaining thermal control define the control system design objectives. These design objectives are not stringent and thus make it possible to place the emphasis on system simplicity, reliability and minimum weight. The A/C system configuration is based on satisfying the following requirements (See Table 1-1):

a. Stabilization during two midcourse guidance corrections.
b. High-gain antenna pointing.
c. Thermal control.
d. Pointing and slewing of scan platform during intercept.

The requirements in Table 1-1 are compatible with present Mariner-C capabilities, except for comet pointing which requires adding a mechanically gimballed comet tracker and science package with two degrees of freedom.

1.2.2 Midcourse Propulsion

The propulsion system must have a multi-start capability for imparting two velocity increments, one to be less than 100 meters/sec and a second to be less than 50 meters/sec. The guidance system must impart the velocity increment in any orientation with an overall accuracy of 3 percent or better.

1.2.3 Comet Tracking

No comet tracking for the purpose of carrying out guidance corrections is required; the only requirement is to orient the science package. Tracking for purposes of making guidance computations has been deleted due to the following factors:

a. Tracking during the early part of the flight following launch requires unrealistic optical systems to sense comets that are approximately 20th magnitude at that time.

b. Comet brightness does not reach levels that are practical for the purpose of tracking until after a guidance maneuver becomes ineffective.

c. An uncertainty of $\pm$5000 km in the distance of closest approach has been specified in the trajectory and guidance analysis.

d. Tracking for the purpose of guidance computations can be done by Earth observatories. A pre-recovery study of comet orbits is to be completed prior to launch in order to improve the predicted time of their passage through perihelion.

TABLE 1-1

A/C REQUIREMENTS

Subsystem	Requirement	Tradeoffs
Cruise Science	Orient instruments along the S/C velocity vector, S/C x-y-z axes, and toward Sun within $\pm 0.5^{\circ}$.	---
Intercept Science	Orient TV, photometer and spectrometer toward nucleus within $\pm 0.5^{\circ}$ accuracy and at a maximum rate of 1°/sec.	1. Gimballed scan platform vs gimballed S/C. 2. Scientific value vs pointing accuracy.
Guidance	Control midcourse thrust direction.	Attitude accuracy vs terminal aiming error.
Telecommunication	Point high-gain antenna toward earth within $\pm 1^{\circ}$ accuracy at a 1°/sec rate.	---
Power	Orient solar panels toward Sun within $\pm 5^{\circ}$.	---
Thermal	Establish Sun line within $\pm 5^{\circ}$.	---

SECTION 2

ATTITUDE CONTROL SUBSYSTEM

2.1 MODES OF OPERATION

Three distinct modes of operation are indicated to accommodate the A/C system requirements:

a. Cruise Mode. Three-axis active stabilization using mass expulsion, derived rate information, solar pressure vanes in pitch and yaw, and roll stabilization via a star tracker.

b. Maneuver Mode. Reacquisition of the celestial reference bodies using programmed search modes.

c. Encounter Mode. Three-axis stabilization as in the cruise mode and operation of a platform-mounted comet tracker. Onboard tracking or pointing toward the Comet is to be accomplished by utilizing a gimballed tracker during the encounter phase of the trajectory. Orientation requirements for the scientific equipment and other spacecraft subsystems form the basis for the design objectives.

2.1.1 Sequence of Events for A/C

The following summarizes the Comet Mission A/C system sequence of events:

Acquisition. Following separation from the upper booster stage, the spacecraft acquires the Sun and Canopus references. The separation interface from the booster upper stage results in an uncertainty in spacecraft attitude and angular rates. Acquisition is accomplished by first stabilizing with respect to the Sun and then searching for the stellar reference by rolling the spacecraft about the Sun-line. The design permits acquisition of the Sun-star references at any time following the initial acquisition and before intercept. Initial acquisition has several requirements which must be allowed for in the formulation of a sequence of events.

These are the following:

a. Initial search of the star field must avoid bright sources of interference to the star tracker; notably spacecraft reflections of earth albedo and comet albedo, and stellar objects having a brightness comparable to the celestial reference.

b. Payload separation rates from the upper stage of the launch vehicle must be within the range of the sensors. The problem of initial acquisition requires that boundary conditions be established regarding maximum separation rates. Inertial rate gyros are capable of sensing rates up to $22{,}000^{\circ}$/hr; however, separation rates are much less than this (estimated to be less than 0.1°/sec). Initial acquisition can be carried out without the use of gyros for a Centaur separation; however, this has not been verified by simulation, although related experience on similar control systems supports this conclusion.

Cruise. The A/C operates in a combinational mode consisting of derived-rate deadband ($\pm 0.5^{\circ}$) operation about the three reference axes plus the use of a solar vane system for stabilization with respect to the Sun. Following acquisition of the Sun reference and the stellar reference, spacecraft angular rates are reduced to a minimum level. Minimum rates are obtained by limit-cycle operation set by the minimum impulse obtained from the mass expulsion system. Deadband rates of 2.0×10^{-3} degree/second, are practical and within the requirements for the Comet Mission. The use of solar vanes for the pitch and yaw axes further reduce the rates about these axes. The low rates enhance the scientific objectives by reducing the amount of skewing of the optical sensors. This is particularly so if the A/C thrusting subsystem were to use hot-gas propellant expulsion for active control. The system indicates spacecraft attitude to a 3-sigma value of ± 0.1 degrees. Detailed descriptions of this operational mode can be obtained from JPL specifications of the Mariner-C A/C System, and from the Solar Probe Study (Philco, 1964).

Maneuver. The A/C system accepts maneuver commands via the spacecraft command subsystem. The maneuver sequence consists of a roll turn followed by a pitch (or yaw) turn. The 3-sigma accuracy of orientation at the end of the maneuver does not exceed ± 2.0 degrees and the time required to reach the desired orientation and return does not exceed one hour. The inertial system serves as a reference attitude sensor, provides control signals to the autopilot, and has a 3-sigma drift rate better than 0.5°/hr. Attitude control is accomplished by inserting vanes in the nozzle for thrust-direction control.

Encounter. The encounter mode is initiated approximately 30 days prior to closest approach. Initiation of this mode consists of actuating a gimballed TV/Tracker which records a complete scan frame for purposes of determining the acceptability of the picture to the tracker and of establishing an empirical comet brightness model. The uncertainty in the comet illumination model requires that the tracking illumination pattern be inspected and a decision to track from on-board be made. In the event that tracking is not possible, due either to a bright stellar background or a large anomaly in the predicted illumination model, tracking is carried out with a pre-programmed combination of gimbal angles. This latter case is a precautionary measure to allow for the possibility that the tracker cannot operate on the actual comet illumination pattern.

An inertial system stabilizes the spacecraft during encounter to insure against the possibility of having the sun sensor lose track or the startracker lose Canopus. An interference-free condition cannot be guaranteed although the predicted particle density is extremely low within the coma.

2.2 STABILIZATION SYSTEM REFERENCES

The selection of the Sun and Canopus as references for a 3-axis stabilization system has considered the probe orbit inclination with respect to the ecliptic plane to be less than ± 2 degrees. The orbit inclination affects the required size of the Canopus tracker field of view since,

for a worse case condition, it is within the present Canopus trackers field of view. The need to orient the solar panels for power and to stabilize the communications antenna toward earth without using a complicated gimbal arrangement are the principal reasons for stabilizing with respect to the Sun. During the encounter mode, the celestial references must not be obscured. Considering that the probe aiming point is biased on the Sun side of the comet at closest approach, present estimates are that the particle density is too low for obscuration of celestial references. However, as a matter of precaution, it is recommended that the inertial system be used as the stabilization reference during the last hour prior to fly-through until the experimental objectives have been completed.

2.2.1 Spin Stabilization vs 3-Axis Control

The need to spin-stabilize has been discounted on the basis that the experimental objectives, midcourse maneuvers, and the need for high-gain communication during and after encounter require 3-axis stabilization. Once the need for this capability is demonstrated, the use of spin stabilization is unrealistic in terms of system weight. The three-axis stabilization system can be designed to use a few pounds of N_2 per year or less.

2.3 MIDCOURSE MANEUVERS

Midcourse attitude maneuvers for orienting the engine to any attitude cannot be accomplished using the normal Sun sensor and Canopus tracker. An inertial reference package is needed to stabilize the spacecraft for a period of several hours without incurring large attitude errors. The maneuver consists of a warm-up period for the inertial package followed by the switching from the star-tracker and Sun-sensor outputs to the inertial output. The spacecraft is then rolled and pitched to the command attitude; the turns are commanded from the ground by pulsing the gyro torquers. The propulsion system is actuated and during the burn is stabilized using the inertial package to sense attitude. After the velocity correction is complete, the vehicle is reoriented to the normal cruise attitude and a reacquisition mode initiated.

2.3.1 Gyro Performance

The present Mariner-C inertial package performs adequately. However, improvements in reliability would result by using recently developed gyros such as the Litton Industries Vibrarotor gyroscope; the performance details are classified. Since JPL is planning to evaluate this gyro in the near future, no more shall be said here. Large corrective thrust levels require thrust-direction autopilot stabilization using jet vanes in the plume. Somewhat lower thrusts of longer duration would use the cruise A/C system to maintain the attitude during the burn. A micro-thruster using ion propulsion would also use the cruise stabilization system for stabilization. It is important to note that if the burn time is very long for low thrusting devices, e.g., in excess of one hour, the drifts resulting from inertial stabilization for the present system are approaching the basic cruise mode sensor accuracy limit of ± 0.1 degree.

The effect of the increased velocity increment on the gyro drift during the midcourse propulsion burn is negligible as indicated in the following paragraphs. The attitude maneuver is commanded by torquing gyros through the desired attitude prior to the corrective burn. The spacecraft is to be stabilized in the command attitude for a length of time; then following burn termination, the gyros are torqued to the initial attitude or at least as close as is practical in order to reacquire the cruise celestial reference.

The estimated accuracy of such a system is carried out assuming that the indicated accuracy is ± 0.1 degree, even though the attitude control system permits attitude excursions to the limits of a deadband of at least ± 1.0 degrees. The Kearfott specification of maximum torque uncertainty for the King Series gyro (Model C702519005) is equivalent to 0.2°/hr based on a nonimal operating temperature of 115°F and a maximum spread of five fixed-torque levels taken during separate running periods with cool-down to 70°F between each period. The maximum unbalance drift is 0.5°/hr-g about the

most unfavorable axes. In addition, torquer linearity is 0.02 percent; however, the autopilot command accuracy is limited by the ability to command a specified bias torque current. Using a precision feedback current resistor having a tolerance of 0.5 percent for the command torquer, the ability to command an attitude is a function of the maneuver sequence. Thus, for a 180 degree pitch and 90 degrees yaw, the autopilot command errors alone are $\pm$0.9 degree in pitch and 0.45 degree in yaw.

The magnitude of the gyro unbalance error is estimated by assuming a correction velocity requirement of 300 feet/sec, a spacecraft weight of 700 pounds, and a nominal midcourse-engine thrust of 50 pounds. The required burn time for the correction is approximately 130 seconds during which the gyro unbalance error is 0.028 degree, a negligible drift. Assuming the maneuver mode operates with the inertial reference for one hour, the gyro drift produced by constraint torques is 0.2 degree.

The contribution of the time-dependent gyro drift to the overall error in the orientation of the midcourse corrections is well within tolerance for the 3 percent total uncertainty specified earlier. In the event that lower thrust levels were to be used for the midcourse correction, it would be possible to accept burn-orientation errors up to approximately 2 degrees without seriously degrading the guidance correction accuracy. The time it would take for the drift to degrade the system to 2 degrees is several hours. Depending upon the capability of the electrical power subsystem to supply this additional power, the burn time could be extended to a duration of several hours. Present considerations for the propulsion system using lower thrust levels (four one-pound engines) extend the burn time by approximately 12.5 times if a bipropellant system of attitude control and midcourse propulsion were adapted. This results in a burn time of approximately 30 minutes instead of 140 seconds.

2.4 WEIGHT AND POWER

Table 2-1 contains a summary of the weight and power of major components in the A/C subsystem. All components operate continuously with

a warm-up period (30 watts for one hour) followed by an operating mode (54 watts for one hour). The system weight is essentially that of the Mariner-C attitude control and midcourse propulsion subsystems except for possible midcourse propulsion capability, and for comet tracking of the nucleus at encounter. The weight of the comet tracker assembly includes the tracker and a gimballed platform capable of scanning over a hemisphere.

TABLE 2-1

GUIDANCE AND CONTROL

Subsystem	Weight (lbs)*		Temperature (°F)**	
	Comet Probe	Mariner-C	Minimum	Maximum
1. Propulsion	75.0	50.22	35	125
2. Comet Tracker & Gimbal	15.0	-	-30	+100
(Planet Scan)	-	18.0	-	-
3. A/C Electronic Assembly 7				
Gyro & Electronics	11.0	11.04	30	131
Electronic Assembly 7 less Gyro & Electronics	27.0	27.0	30	131
4. A/C Gas System				
Pneumatic System	39.0	29.0	40	140
Solar Pressure Vanes	4.0	4.0	-200	+250
5. A/C Sensors				
Sun Sensor	0.93	0.93	30	130
Earth Detector	0.25	0.25	30	130
Canopus Sensor	5.5	5.5	-30	+100
TOTALS - A/C	92.68	95.72		
Propulsion	75.0	50.22		

* Based on the weight profile for Mariner C given in JPL EPD-224
**Based on temperature profiles for Mariner C given in Specification MC-4-120B.

A simplified block diagram of the attitude control system is shown in figure 2-1. That diagram does not include the solar vanes, the micro-thrusters and the interface with the telemetry and command sequencer. The effect of these interfaces can be evaluated without their inclusion in the diagram. Appendix B contains several block diagrams showing the control system, considering small-angle operation.

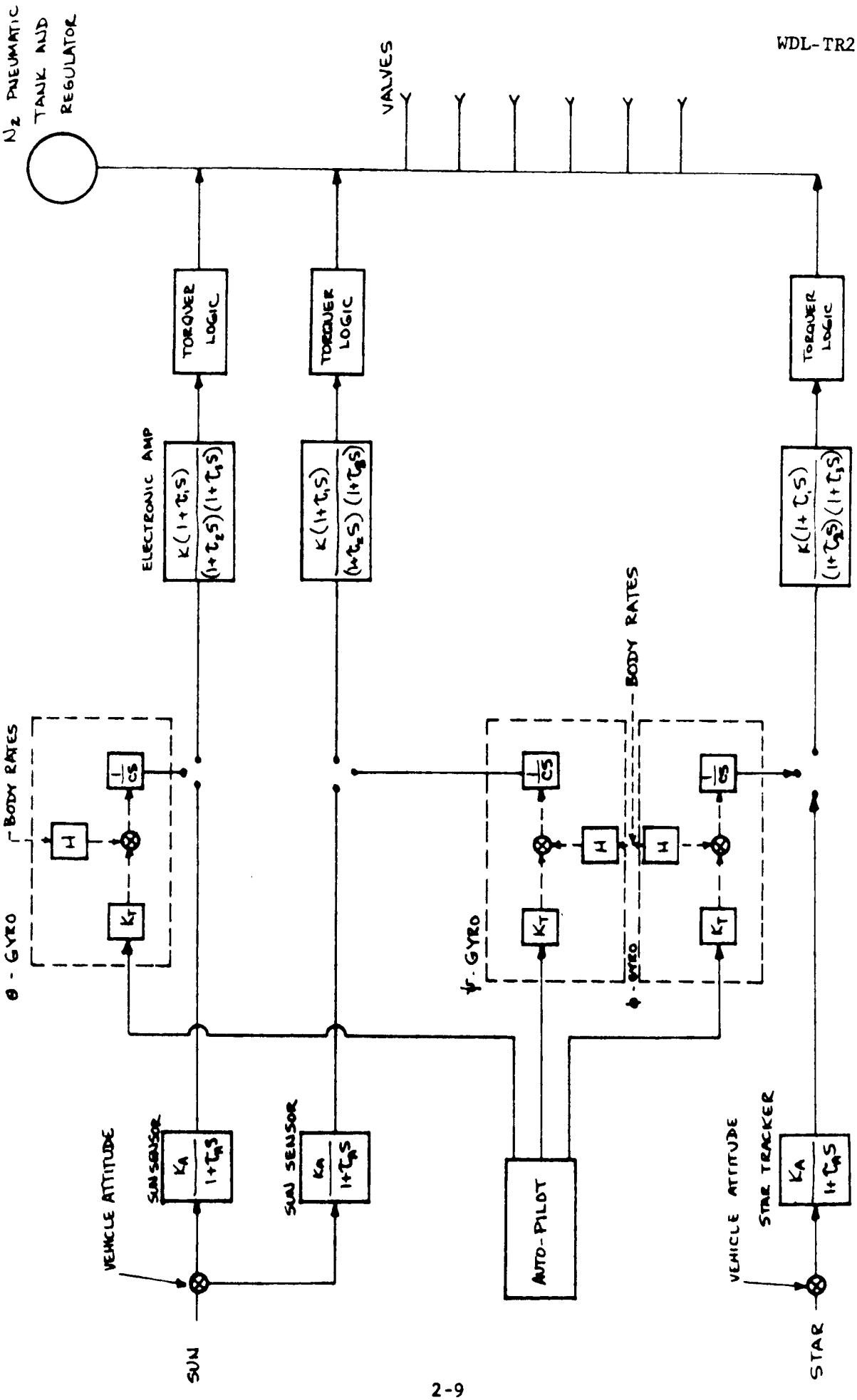

Fig. 2-1 Simplified Attitude Control System

SECTION 3

MIDCOURSE PROPULSION SUBSYSTEM

3.1 SYSTEM CONFIGURATIONS

The propulsion subsystem required for comet missions must have the capability of imparting two velocity corrections, one to be less than 100 meters/sec and a second, less than 50 meter/sec. For some missions the total is nearly twice the capability required for the Mariner-C mission, 80 meters/sec. Propulsion system studies have resulted in a system sizing using two propulsion systems. The first is a 50-pound hydrazine engine which uses jet-vane actuators to thrust-vector control for attitude stabilization during the burn. This system is merely an extension of the Mariner-C propulsion system adopted to provide additional impulse. The second system uses a bipropellant motor having a lower nominal thrust. This system also serves as an attitude control system acting in conjunction with solar vanes to reduce the angular rates in the pitch and yaw axes. A similar bipropellant system without solar vanes is being built by Marquardt Corporation for use on the Lunar Supply Module. The angular rates about the roll axis of the comet probe are reduced to 5×10^{-4} rad/sec and limited by the minimum repeatable impulse obtainable using presently avaiable bipropellant thrusters. This deadband rate compares with a 4.45×10^{-6} rad/sec rate for the Mariner-C, assuming a 20-millisecond minimum on-time for the control jets.

The bipropellant system deadband rates can be removed in pitch and yaw by the solar vane system as is demonstrated in the analog simulation reported in Appendix B or this report. The roll axis could use a microthruster to further reduce the roll-axis rates. Present data on the WDL microthruster is summarized in Section 3.4 of this report. In fact, the microthruster could substitute for the solar vanes in view of mounting freedom and packaging ; weights and power requirements for both systems are available.

The midcourse velocity increment could be obtained by the same motors used for attitude control by orienting pitch and yaw motors aft. To do this, all engines looking aft and also used for control in pitch and roll would be operated simultaneously to impart the velocity increment to the vehicle. Attitude control during thrusting would be carried out by shutting down the appropriate pitch or yaw motor; this logic being reversed from the logic for the non-propulsion modes in that attitude control logic turns the jet on instead of off. This system requires further study before its use can be recommended in place of the operational propulsion system presently used on the Mariner-C.

3.2 MONOPROPELLANT SYSTEM

Anhydrous hydrazine monopropellant is a proven fuel for post-injection velocity correction. Its Isp is of the order of 240 seconds. The reaction temperature of hydrazine is 1800°F, the upper temperature limit for using jet vanes for thrust vectoring. A recent development of the Shell Oil Company catalyst gives hydrazine a restart capability not available in the past. The thrust level is sized so that variations in starting and stopping transients do not have an appreciable effect on the programmed impulse. Thrust is also kept low to reduce the weight and response characteristics of the deflection vanes. Hydrazine must be conditioned to +25°F minimum before firing. The weight of a hydrazine midcourse motor subsystem with deflection vanes and pneumatic attitude control is as follows:

Component	Weight
N_2H_4 Storage Tank	15.0 pounds
Valve, Catalyst Chamber and Nozzle	2.6
N_2 Pressurization Storage Tank	2.0
N_2 Regulator and Plumbing	1.5

Component	Weight
Deflection Vanes	2.5
N_2H_4	45.0
N_2	2.0
TOTAL:	70.6 pounds

3.2.1 A/C with Monopropellant System

The study has investigated the possibility of integrating the attitude control subsystem with the propulsion subsystem by using the same nitrogen supply for both systems. A cold-gas nitrogen system can be used for attitude stabilization with or without interfacing with a solar-torque stabilization system. A pneumatic system for the Solar Probe was investigated at Philco (1963) and the same system can be used here. Total weight of reaction elements was 19 pounds including 6 pounds of nitrogen stored at 300 psi. Limit cycle operation required 37 percent of the fuel so from a weight standpoint little was gained by adding the solar vane stabilization system, although reliability and platform stability are increased by not having to actuate the gas system in the cruise mode.

If the nitrogen supply for the attitude control subsystem is combined with the nitrogen pressurization in the hydrazine system, weight savings accrue by thrusting with the nitrogen in the spent hydrazine system and by using common filters, fill valves, tanks and telemetry. The weight saving from this is approximately 4 pounds at the sacrifice of making both functions vulnerable to a tank failure. A high-pressure, stored-gas system has recognized drawbacks. Storing high-pressure gas during launch at reasonable tank weight entails a high degree of refinement of structural design. Leakage of gas past the dynamic seals affects long-term reliability. System reliability can be increased in some areas by adding redundant valves, seals and relief systems. Two separate gas systems can increase reliability by lowering the required tank size or pressure, which also

makes each system immune to failures in the other and thereby increases the probability of mission success.

Low-storage-pressure subliming systems and vapor systems are being developed to augment cold-gas system. Some of these use isotopic heaters to achieve high-performance operation. One such system is reported on in Section 3.4 of this report.

The weight of the nitrogen cold-gas system for attitude control with a monopropellant midcourse correction subsystem is as follows:

Components	Weight
N_2 Tank	11.0 pounds
Fill Valve	0.5
Filter	0.4
Pressure Regulator	0.3
Pressure Transducer	0.1
6 Valves and Nozzles	0.4
Fittings and Plumbing	0.4
N_2 Charge	6.8
TOTAL:	19.9 pounds

The combined weight of the hydrazing-nitrogen thrusting subsystem is therefore 90.5 pounds.

The Mariner-C system by comparison uses a redundant gas supply for the attitude control system and a separate hydrazine pressurant supply in order to increase the probability of mission success by the use of redundant systems where practical. The present attitude control system is capable

of performing this mission without modification. The propulsion system may be required to carry more fuel and oxidizer to satisfy increased midcourse velocity requirements.

3.3 BIPROPELLANT SYSTEM

A hypergolic bipropellant thrusting system has several desirable attributes for a comet mission. Its Isp is considerably higher (290 sec for N_2O_4-50/50 N_2H_4-UDMH). Radiation-cooled nozzles and film-cooled thrust-chamber walls permit continuous thrusting with no hardware degradation. The high exhaust temperature precludes using deflection vanes for thrust vectoring. A gimballed vectoring system is undesirable because of its weight (approximately 5 pounds for a 25-pound thruster) and is considerably more complex than a vane system. However, if pulsed low-thrust, high-response hypergolic roll-pitch and yaw engines are used to vector the midcourse engine, the same engines can be used for attitude control. The minimum reliable impulse from the thrusters is greater than can be tolerated in cruise mode operation. However, if the system is used to acquire the thermal stabilization system, significant overall system simplicity is achieved.

The thrust of the midcourse motor must be compatible with the vectoring available from the one-pound motors. The weight of a bipropellant midcourse correction attitude control subsystem is as follows:

Component	Weight
N_2O_4 - N_2H_{41} VDMH Tanks	10.0 pounds
Regulators and Valves	4.0
N_2 Bottles and N_2	5.0
5 lb. ΔV Nozzle and Valve	1.5
6 - 1-lb. Attitude Nozzles and Valves	7.2
Fuel and Oxidizer	39.0
TOTAL:	66.7 pounds

3.3.1 Minimum Deadband Rates

A typical low-thrust engine considered for attitude control is the one being developed by Bell Aerosystems. Test results on this engine show pressure (thrust) response with as little as a 2.5-millisecond pulse (vacuum test data are not available yet). At 10 milliseconds the impulse from this thruster is approximately 0.006 pound-seconds. Maximum deadband rates for this impulse about the roll axis can be estimated on this basis, since the moment of inertia about the roll axis is lower than about the pitch or yaw axes. The thruster is mounted on a 2.5-foot arm. The ratio of impulse-radius to inertia is thus 5×10^{-4} rad/sec; the deadband rate is $\pm 2.5 \times 10^{-4}$ rad/sec.

Pending the establishment of the acceptability of this angular rate, further analysis and limited testing of existing hardware under vacuum environments is recommended to better define first pulse and steady state impulse characteristics. These high deadband rates can be removed entirely by the microthruster system of attitude control and by the solar-vane system which would operate during the cruise mode.

3.4 MICROTHRUSTER

The hydride microthruster is a new concept in low-thrust attitude control actuator design which is at present being actively developed in the WDL Power Subsystems Laboratory. The basic thruster is powered by a radio-isotope and consists simply of a volume of hydrided material which encloses the isotope, a thermally insulated container and a thrust nozzle. Elaborations on this basic device are being developed and include a static thrust-control device and a high-temperature heater for high performance.

The basic thruster is a continuous-thrust device and cannot be modulated or shut-off by itself. It is, however, essentially unchanged by the addition of the control and performance devices mentioned above. The thruster utilizes the inherent capabilities of certain classes of metals to absorb large quantities of hydrogen and to store them with no leakage at room temperature and pressure and to release it as a gas when

the temperature is raised. By judicious choice of isotope volume and thermal insulation design, exact control of the hydrogen evolution rate can be obtained for long periods of time, thereby achieving accurate thrust levels from very low (10^{-6} lb.) to moderate (10^{-3} lb). Power requirements to evolve the hydrogenare low so that large amounts of the isotope fuel are not required. For example, a thruster operating at 10^{-5} lb. of thrust will require only 1/3 watt of thermal power with the required amount of Pu-238 contained at the center of the hydride, which will effectively act as radiation shielding. The resulting gamma photon flux at 1 meter from the center will be only 0.1 photon/cm^2-sec.

Thrust control is provided by means of a static or "solid state" propellant valve. The concept of this device presently under development takes advantage of the variable permeance of certain materials for hydrogen. Thus a diaphragm placed downstream of the hydride/isotope propellant generator will act as a valve with no moving parts, actuation being accomplished simply by raising or lowering the diaphragm temperature. A 1 to 2-watt electric heater will provide the heat.

Figure 3-1 is a schematic of the basic microthruster with a "solid state" control valve and a high temperature electric after-heater included. This latter accessory is a small (less than 0.5 watt) electric heater which increases the propellant temperature in order to reach high nozzle specific impulses. Figures 3-2 and 3-3 are photographs of the laboratory test models of the basic hydride thruster using titanium hydride and the "solid state" valve using a silver-platinum diaphragm. Figure 3-4 indicates the performance of this type of thruster relative to other concepts.

As indicated in this figure, weight advantages over several other systems are inherent in this concept only at lower total impulse values (N_2 system excepted). This would be the region of Comet Probe application. Many advantages, however, are not implied by Figure 3-4. These include the following:

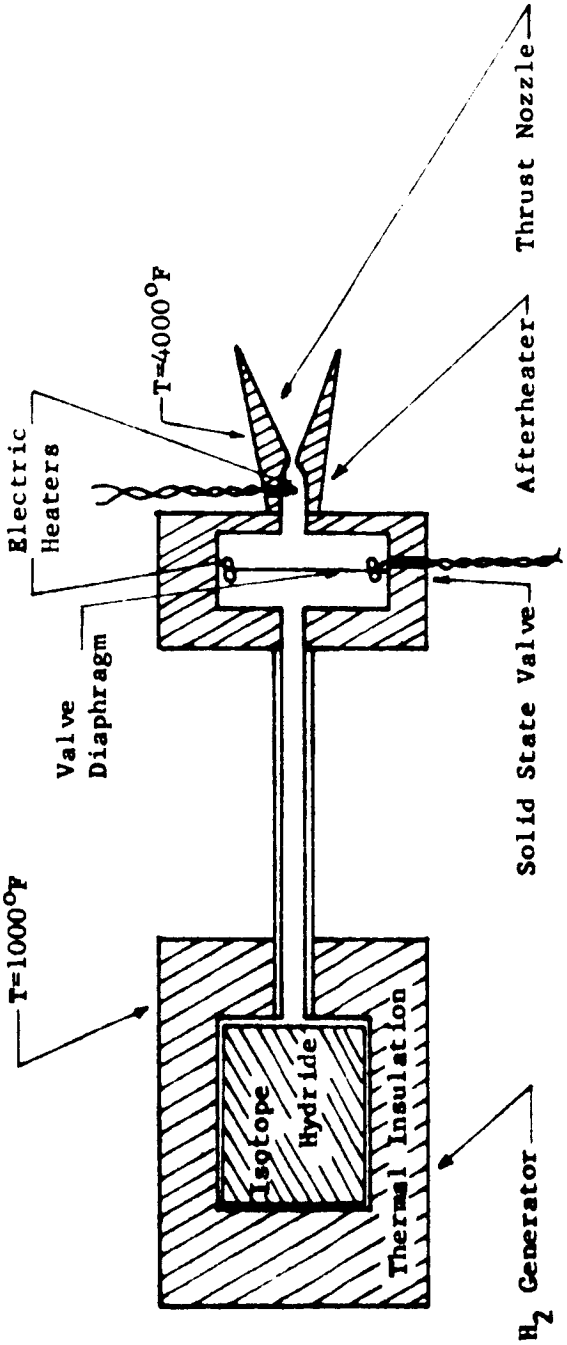

Fig. 3-1 Isotope/Hydride Microthruster

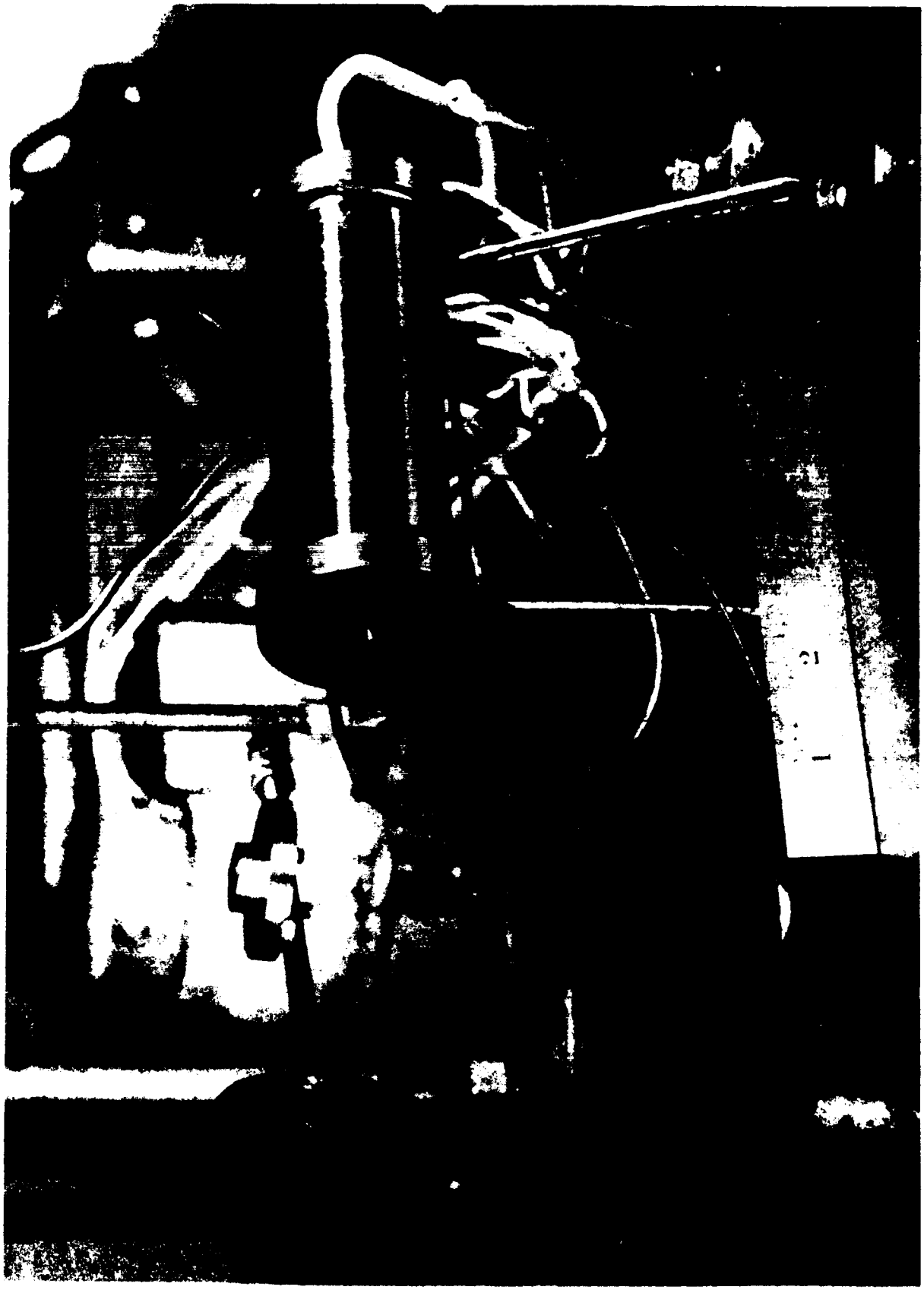

Figure 3-2 Feasibility Model Hydride Thruster (Deflection Vane Pulled Away)

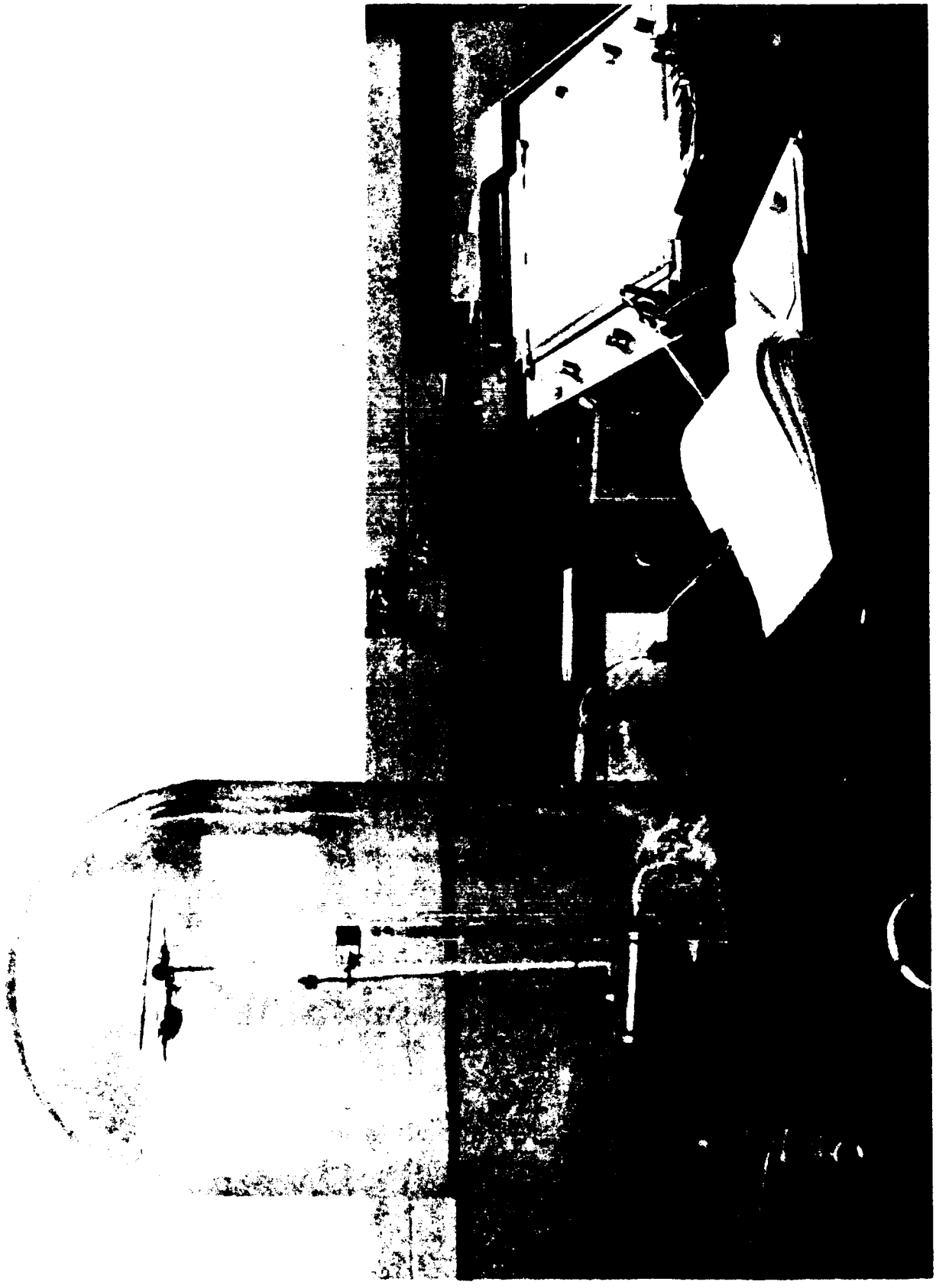

Fig. 3-3. Preliminary Thruster Test Set-Up

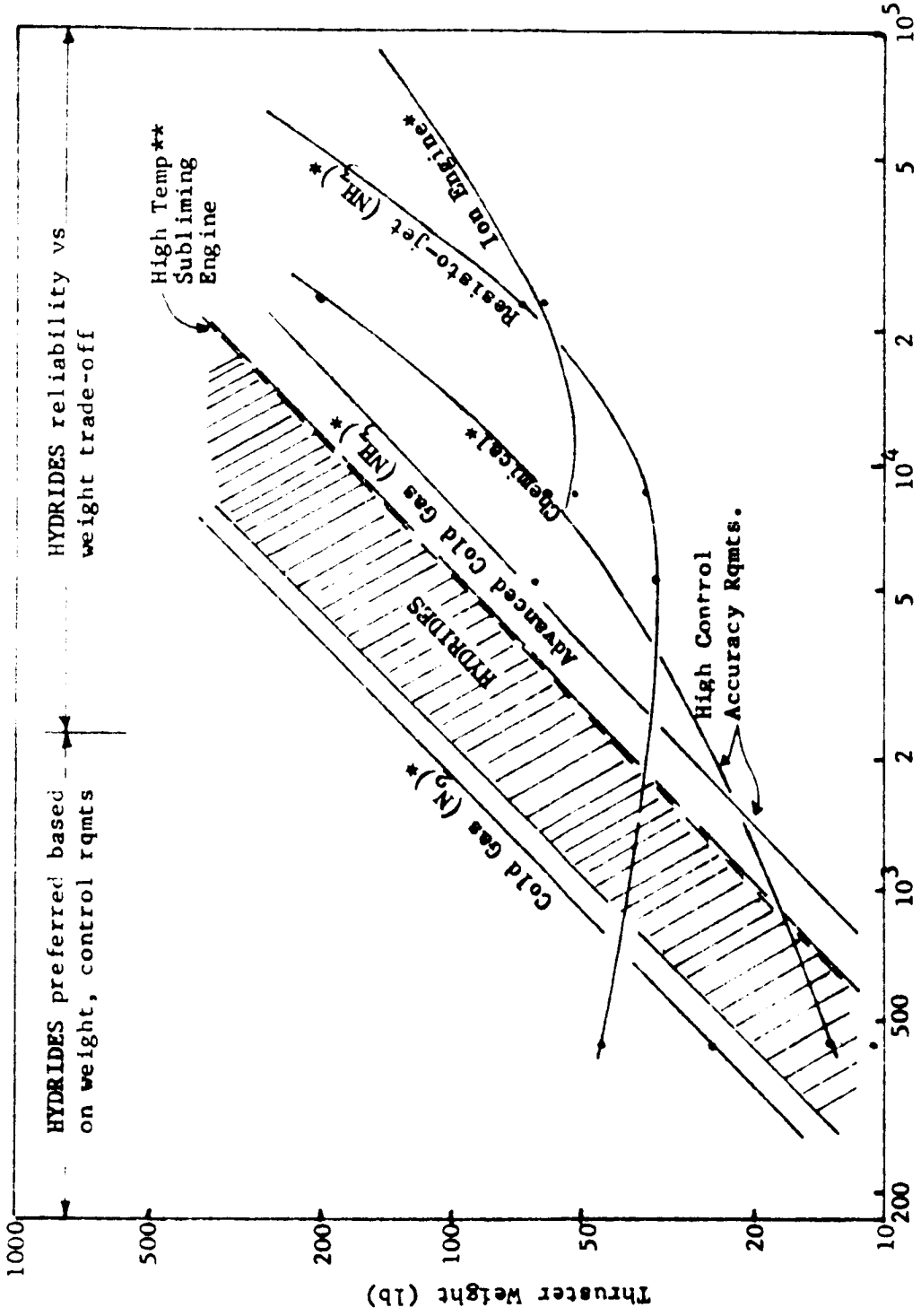

Fig. 3-4 Thruster Performance - Weight Comparison

* Ref. 1 - Journal of Spacecraft and Rockets, March-April 1964
** Ref. 2 - Missiles and Rockets, September 28, 1964

1. No moving parts - High reliability.

2. Low pressure system - No valve, metering, or storage problems.

3. Low sensitivity to environment - No performance perturbations due to temperature changes.

4. Self-contained unit - No plumbing or external services required, easy to locate.

5. Low molecular weight propellant - High specific impulse, no propellant plating out or solidifying problems.

SECTION 4

ON-BOARD COMET TRACKING

4.1 EARLY-FLIGHT TRACKING

The need for refining the aiming point accuracy during the terminal phase of the mission has led to the suggestion that the comet be acquired and tracked early during the flight (Narin and Pierce, 1964; STL, 1963) and that pictures be telemetered to earth for analysis prior to the second midcourse maneuver. This problem area is unique to comet mission studies and, therefore, has received much attention during the attitude control system studies. The principal problem of sensing the position or presence of a comet is that optical models are not well agreed upon in the existing literature. Unfortunately, what is available indicates that comets are too faint to track optically on-board at large distances from the comet and whenever the comet is beyond heliocentric distance of 1.5 A.U. Available references report wide variations in the brightness of the comets of interest to this study; but, all models indicate that the comets are not as bright as a 10 magnitude star when observed from earth at the time the probe is launched. The weight required to track a star of 10 magnitude is about 350 pounds. The comet does not become this bright until just before intercept and after the usefulness of the measurements for computing guidance corrections is lost.

4.1.1 Scope of Analysis

The early-flight comet tracking study includes the definition of comet brightness models and the star background, an evaluation of two sensitive photo-detectors, an image dissector and an image orthicon, and an extrapolation of comet-tracking optical system weights based on optical systems used in space flight experiments. The image dissector is less sensitive for this application; however, it is inherently more rugged than the image orthicon. The optical systems used for this comparison are the Orbiting Astronomical Observatory and Celescope systems, since the weight of these systems are comparable to the total payload capability of a comet probe.

4.1.2 Implementation of Optical System

The possibility of using a slow-scan TV system appears possible if large optical systems and telemetry requirements can be accommodated. Considering the most sensitive system using an image orthicon and a 100-second exposure time, the weight of an optical system required to observe a 10 magnitude comet is 180 pounds (360 pounds for an 11 magnitude comet). Threshold levels have been defined on the basis of the ratio of peak signal-to-rms-noise level. A ratio of 6 has been selected as the criterion for observing a signal in the presence of background random noise. TV resolution limits the accuracy to which the position can be determined with respect to a known stellar background pattern. The use of an 0.5 degree optical field would be practical for an optical system of this size, would be easy to orient using standard attitude control system components, and would have sufficient resolution to observe the comet position to 10 or 20 seconds of arc.

However, the large weight of the optical system requires a major re-design of the Mariner-C spacecraft structure. Furthermore, pointing of the optical system requires either maneuvering the spacecraft or accurately pointing a gimbal system, both of which require re-designing the spacecraft structure and changing the attitude control and thermal control subsystems. Probably the most demanding of these re-designs is the thermal control necessary to maintain optical alignment and to eliminate thermal stress in the optical materials.

The data presented in Figure 4-1 shows the weight trade-off for the most sensitive system. The complete analysis is presented in Appendix A.

4.2 ENCOUNTER TRACKING

The purpose of this study is to define the feasibility of tracking a periodic comet just prior to, during, and after probe intercept. The system must provide tracking signals for the purpose of pointing experimental packages toward the comet. Several instruments, such as the TV, spectrometer,

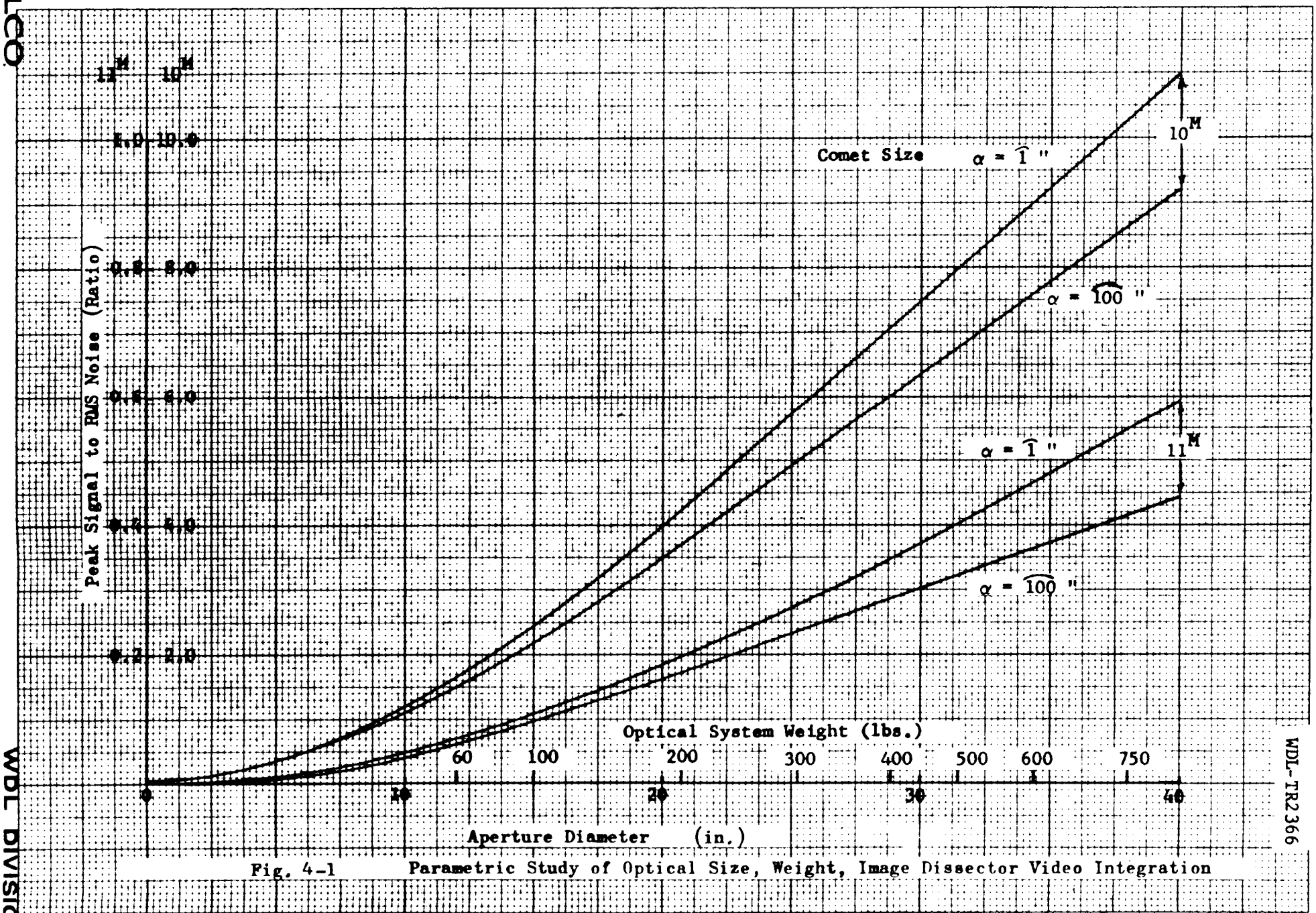

Fig. 4-1 Parametric Study of Optical Size, Weight, Image Dissector Video Integration

and photometers, require that the comet appear within their respective fields of view. The objectives of this phase of the study are to (a) define the system requirements for such a tracker, (b) establish feasibility, and (c) recommend a system.

A model of comet illumination is discussed and forms the basis for this investigation. Scattered sources of comet models disagree and the data obtained from Dr. Cunningham (1964) strikes a reasonably good median range. The large uncertainty in these models normally imposes a limitation on the firmness of recommended designs. However, this investigation has allowed for some changes by setting system constants at a safe level.

4.2.1 Encounter Comet Brightness Distribution

Cunningham has indicated that in the region of maximum brightness, the brightness distribtuion of both the coma and the nuclear condensation of faint, periodic comets near perihelion can be described by exponential functions of angle away from the center of the nucleus. That is,

$$B = B_o e^{-kL^2} \qquad (2\text{-}3)$$

where

- B = brightness measured in stellar magnitudes per (minutes of arc)^2
- B_o = brightness at center
- L = angular distance measured in minutes of arc away from the center by an observer at 1.0 A.U.

This brightness pattern applies to the coma and the nuclear condensation in which the coefficient k and B_o for Pons-Winnecke are approximately as follows:

Region	k	B_o
Coma	8	$4.0^M/(\text{min.})^2$
Nuclear Condensation	2000	$6.0^M/(\text{min.})^2$

The above model can be converted to stellar magnitudes M at 1 A.U.:

$$M = M_o + 2.5\ kL^2\ \log e \qquad (4\text{-}2)$$

where M_o is the absolute magnitude.

Both coma and nuclear condensation have the same spectral intensity distribution as the Sun, assuming that practically all the radiant energy from the comet results from reflected sunlight. If we consider the radius from which 99 percent of the energy is radiated, then, for the coma, the radius as measured at 1.0 A.U. is

$$L_{rc} = \frac{3}{\sqrt{2k}} = 0.75 \text{ min of arc (coma)} \qquad (4\text{-}3)$$

$$L_{rc} = 0.0475 \text{ min of arc (nuclear condensation)} \qquad (4\text{-}4)$$

with the comet assumed to be at perihelion. Cunningham recommends a model whereby B_o is a function of r^6 for the various comets to account for comet activity as perihelion is approached.

The angular size of the coma as a function of comet-to-observer distance is

$$\tan L_{RC} = \frac{r_c}{d} \qquad (4\text{-}5)$$

where the coma's effective radius, r_c, is assumed to be the encounter mode. Substituting L_{RC} and using d = 1.0 A.U., the value for r_c is

$$r_c = d \tan L_{RC} = 3.24 \times 10^4 \text{ km} \tag{4-6}$$

Similarly, the effective radius of the nuclear condensation is

$$L_{RN} = 1.92 \times 10^3 \text{ km} \tag{4-7}$$

Figure 4-2 may be used as a computational aid to determine angular size as a function of distance from the comet for small angular widths in which

$$L_R = \tan \frac{r_r}{d} \cong \frac{r_r}{d} \tag{4-8}$$

is a valid approximation.

The brightness model can be constructed from the geometry shown with the help of the simple sketch below:

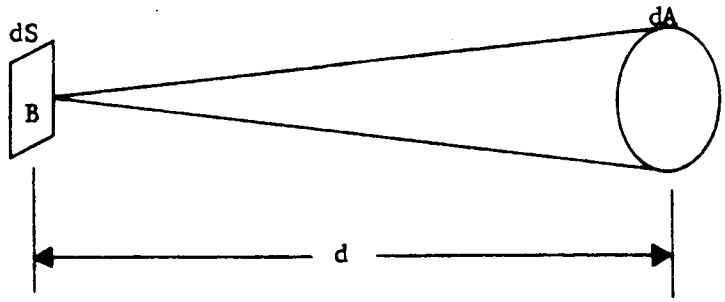

The luminous flux from the element dS at a given distance d is given by

$$dF = B \frac{dA}{d^2} \tag{4-9}$$

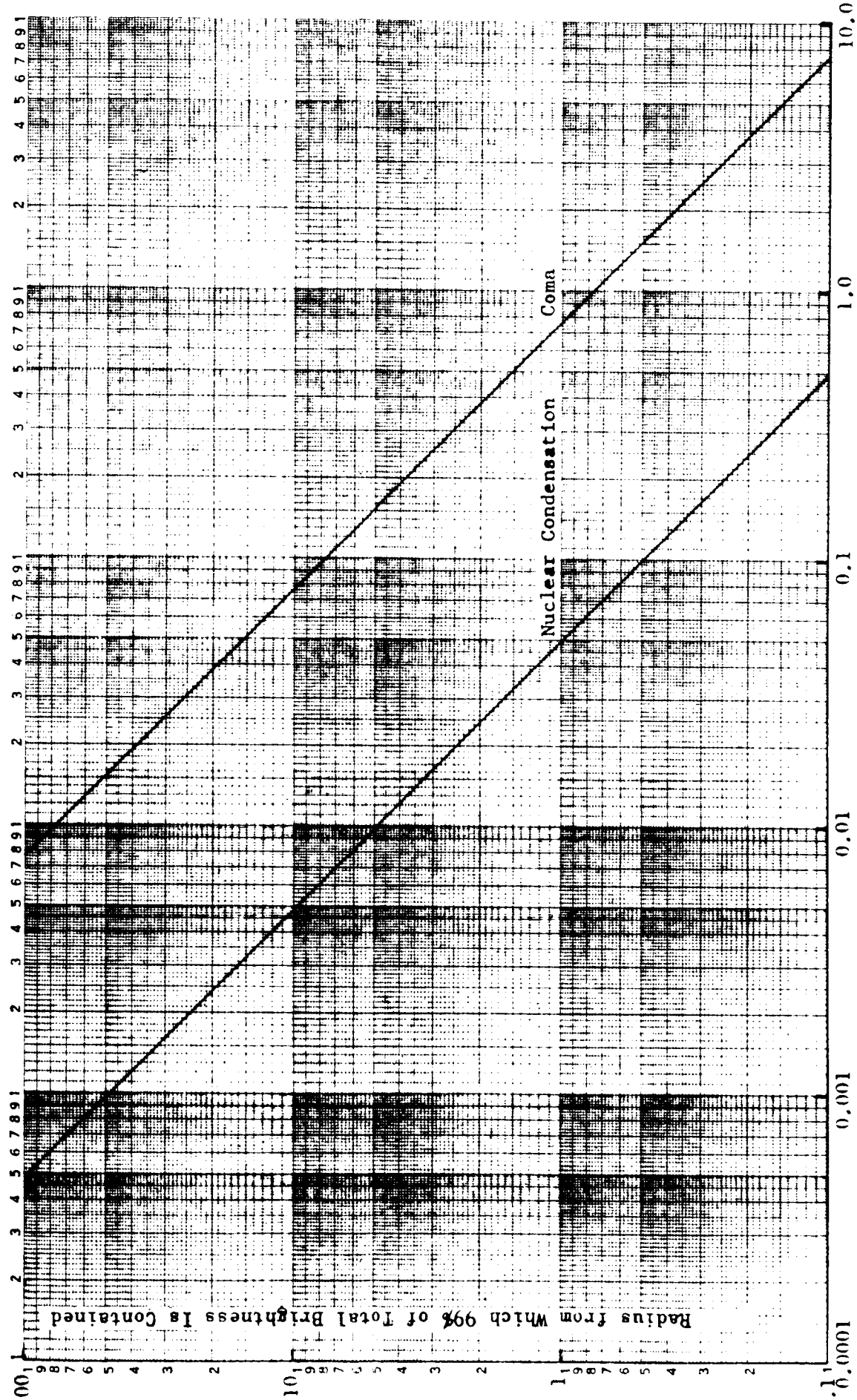

Fig. 4-2 Angular Size vs Distance to Pons-Winnecke

where the constant B is the brightness, or the luminance, of the source dS and the elemental area dA is assumed to be at right angles to the line of sight toward the element dS. Holding dA constant and varying d from d_o, some initial distance,

$$\frac{dF_o}{dF} = \frac{B\frac{dA}{d_o^2}}{B\frac{dA}{d^2}} = \frac{d^2}{d_0^2} \tag{4-10}$$

The illumination E of a surface is given by

$$E = \frac{dF}{dA} = \frac{B}{d^2} \tag{4-11}$$

so that

$$E = \frac{E_o d_o^2}{d_1^2} \tag{4-12}$$

This form is used to predict the illumination as a function of distance from an element having a stellar brightness of 4th or 6th magnitude, as shown in the table below:

B_o	E_o
4th	5.1×10^{-12} lumen/cm^2/min^2
6th	8.2×10^{-13} lumen/cm^2/min^2

Substituting these constants in accordance with Equation (4-1) we have the illumination as a function of probe-to-comet distance of

$$E = \frac{5.1 \times 10^{-12}}{d^2} \exp\left[-2000\, L^2 d^2\right] \tag{4-13}$$

where d is expressed in A.U. and L in minutes of arc.

The graphical representation of these illumination distributions is shown in Figure 4-3 using $\Delta = d = 1.0$ A.U. The variation of brightness for the cometary coma and nuclear condensation is estimated to vary as the sixth power of heliocentric distance. Converting to magnitudes,

$$m = m_o + 15 \log r. \qquad (4\text{-}14)$$

Figure 4-4 is a plot of this relationship. As the comet heliocentric distance increases, cometary activity decreases and the size of the coma decreases until, at a large heliocentric distance, only the nucleus is observed. Figures 4-5 and 4-6 plot apparent size as a function of time to intercept and of approach distance from the center of the nuclear condensation. This work disregards the effects of cometary activity. Figures 4-7 and 4-8 plot the variation of E or apparent magnitude with time and with approach distance from Pons-Winnecke. The variation in apparent size and brightness is expected to be of a lower rate following the point of closest approach.

4.3 COMET TRACKING SUBSYSTEM

The encounter mode can use electronic scanning to track the comet from the spacecraft and to provide video for TV transmission of the cometary image. Both of these functions can be made compatible without compromising the performance of either the tracking or the TV scanning functions. The discussion below develops tracking requirements only; the TV subsystem is discussed in Volume 6 on Telecommunication. In a combined tracking-TV system, the tracking mode acts to stabilize the TV scan to the same point continuously. Pointing can be accomplished by the use of bias signals as long as the reference target is not distorted or lost from view.

4.3.1 Optical Field

The optical field of view required to track during encounter must be large enough to include the unique optical pattern on which tracking can be accomplished plus any alignment uncertainty due to an attitude stabilization of ± 0.5 degree and a pointing accuracy of ± 10 to 20 minutes.

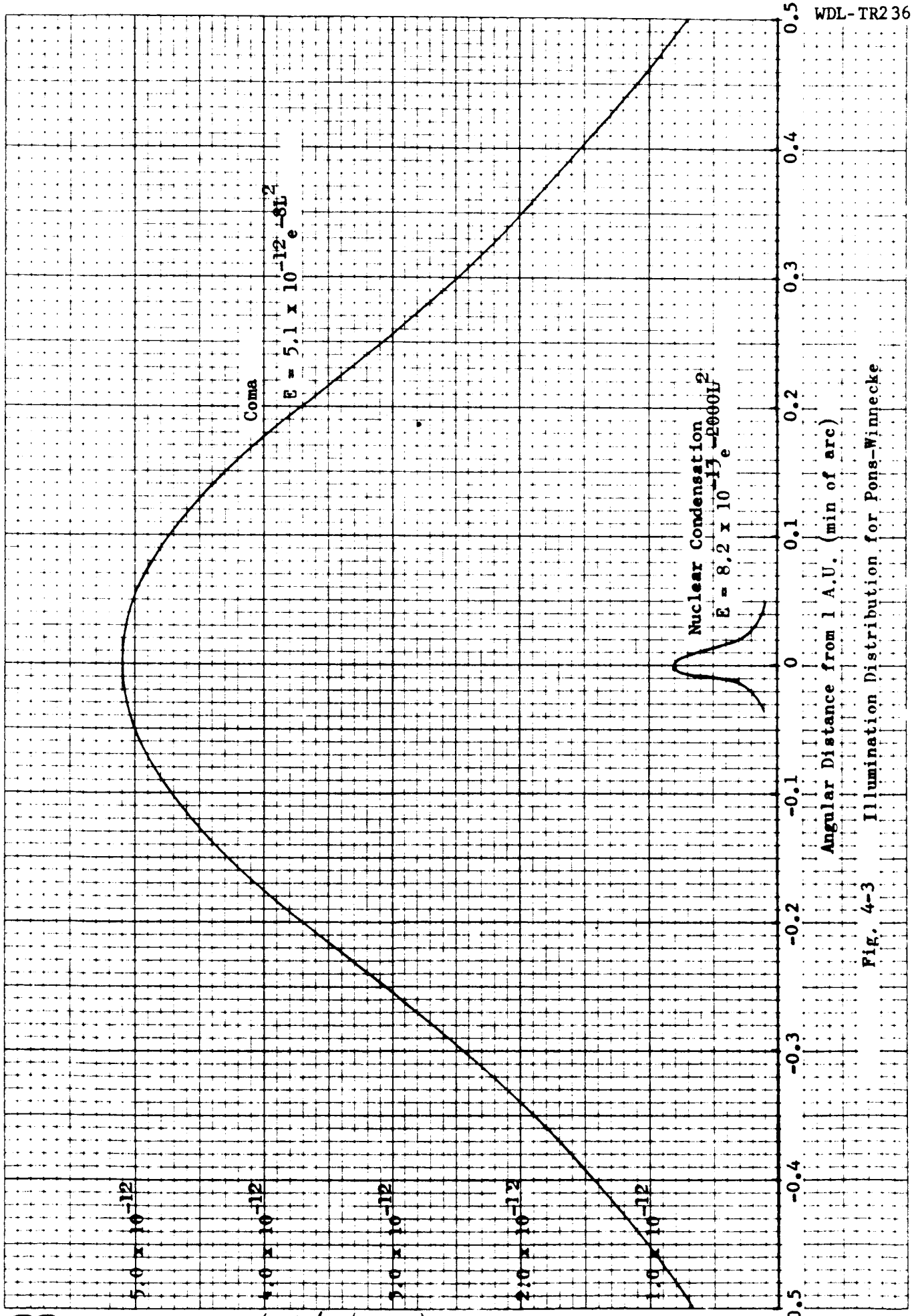

Fig. 4-3 Illumination Distribution for Pons-Winnecke

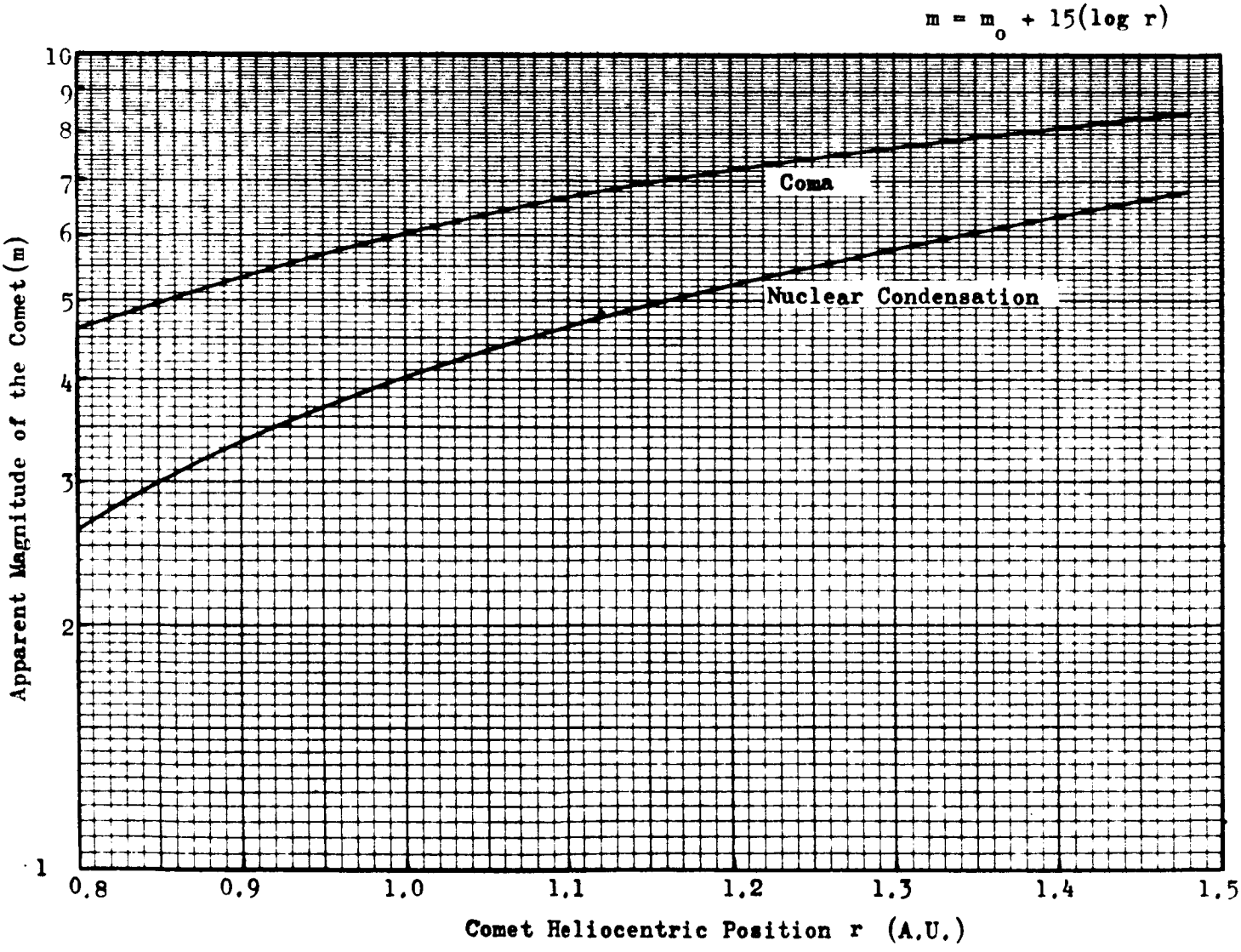

Fig. 4-4 Apparent Magnitude vs Heliocentric Distance

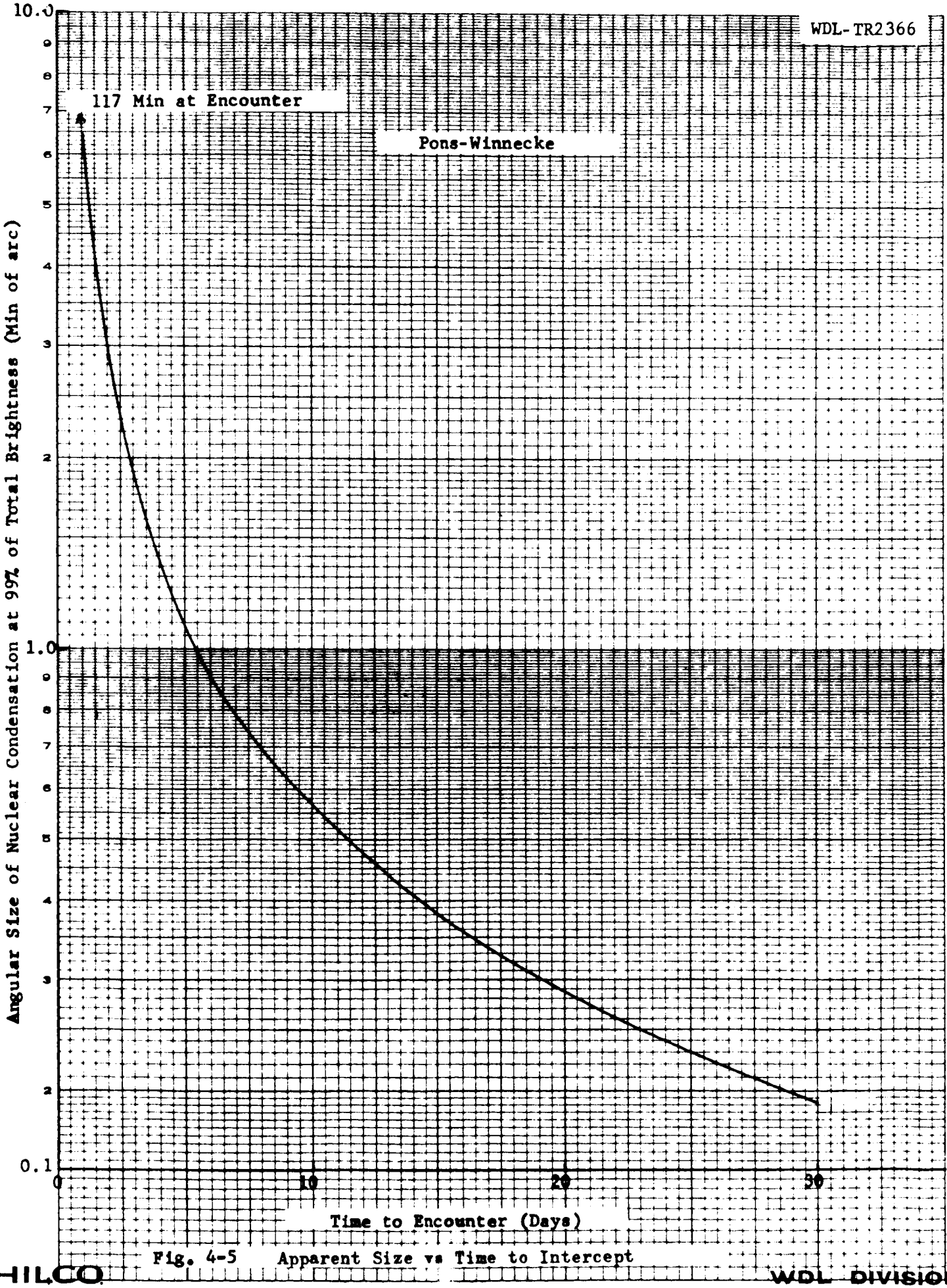

Fig. 4-5 Apparent Size vs Time to Intercept

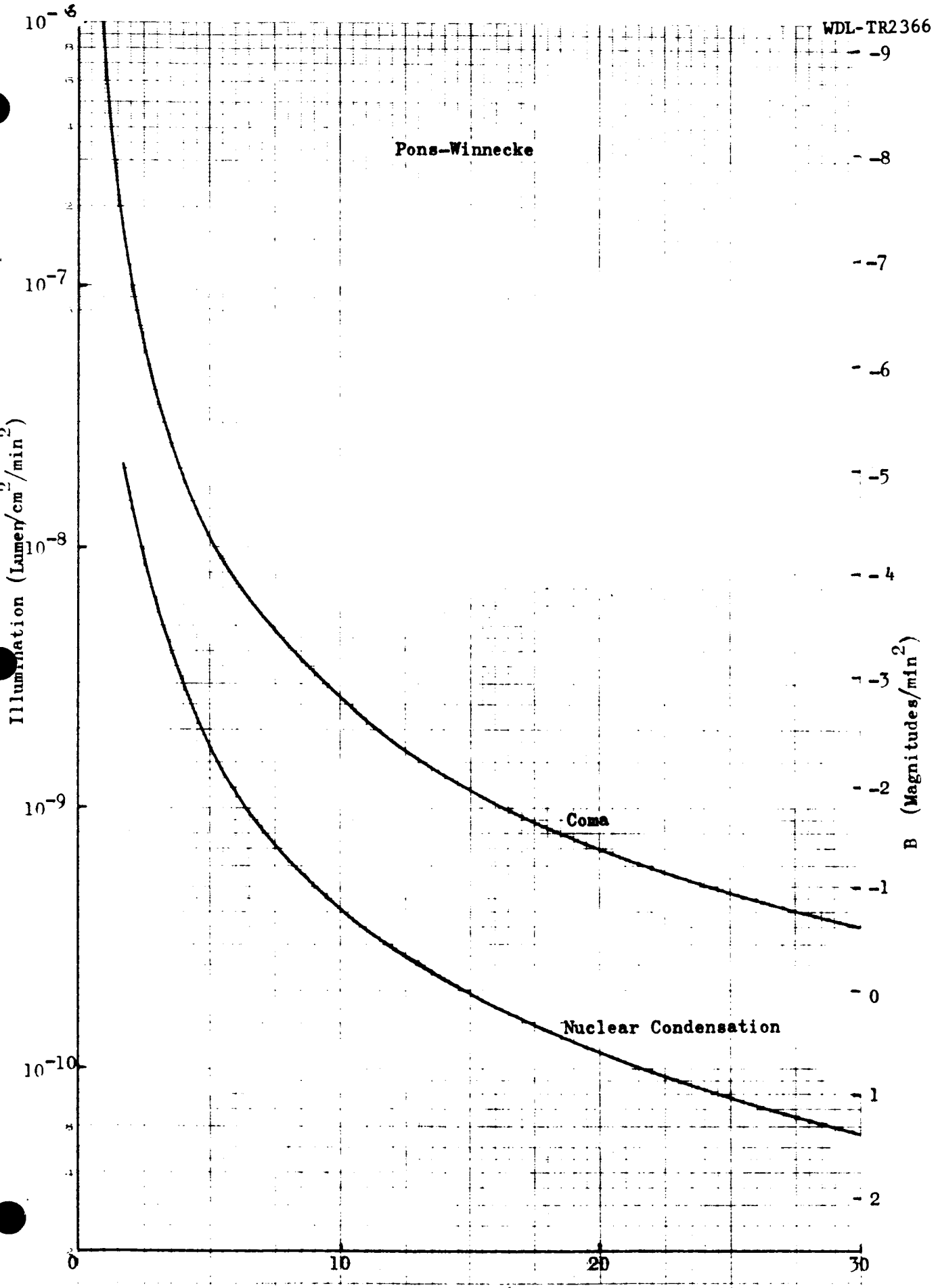

Fig. 4-6 Illumination vs Time to Intercept

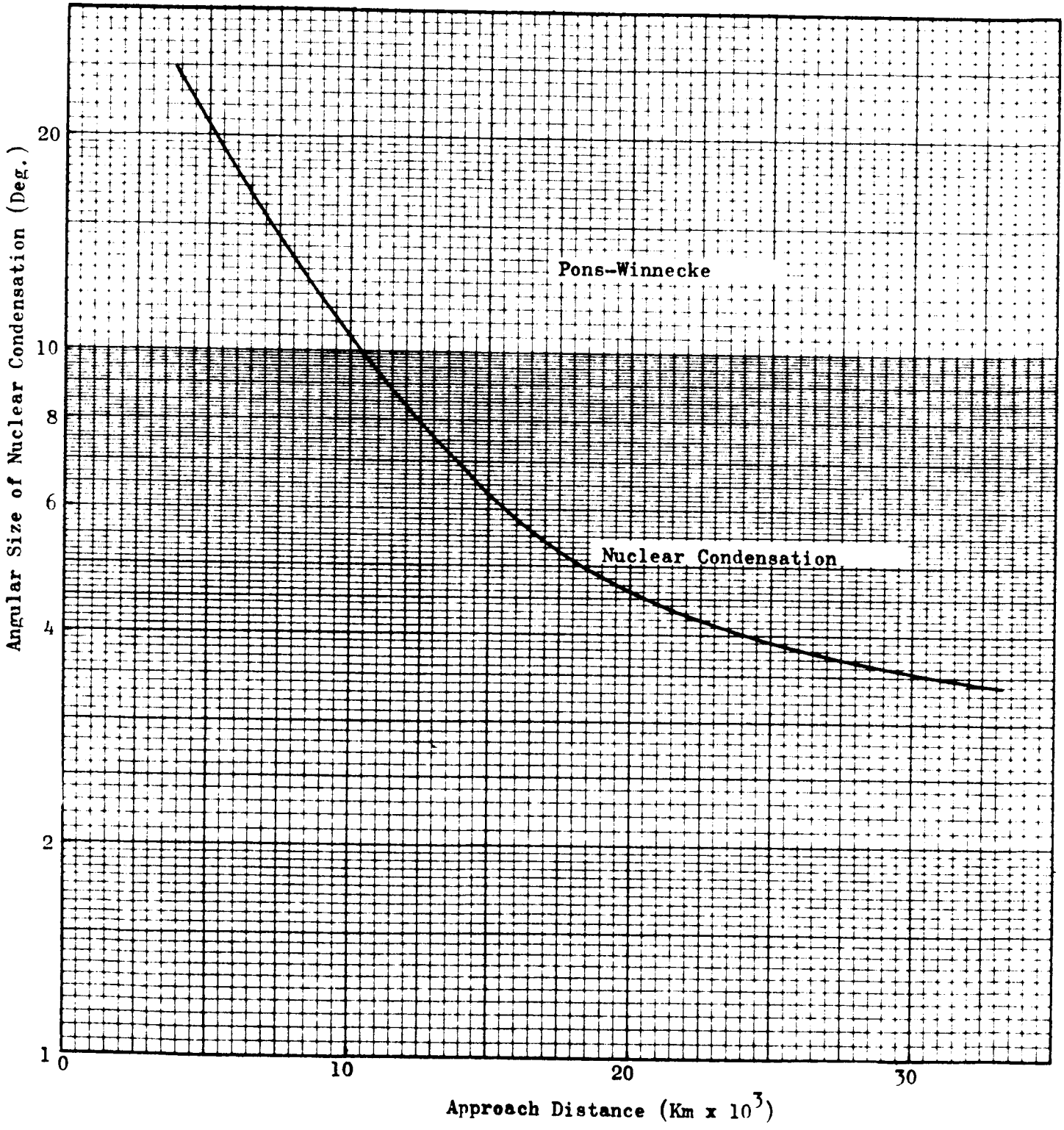

Fig. 4-7 Apparent Size vs Approach Distance

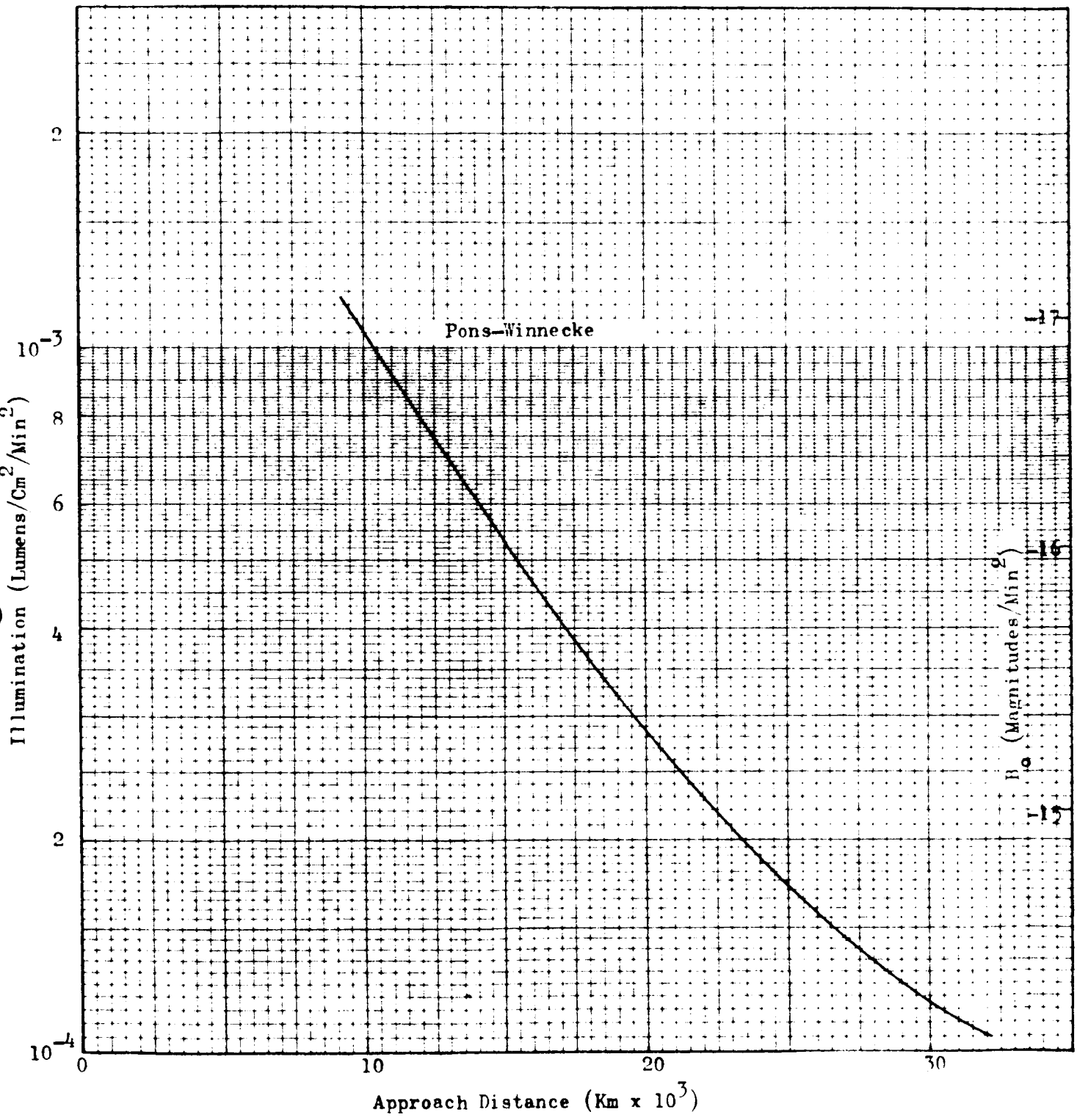

Fig. 4-8 Illumination vs Approach Distance

Considering that the unique optical pattern being considered is cometary coma against a stellar background, the optical field must include the nuclear condensation at encounter. In the case of a 10,000 km miss distance from Pons-Winnecke, the cone angle is approximately 12 degrees. Considering the total stabilization and pointing accuracy, the minimum optical field is a cone of 14 degrees or a square field of 14-by-14 degrees. A larger field is required to observe the coma; present data indicates the coma size to be 2 arc tan (r_c/d) - 146 degrees.

4.3.2 Tracking Subsystem

The total subsystem comprises the following essential elements: optics, scanner, detector, signal-processing electronics, and mechanical configuration. The scanner, detector, and signal-processing electronics hold the key to the performance that is attainable. This section, therefore, analyzes the system alternatives in these categories. Using available design information, it has become apparent that at least two schemes should be investigated for the comet tracker. The two systems, illustrated in Figure 4-9 and showing the most promise, use a scan raster to detect relative image position, but differ in that in one system the scan raster is repositioned such that the image always appears at the null position, while in the second system it does not. These systems are considered to be either closed-loop or open-loop trackers. The latter system offers the advantage of equipment simplicity but operates with a lower S/N, has a restricted linear region, and is more sensitive to comet size. Figure 4-10 is a functional diagram of the tracking subsystem.

Open-Loop Subsystem. This system depends entirely on a knowledge of the effects of non-nominal operation, where knowledge of the uncertainty in the estimated comet magnitude can be simulated to insure that the uncertainty is tolerable. Some of these conditions can be investigated with the available data.

Closed-Loop Subsystem. The servo-loop system operates by moving the scan raster such that the planet image is centered. The system operates

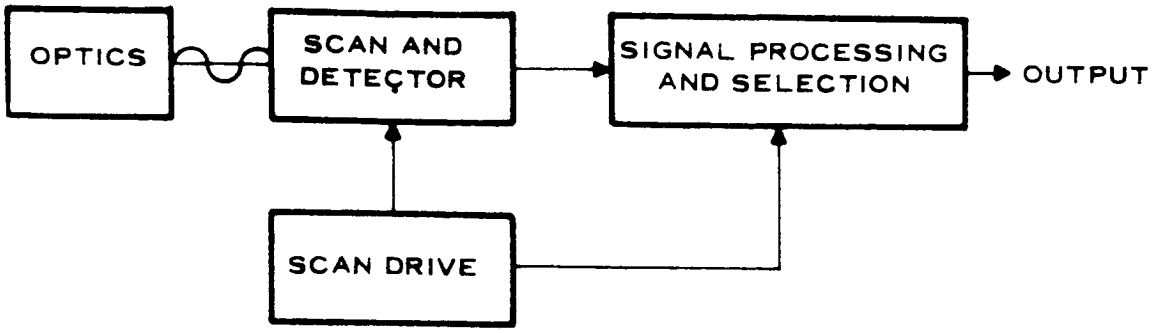

(a) Simplified Block Diagram Open Loop Subsystem

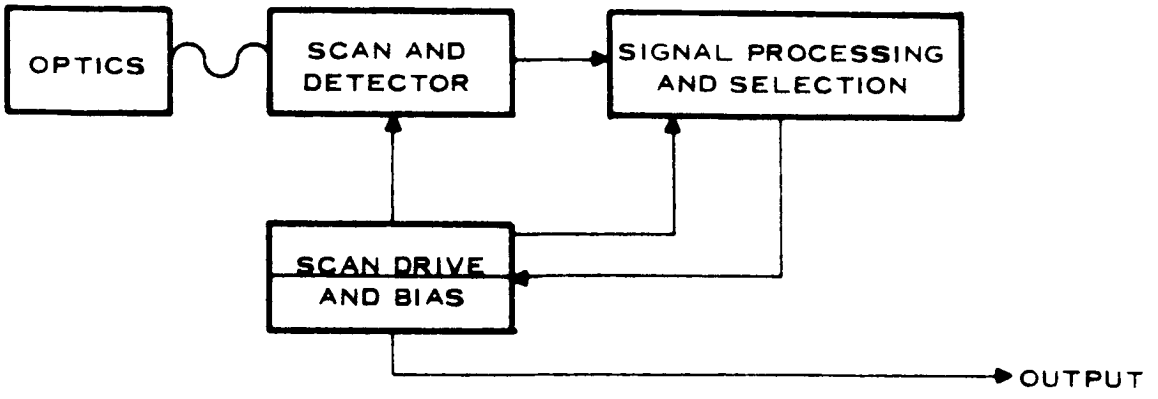

(b) Closed-Loop Subsystem

Fig. 4-9 Simplified Block Diagrams - Open and Closed - Loop Subsystems

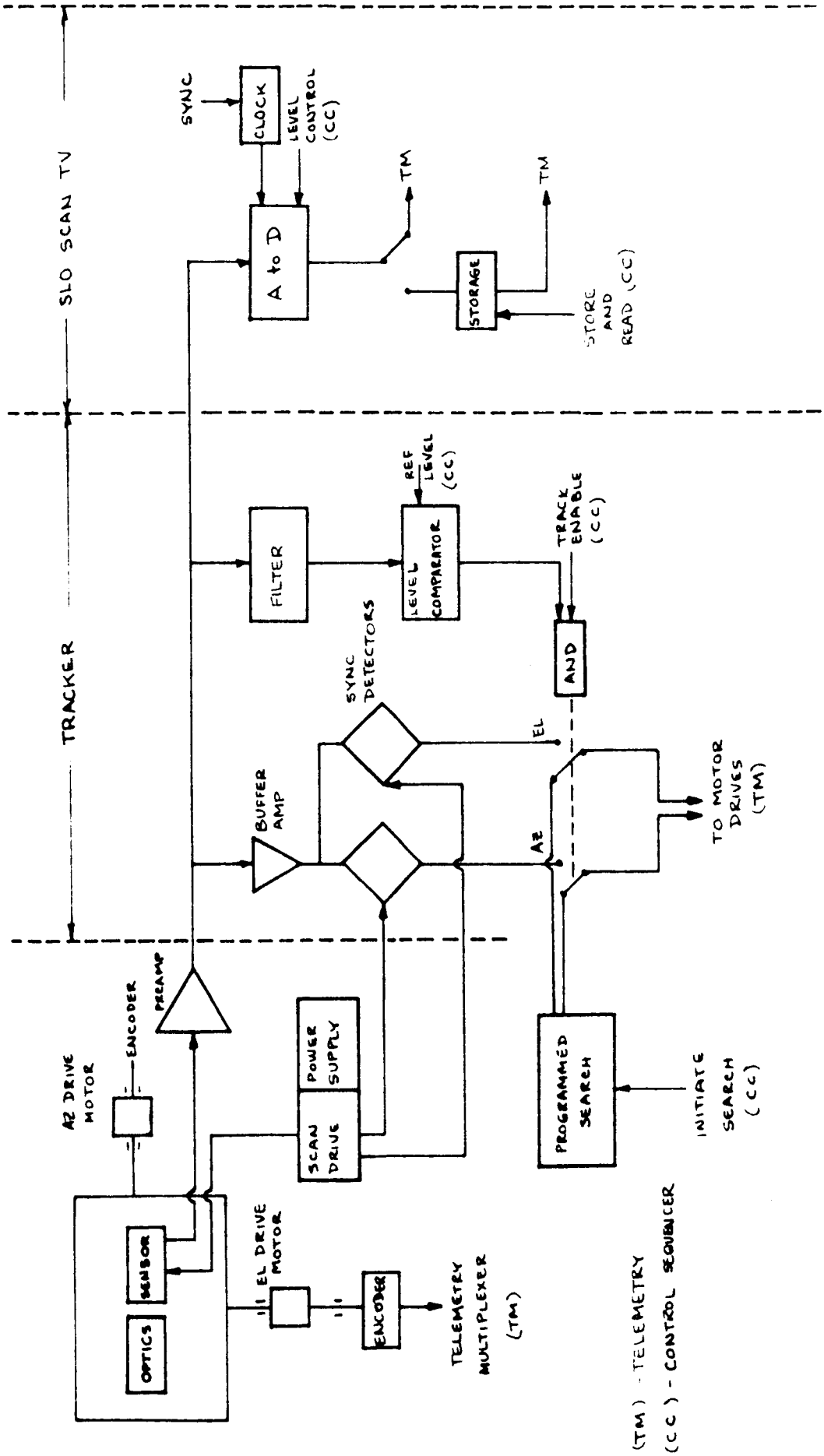

Fig. 4-10 Comet Tracker Functional Diagram

with the additional complexity required of the deflection drive circuit, a penalty accepted to avoid the sensitivity of the tracker to comet size. In this configuration, the most significant problem to study is the effect of gain variations on tracker stability. The variation in open-loop system gain results from comet size variations and from gain variations due to cross-coupling between X and Y channels. The limiting accuracy of this type of system is set by linearity of the deflection system. The operating accuracy on the less bright comet levels depends on the noise plus the linearity of the deflection system, and optical alignment. Acquisition is carried out with a sufficiently large scan raster to cover the optical field of view. After the raster is centered on the comet, it is possible to electronically decrease the size of the raster; decreasing the raster size increases the open-loop gain. While the need for this option is presently undefined, it is available for reducing the over-all system-pointing accuracy. The first system uses the same size raster for acquisition as for the normal operating mode. In this case, the raster size fills the field of view at the beginning of the acquisition mode and simply uses that same raster during the normal modes.

4.3.3 Scanning

Philco WDL has developed single- and dual-axis scan simulations for determining performance characteristics and as design aids for parameter optimization. These include a single-axis simulation on a small desk computer (RECOMP II) and both single- and dual-axis simulations on the WDL analog computer. These simulations have been developed to provide insight into the parametric behavior during the intercept phase. The simulation has demonstrated a relatively inexpensive method of accumulating design data before breadboarding a tracker, thereby insuring that the selected design is optimum. The subsection below discusses scanning techniques. An attempt has been made to keep the discussion (and the simulation used in the discussion) general so that it is applicable for most scan implementations. The information presented is intended to illustrate both some of the problems considered in arriving at the proper scan and the tools for attacking these problems. Subsequent subsections indicate the options that are available in implementing such scans.

All scanning techniques either move an image across a fixed aperture or move the aperture across the fixed image, thereby chopping it. A single analysis is sufficient for both cases. Analyses to date are based on simple apertures (single rectangular, square, or circular apertures in the aperture plate), and indicate that required performance is attainable with straightforward approaches. The output of a detector on the image of the comet is a series of video pulses. This pulse train contains the information required, i.e., the position of the image in the scan plane. The model to be used in these situations is based on the system geometry depicted in Figure 4-11 which shows the center of the aperture with a maximum scan deviation δ, a round (or square) aperture of radius d, a comet of radius r_c, and a comet centroid location of φ relative to the null (optical) axis. It is worth commenting that, with the electronic scan drive using a triangular scan drive such as commonly used for TV systems, processing circuitry logic is available to make the transfer function extremely linear over the entire operational range. Such a system is included in the simulation examples.

Sinusoidal Drive System. A typical example of an ideal detector output is shown in Figure 4-12 for a single-axis scanning system. Using this single-axis model, the pulse train is seen to be symmetric about the chosen reference axis, and the pulse position, assuming a sinusoidal drive, is defined by

$$\theta_{11} = \arccos (\varphi + d + r_c)/\delta \qquad (4\text{-}15)$$

$$\theta_1 = \arccos (\varphi + d - r_c)/\delta \qquad (4\text{-}16)$$

$$\theta_2 = \arccos (\varphi - d + r_c)/\delta \qquad (4\text{-}17)$$

$$\theta_{22} = \arccos (\varphi - d - r_c)/\delta \qquad (4\text{-}18)$$

The pulse train contains a measure of the image position with respect to the optical axis such that, with proper processing, the output error signal

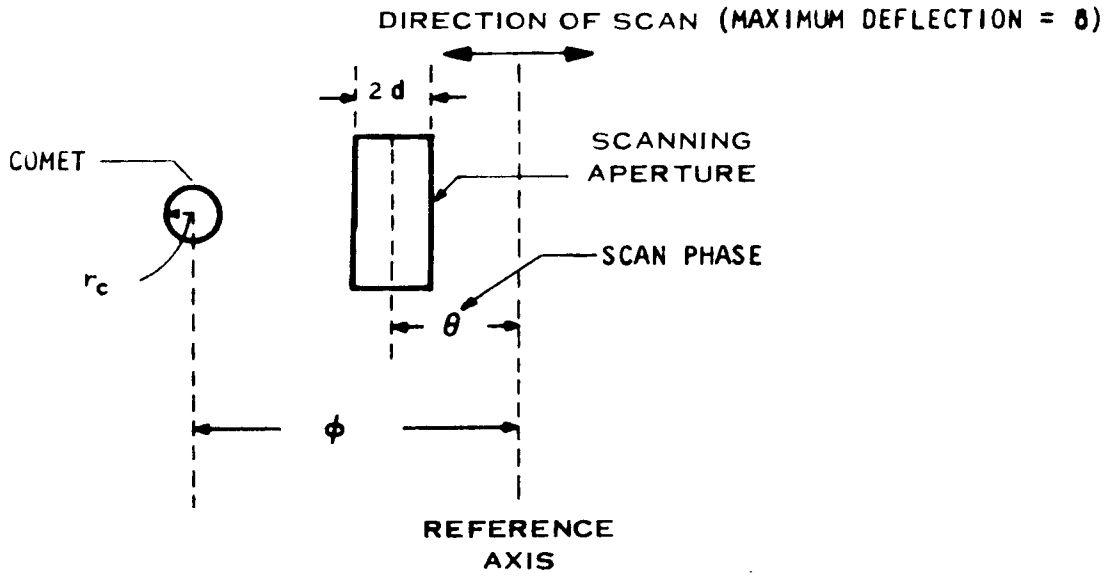

Fig. 4-11 Scanning Geometry

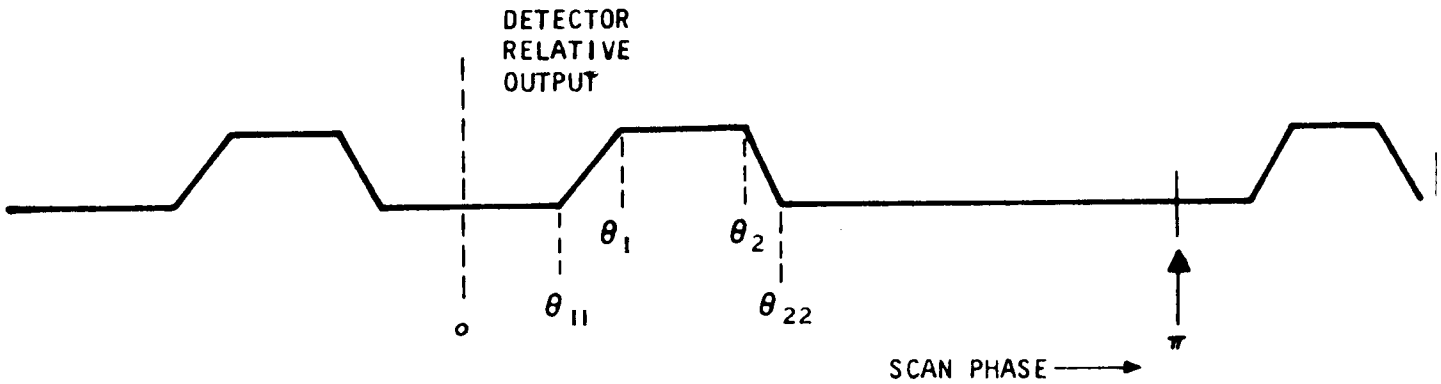

Fig. 4-12 Typical Detector Output

provides an analog-signal indication of φ. Considerations of power and signal processing simplicity restrict the processing network to the use of the first harmonic components in the signal.

Since most of the characteristics of the output error curve can be derived from the Fourier series of the wave train, several general comments can be made which apply to all scanning systems of the type described thus far. The Fourier coefficient, a_n, is given by

$$a_n^2 = \frac{2e_o}{T}\left[\int_{\theta_{11}}^{\theta_1} k_1(t_{11} - t)\cos n\omega t\, dt + \int_{\theta_1}^{\theta_2} \cos n\omega t\, dt + \int_{\theta_2}^{\theta_{22}}[\,1 - k_2(t_2 - t)\,]\cos n\omega t\, dt\right] \tag{4-19}$$

where a_n = amplitude of the Fourier coefficient corresponding to the n^{th} harmonic

$\theta_1, \theta_{11}, \theta_{22}, \theta_2$ = pulse position (see Figure 4-11)

t_{11}, t_2 = the times corresponding to the angles θ_{11}, θ_2

T = the scan drive period

e_o = the detector output.

The following comments apply:

a. Only the a_n terms are required to describe a steady-state pulse train since the function is always even.

b. The positions of $\theta_1, \theta_{11}, \theta_{22}, \theta_2$, are determined by the scan drive, but the saturation points, zero points, the slope at the null, and the peak power are independent of whether the scan drive is sinusoidal or linear.

c. The use of a dual-axis scan reduces the integral shown above as a function of duty cycle such that the gain of a one-axis scan is always greater than for the two-axis scan, using the same configuration otherwise.

Output Error vs Relative Image Position. Using the geometrical model depicted in Figure 4-11, the output amplitude of the fundamental as a function of the comet image position has been studied parametrically with all linear dimensions normalized to the maximum scan deflection, δ. Assuming a sinusoidal drive, the output error signal (first harmonic) as a function of the image position is shown parametrically with variations in the scan aperture half width, d (see Figure 4-13). The image position φ is shown as the ratio of φ/δ along the absissa with the amplitude of the first harmonic as the ordinate. The principal interest of this curve is the definition of the gain, linear range, and peak power attainable for likely scan configurations. These characteristics are summarized in Figure 4-14. Since these data do not consider comet phase, they represent the best possible performance attainable.

Effects of Coma (or Nucleus) and Scan Aperature Size. The image size of the comet, its phase and the finite size of the scanning aperture determine the shape of the pulses out of the detector. Illustrated in Figure 4-12 are the detector output pulses which can be described as having rise times that are functions of these parameters. As the comet size (r_c) decreases, θ_1 approaches θ_{11} (and θ_2 approaches θ_{22}) thus altering the amplitude of the first harmonic. Figures 4-15 and 4-16 are examples of these effects for aperture sizes d/δ of 0.5 and 0.7, in which r_c has been run through a typical range to demonstrate the effects of tracking various comet sizes using a sinusoidal drive system. The data indicate significant nonlinearities as the comet size is varied. If we return to Figure 4-15, a plot of the linear range can be defined parametrically for the case of $r_c/\delta = 0.5$. The linear range is indicated by the dashed lines in Figures 4-15 and 4-16, using an arbitrary criterion of ± 20 percent.

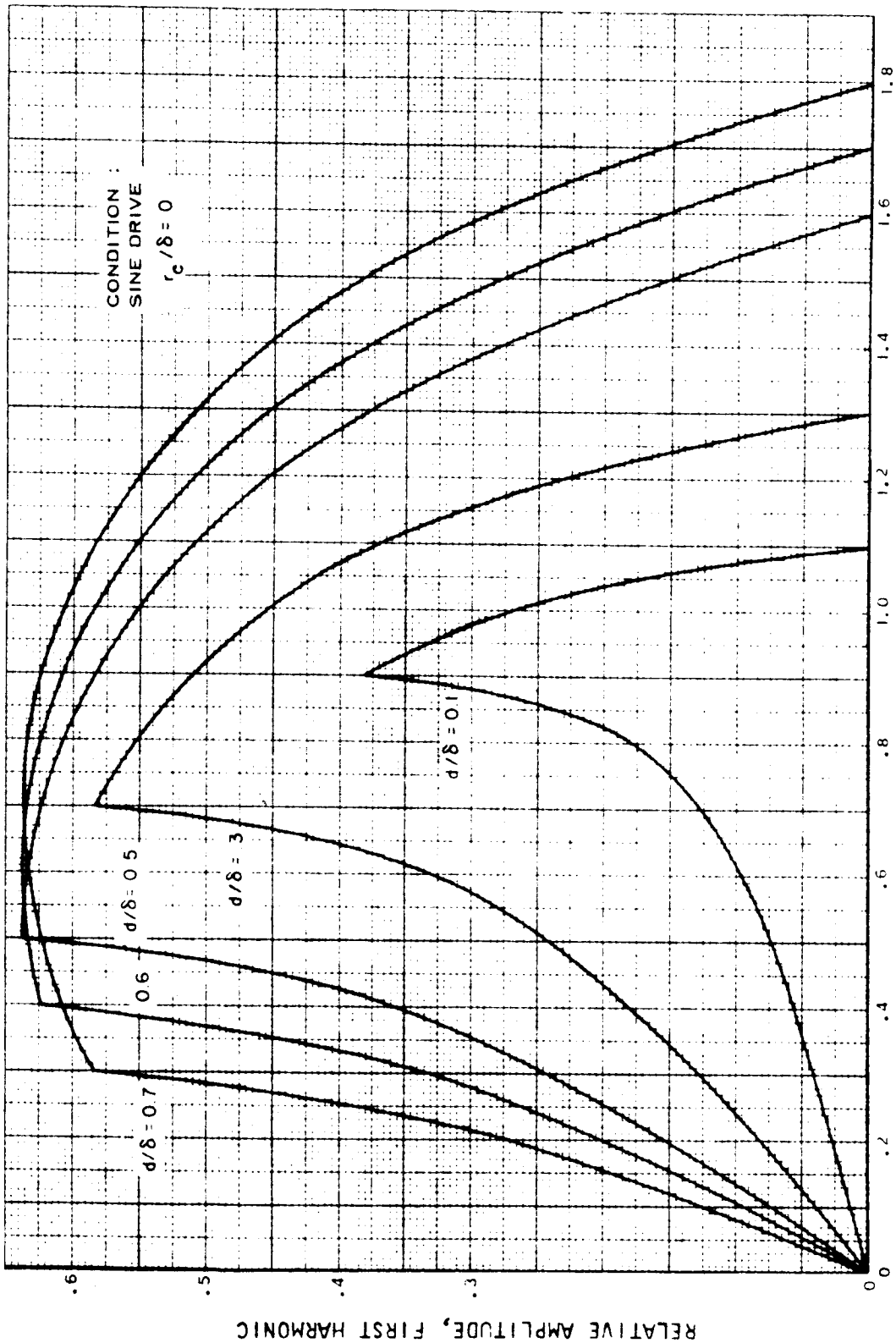

Fig. 4-13 Parametric Study of Comet Size and Aperture Width

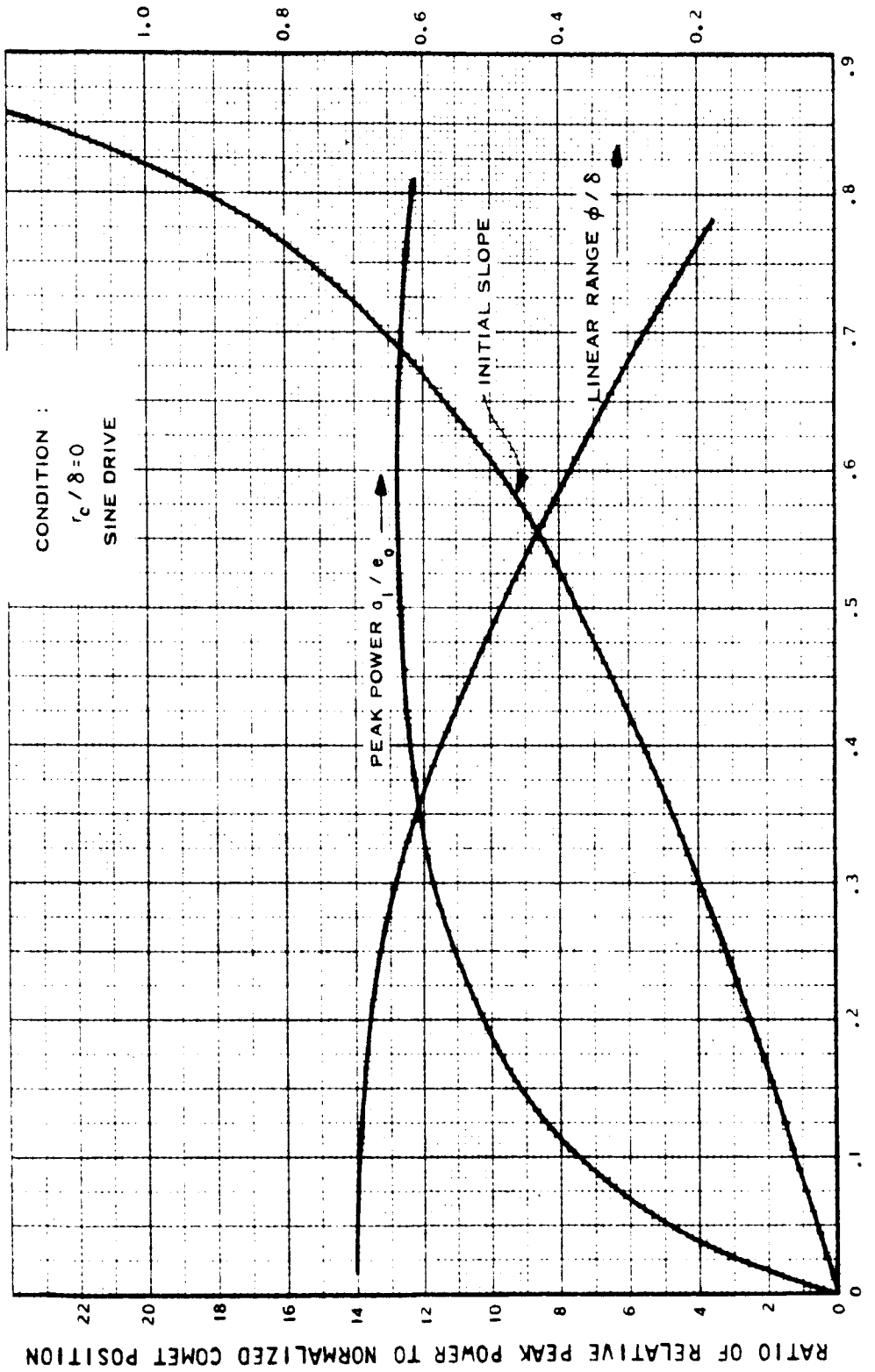

Fig. 4-14 Summary of System Parameter vs Aperture Size

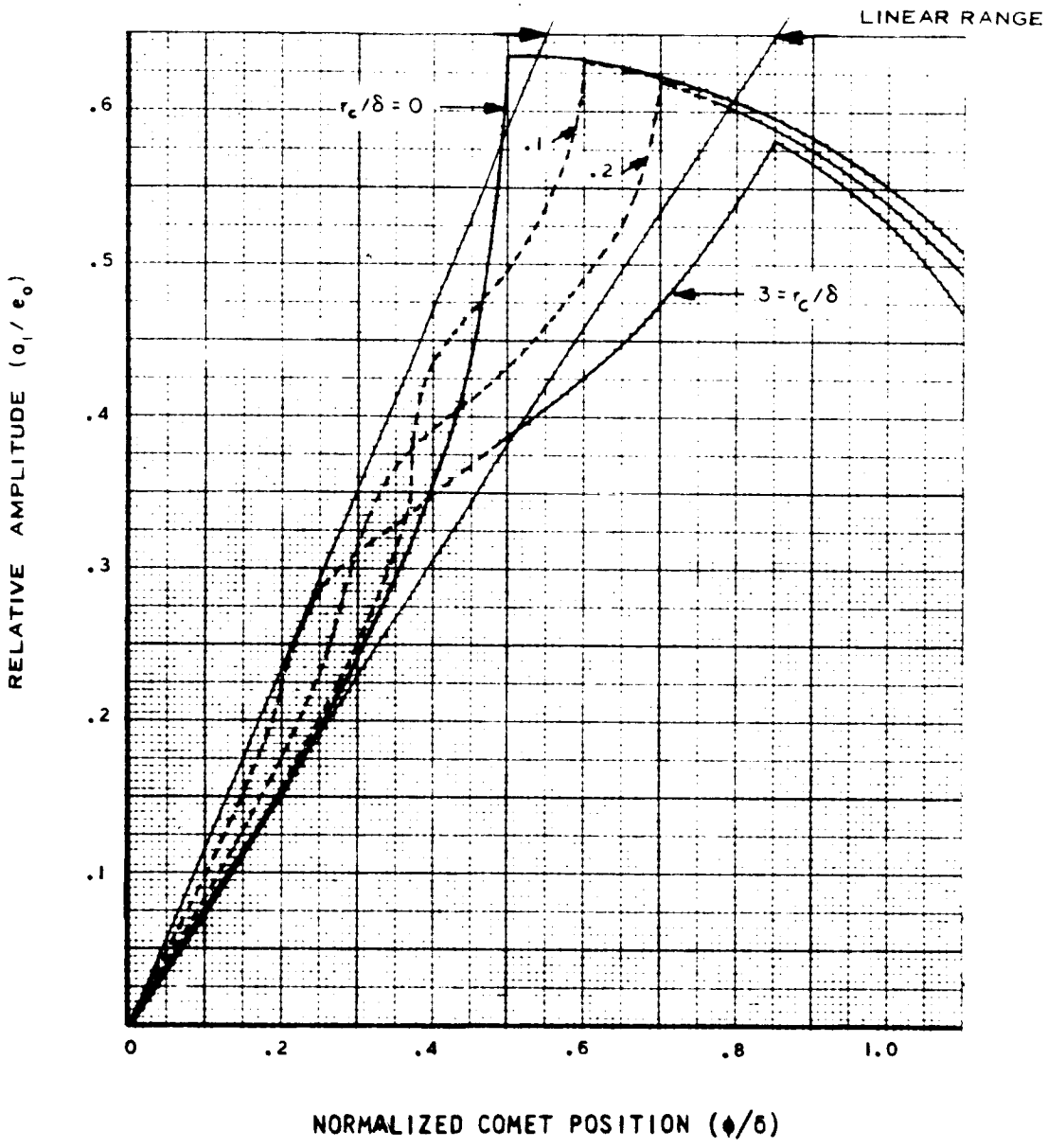

Fig. 4-15 Error Signal Amplitude vs Comet Position, $d/\delta = 0.5$

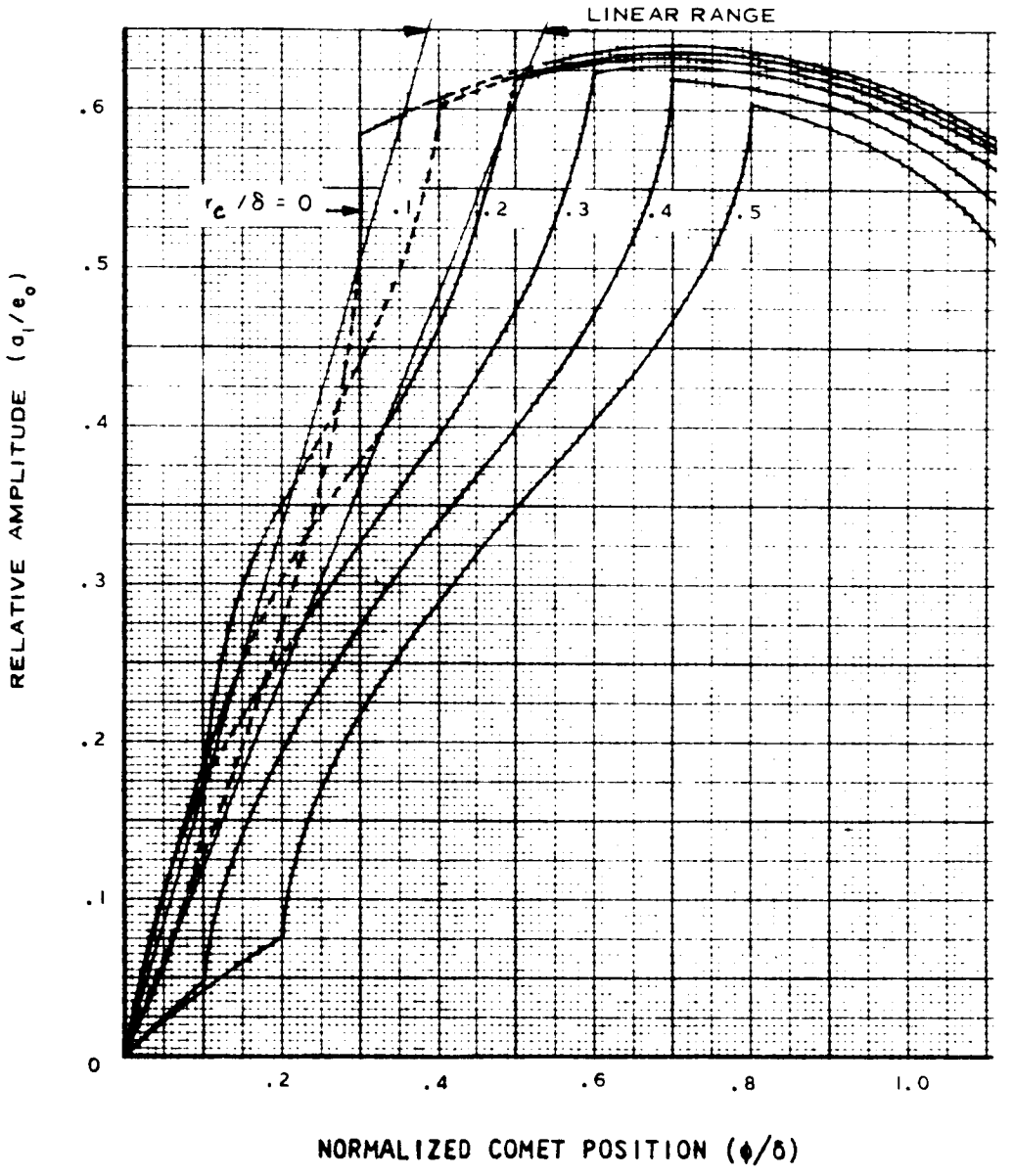

Fig. 4-16 Error Signal Amplitude vs Comet Position, $d/\delta = 0.7$

Two-Axis Scan Effects. The preceding data were obtained from a digital simulation which describes the operation of a single-axis tracker. However, for a system which uses a scan raster to "code" the two-axis information, a two-axis simulation is essential to the generation of design and trade-off information. The more significant effects to be obtained are the following:

a. Verification of the digital single-axis simulation
b. Transfer functions for each axis
c. Cross-coupling effects
d. Comet phase effects.

The first item, which provides the necessary check between the two simulations, has been carried out successfully. The analog simulation consists of stable, adjustable oscillators to generate the two-axis scans, logic circuitry to generate the detector output pulse train, a preamplifier and bandpass network, synchronous bridge detectors, and output-hold circuitry (with provision for gain adjustment, as necessary). Although no noise simulations have been carried out during this study, that capability is available for further work.

The scan raster uses two asynchronous, stable, controlled sinusoidal frequency generators to sweep the desired field of view. Examples of several scan rasters are shown in Figure 4-17 for the several apparent comet sizes to be tracked. The ease of adjustment of scan frequency; apparent size, position, and phase; and bandpass and network configuration made possible the rapid investigation of salient system parameters. Figure 4-17c is an example of a linear scan; the others are of a sinusoidal scan.

The comparison of two-axis scanning with single-axis scanning indicates a need for care in selecting asynchronous scan rates and the bandpass of amplifier circuits to avoid coupling and harmonic beating. Figure 4-18 is a plot of the transfer function for one of the comet tracker channels.

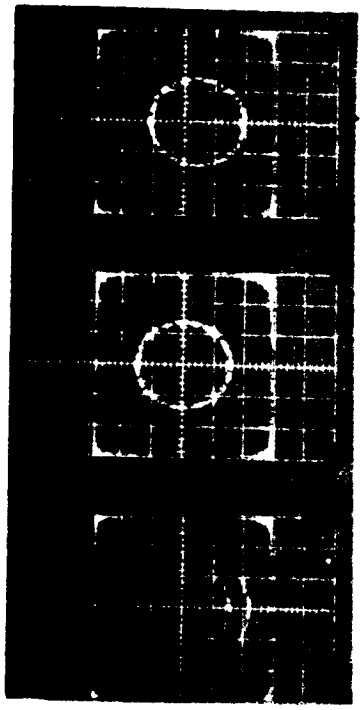

A. Sinusoidal Scan

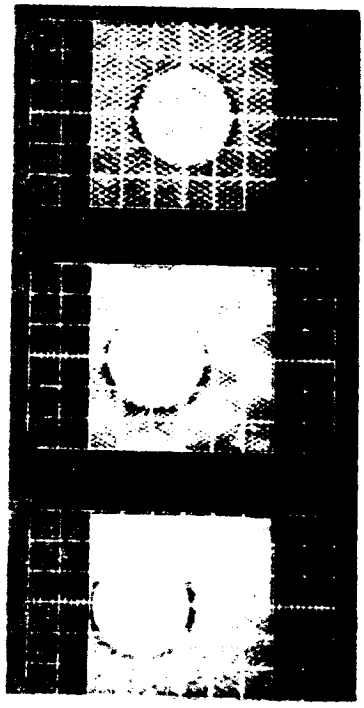

B. Linear Scan

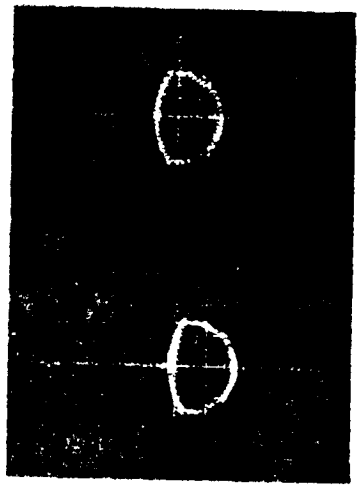

B. Sinusoidal Scan

Fig. 4-17 Examples of Two-Axis Scan Drive Systems

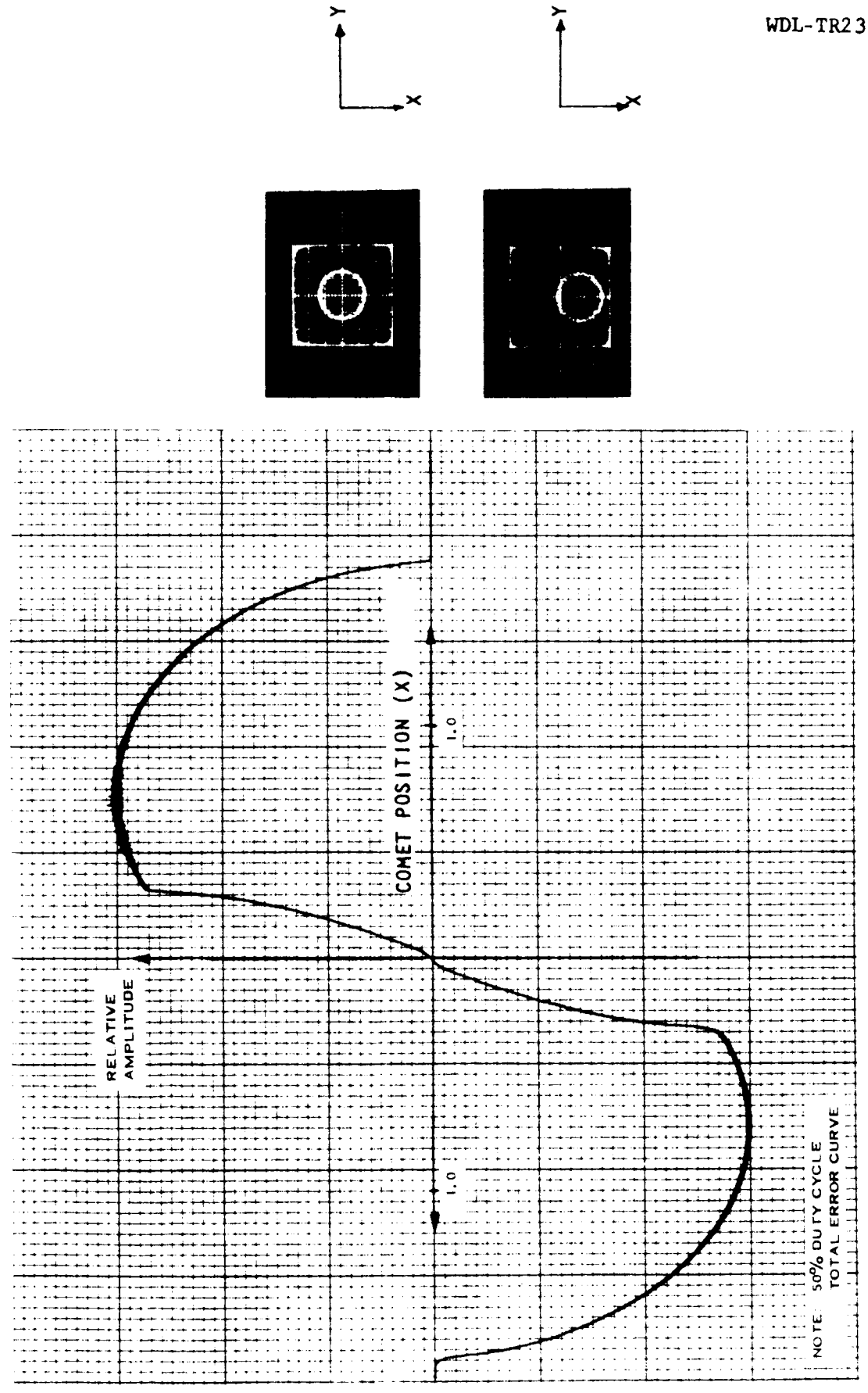

Fig. 4-18 Single Axis Error Curve for Two Axis $d/\lambda = 0.7$

The scan raster frequencies were chosen to minimize the beat-frequency problem in the outputs (300 and 400 cps, scaled). The analog simulation of the two-axis scan raster shows a sensitivity to the adjacent axis duty cycle. The case for $d/\delta = 0.5$ in both axes has been simulated and the error curve for one axis has been compared with the case for a single-axis scan. The results of this comparison are shown in Figure 4-19 for a 50 percent duty cycle, in Figure 4-20 for an 80 percent duty cycle, and in Figure 4-21 for a 30 percent duty cycle.

Cross-coupling. The effects of cross-coupling are demonstrated in Figure 4-22, in which the transfer function has been obtained for successively larger angular offsets in the adjacent axis. The corresponding comet image position for the various parametric curves has been photographed on the monitor display and has been included in the figure. The duty cycle for this simulation is 50 percent and the jitter on the output is due partially to the weak rejection of the scan frequency at the output filter. This jitter was attenuated by using a simple twin-T rejection filter.

Comet Phase Effects. Shown in Figure 4-23 is an example of comet phase simulation. This example includes the full-phase condition and a 50 percent phase condition for comparison of combined conditions which might occur. Interpretation of these data requires some knowledge of the roll position at the time of observation of any particular phase condition. This is essential to the definition of the error curve with respect to a reference point on the comet and is required of any system of this type.

Linear Scan Systems. The transistor implementation of scan drive offers an improvement in stability and parts count if a linear scan can be used, and a constant system S/N over the entire operating range. Figure 4-24 is an example of a system using a linear scan and shows that, if such a system is implemented, the effect of cross-coupling is nearly eliminated. The gain reduction in evidence for the dual-axis scan systems is due to the change in duty cycle. This system is superior in terms of linearity to the sinusoidal scan systems and is preferred in all but mechanically scanned trackers.

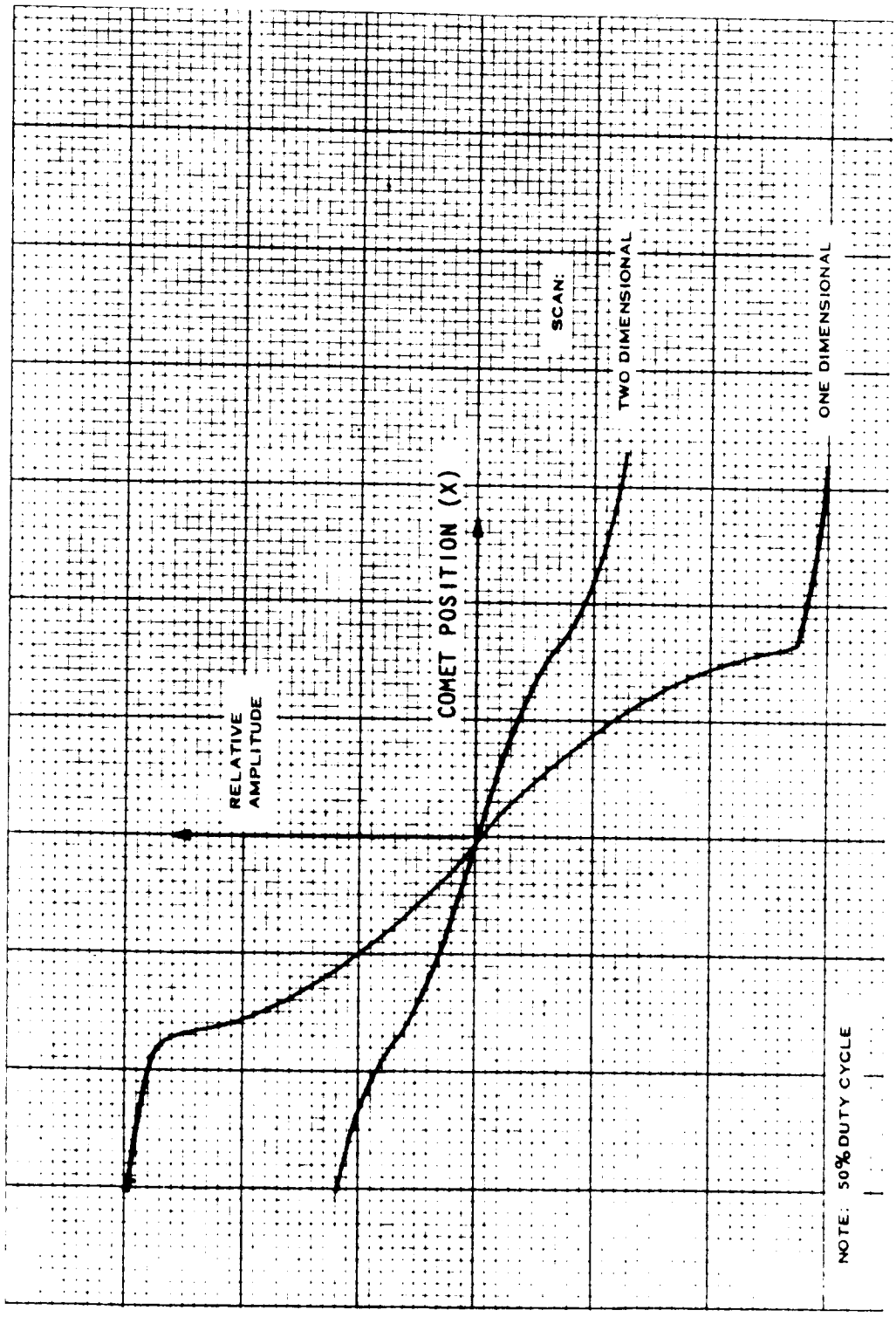

Fig. 4-19 Comparison of Error Curve Using Single- and Double-Axis Scan; 50% Duty Cycle

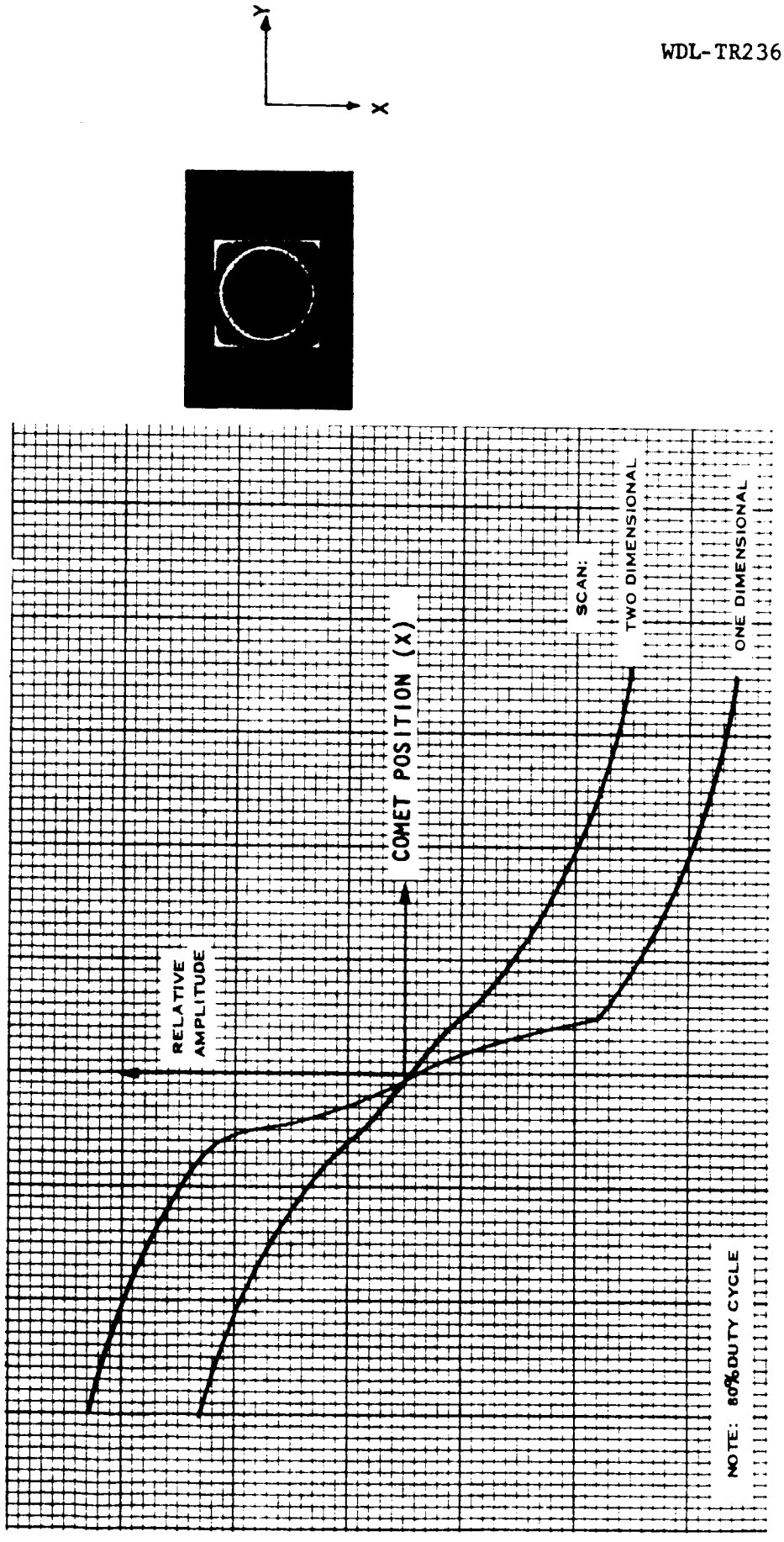

Fig. 4-20 Comparison of Error Curve Using Single- and Double-Axis Scan; 80% Duty Cycle

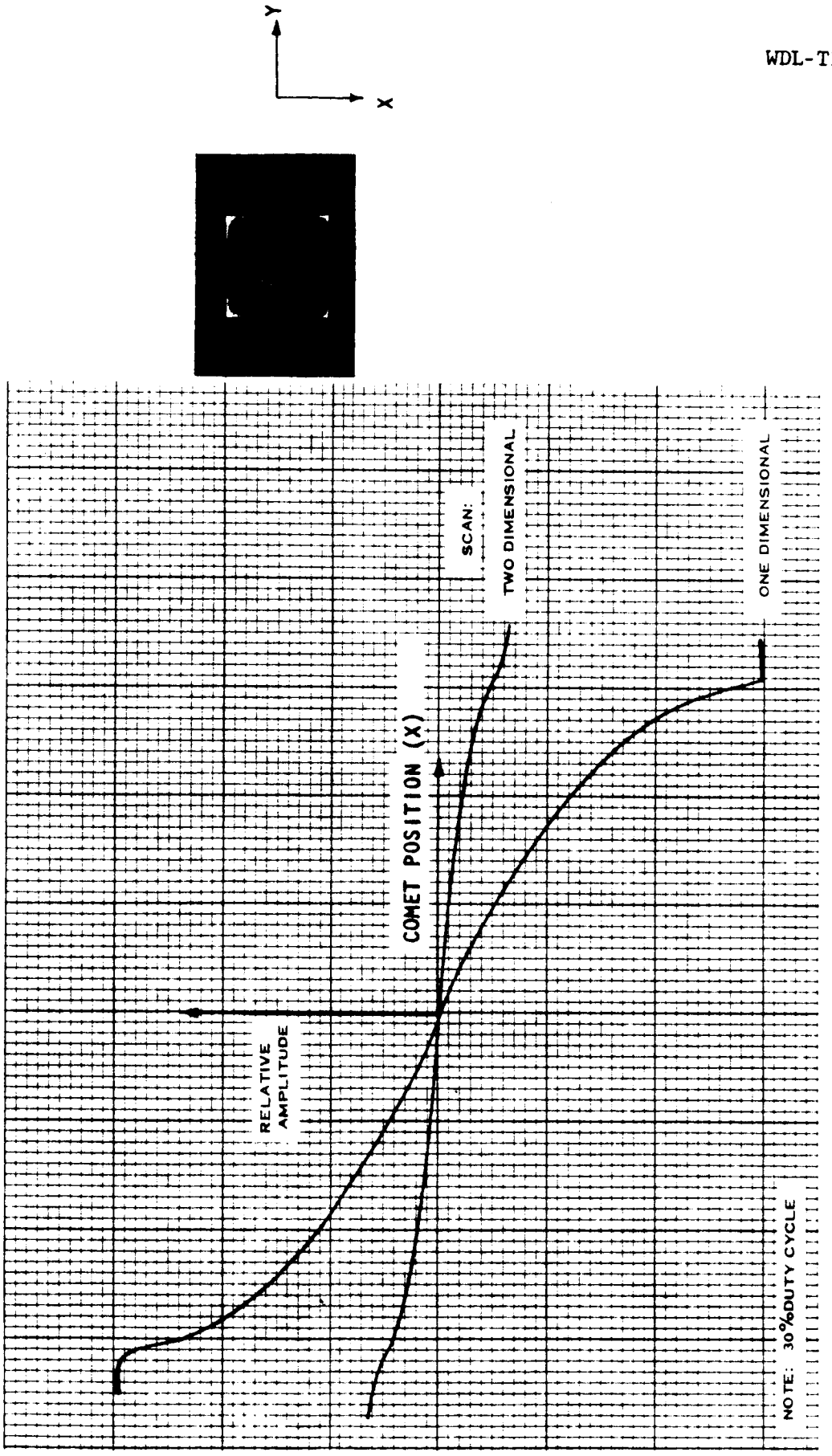

Fig. 4-21 Comparison of Error Curve Using Single-Axis and Double-Axis Scan; 30% Duty Cycle

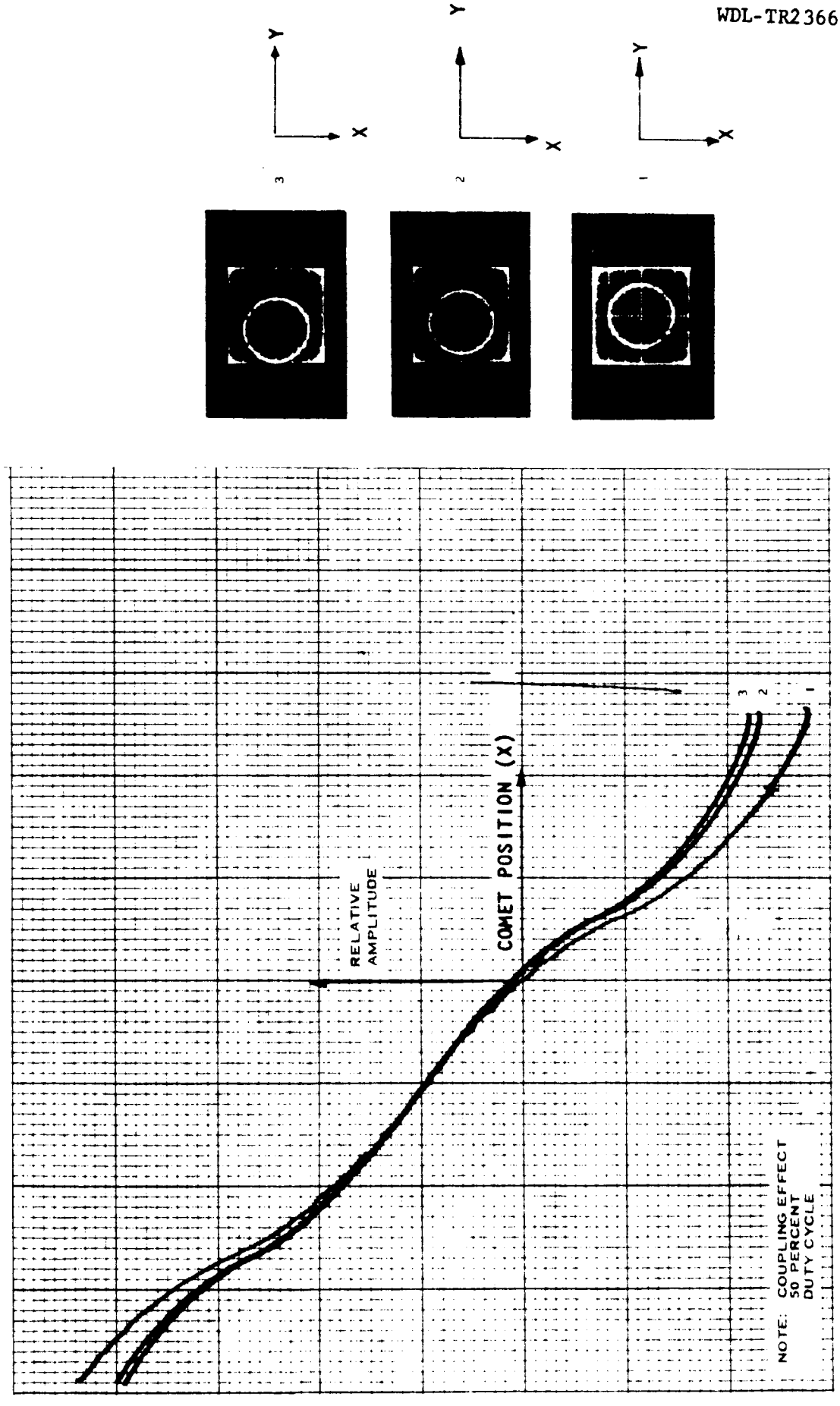

Fig. 4-22 Cross Coupling Effects for $d/\delta = 0.7$, Sine Drive

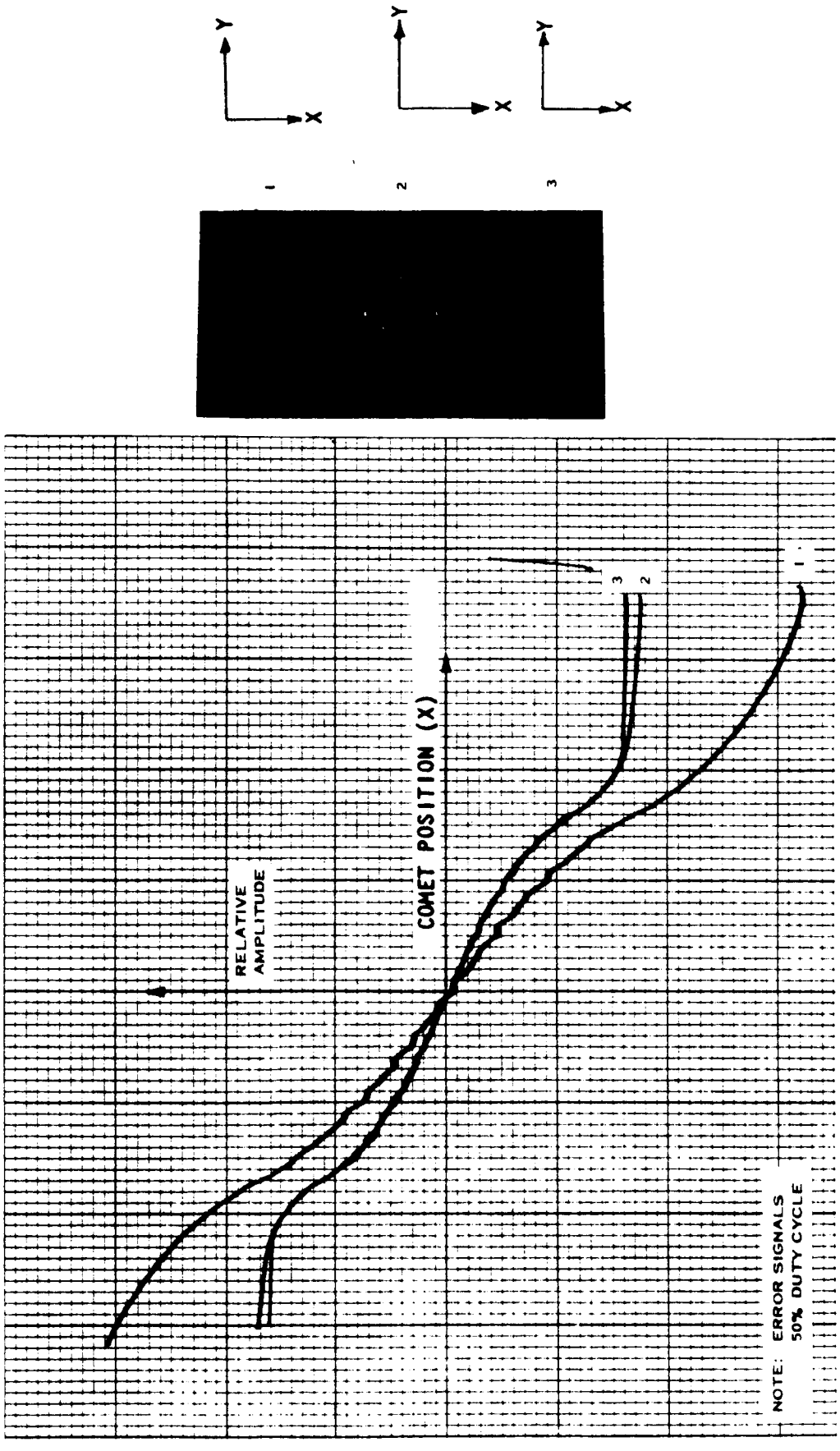

Fig. 4-23 Comet Phase Effects with Cross-Coupling, Sine Drive

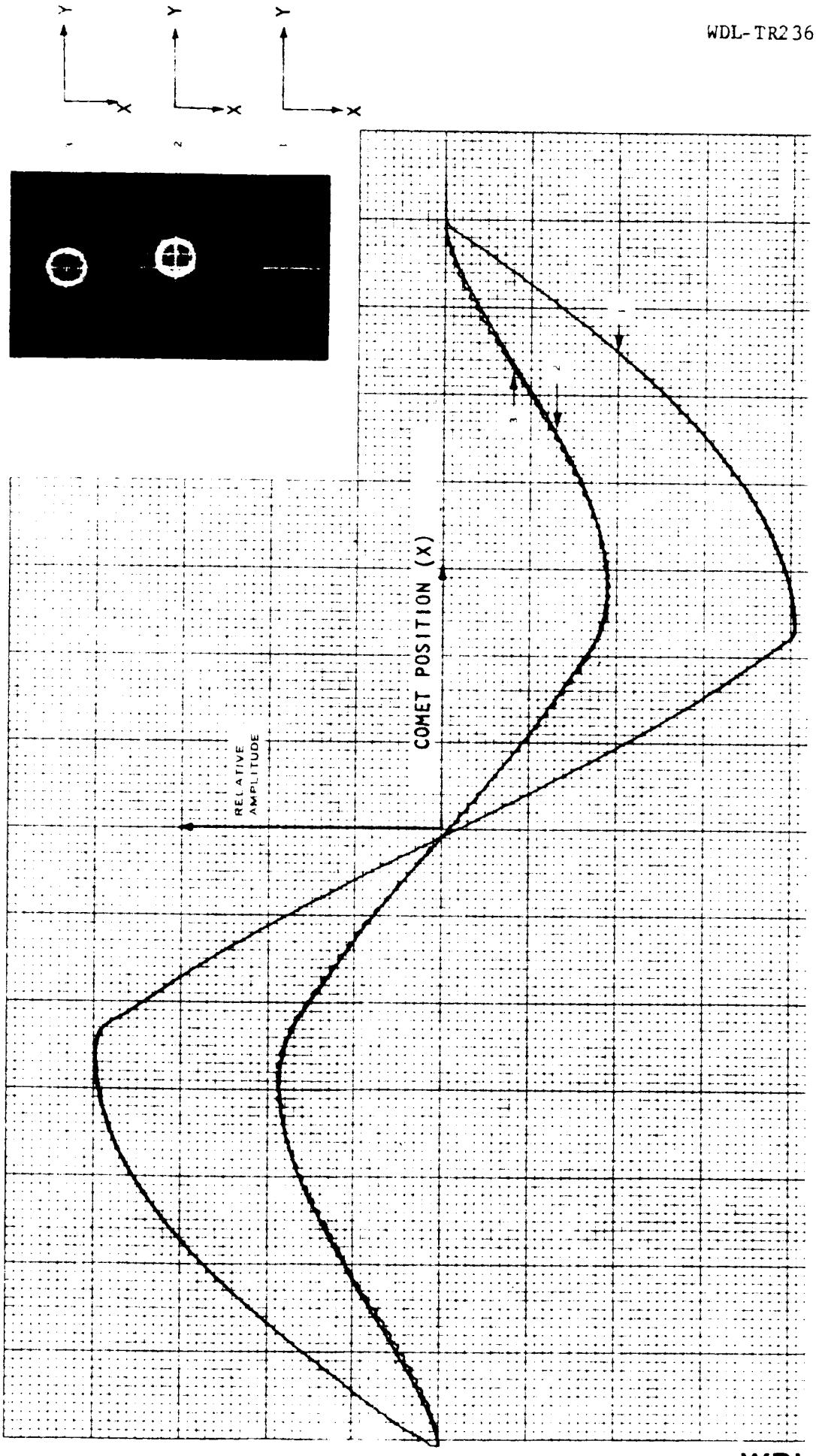

Fig. 4-24 Error Curve Using Single Axis and Dual Axis Scan, Linear Drive

4.4 COMET TRACKER SIMULATION

The parametric data reported in the previous sections were obtained using an analog computer simulation. This consisted of a set of scan generators to drive the x and y coordinates and the sync signals to the synchronous detectors. The simulated detector pulse was obtained using logic circuitry to gate the signal. The system connection diagram is shown in Figure 4-25.

Figure 4-26 is the connection diagram for the single axis tracker demonstration. This system serves as a means of verifying the parametric studies carried out on the analog computer.

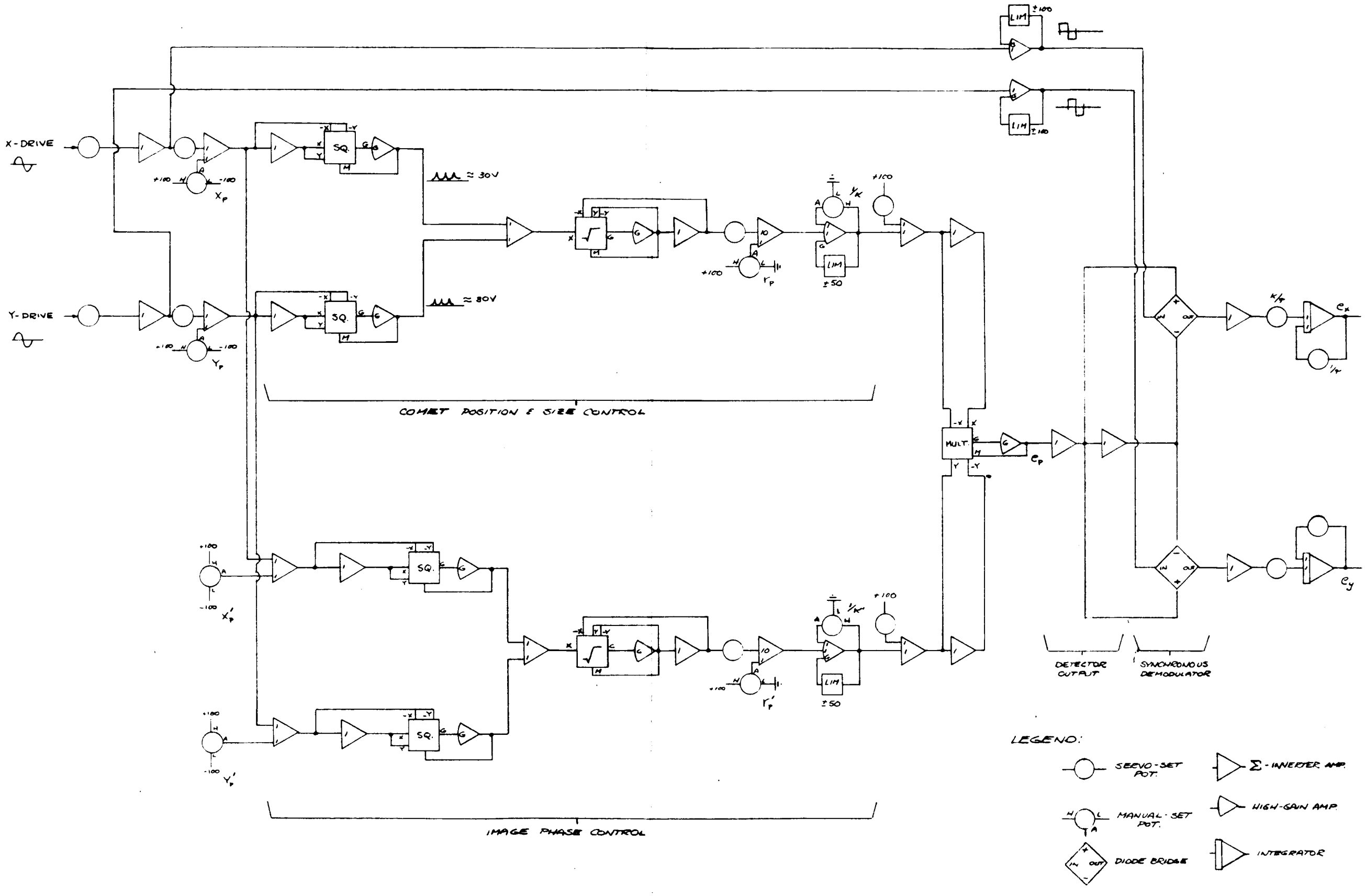

Fig. 4-25 Comet Tracker Analog Computer Simulation

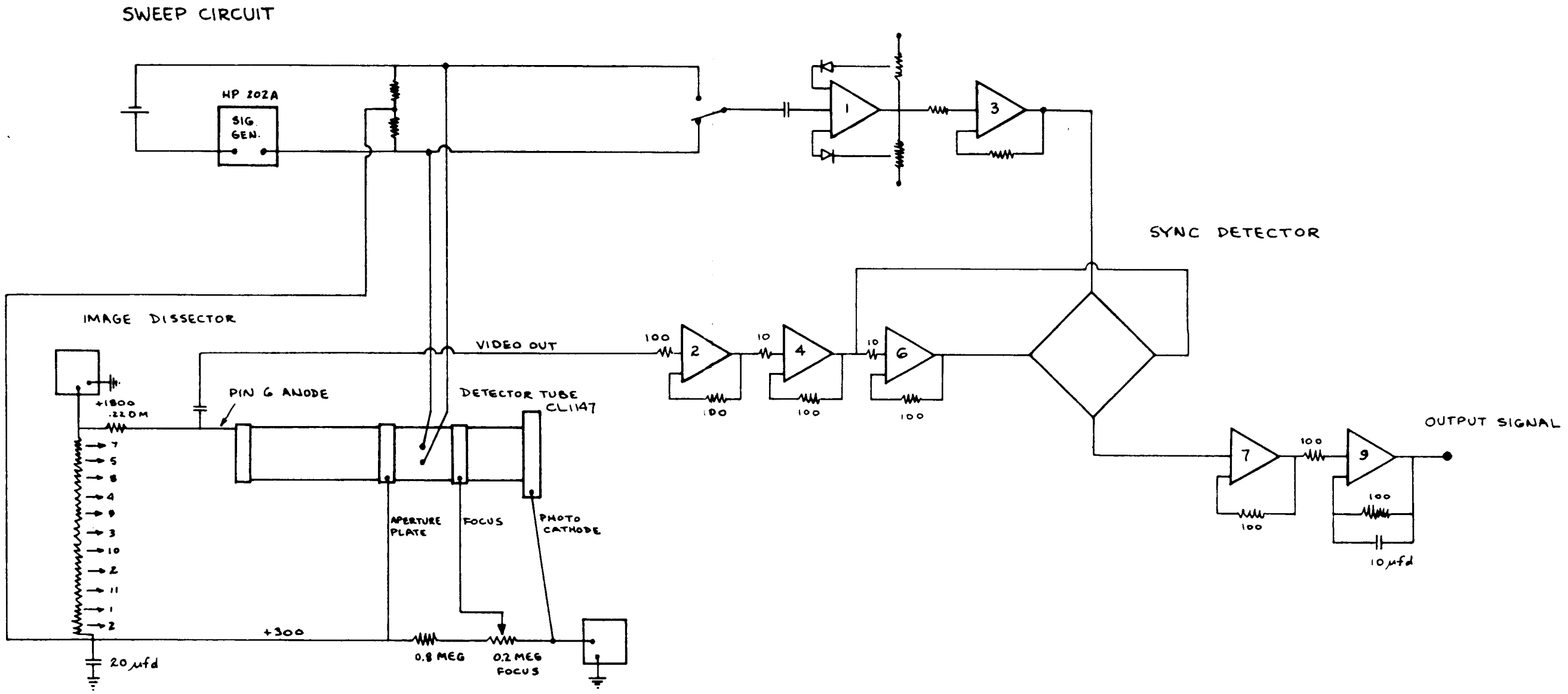

Fig. 4-26 Optical Laboratory Tracker Connection Diagram

SECTION 5

CONCLUSIONS AND RECOMMENDATIONS

5.1 COMET TRACKING

The Mariner-C subsystems for guidance and control have been compared on a systems basis to determine the areas requiring change or improvement. No change to the Mariner-C subsystems is essential with the single exception that a comet tracker must be added to that system for performing observations of the nucleus.

The requirements for sensitivity, range of intensity levels and angular size of the image make the comet tracker unique. As a result of comet tracking studies, it is clear that it is impractical to track whenever light levels exceed 10th magnitude. In fact, present day trackers become complicated with special processing devices, thermal cooling and attitude stabilization requirements for brightness levels exceeding 6.4th magnitude. Pending a special development program, no such device has been identified for use on this program.

Comet tracking is recommended prior to and during intercept when the brightness levels for the comet rise above the threshold light levels for tracker and TV. Early tracking of the comet prior to intercept serves to define the comet brightness model and cometary activity.

5.2 MIDCOURSE PROPULSION AND THRUSTERS

The midcourse propulsion system for the Mariner-C system may have to provide nearly double its present velocity increment capability presently 80 meters/sec for some missions. It is possible to make a 25-pound weight saving if a bipropellant system is used. Since the weight saving is low in comparison to system allotment, no change can be recommended.

The attitude control system thrusters can be improved by the addition of a microthruster. This system removes the deadband rates resulting from the minimum-impulse gas-conserving thruster systems. The advantage of this component is that the number of operations required for the on-off type torquers is reduced. Further advantages derived from this are a freedom of mounting and a higher thrust level than for solar vanes. The weight for a solar vane system is comparable to one using the microthruster.

5.3 INERTIAL COMPONENTS

The use of improved-performance gyros should be considered. Several inertial components exist that have better performance, use less power and have longer life than the Mariner-C gyros. The possibility of direct substitution of these components has not been investigated.

SECTION 6

REFERENCES

Acord, J. D., and Nicklas, J. C., "Theoretical and Practical Aspects of Solar Pressure Attitude Control for Interplanetary Spacecraft", Technical Report No. 32-467, Jet Propulsion Laboratory; May, 1964.

Allen, C. W., Astrophysical Quantities, 2nd edition, The Athlone Press, London, pp. 235, 269; 1963.

Bobrovnikoff, N. T., "Comets", Chapter 7 of Astrophysics, A Topical Symposium, ed. J. A. Hynek, Ohio State Univ., McGraw-Hill, New York; 1951.

Chestnut, H. and Mayer, R. W., Servomechanisms and Regulating System Design, Vol. I, Wiley, New York; 1951.

Cunningham, L. E., Professor of Astronomy, University of California, Consultant to WDL on Comet Mission Study; September-November, 1964.

Davis, R. J., "Project Celescope, An Astrophysical Reconnaissance Satellite", Smithsonian Institution Astrophysical Observatory, SR No. 110, Cambridge, Mass.; December, 1962.

Grabbe, E. M., Ramo, S., Wooldridge, D. E., Handbook of Automatic Computation and Control, Vol. I, Chapt. 22, Wiley & Sons, New York; 1958.

Grumman Aircraft Engineering Corporation, "OAO User's Handbook", Bethpage, New York, Revised; October 15, 1962.

Malling, L. R., "Space Astronomy and the Slow-Scan Vidicon", Jet Propulsion Laboratory, November, 1963.

Narin, F. and Pierce, P. M., "Sighting and Trajectory Analysis for Periodic Comets", Illinois Institute of Technical Research, Rough Draft Report No. T-7, NASR-65(06), Chicago, Illinois; July 22, 1964.

Philco, Weapon System Department, "Notes on Video Sweep Integrator Theory and Design Techniques", Report WS-62-5, Philadelphia, Penna.; April, 1962.

Philco, WDL, "Solar Probe Study", WDL-TR2133; under NAS2-1397; August 30, 1963.

Powers, W. T. and Aikens, R. S., "Image Orthicon Astronomy at the Dearborn Observatory", Applied Optics, p. 157, Volume 2, No. 2; February, 1963.

Russell, N. N., Dugan, R. S., and Stewart, J. Q., Astronomy, Volume II, Ginn and Company, New York; 1955.

Space Technology Laboratories, "Comet Intercept Study Final Report", NASw-414, 8668-6002-Ru-000 Redondo Beach, California; March 28, 1963.

APPENDIX A
EARLY-FLIGHT COMET ACQUISITION AND TRACKING

A.1 INTRODUCTION

The need for refining the aiming point accuracy during the terminal phase of the mission has led to the suggestion that comets be acquired early during the flight [Narin and Pierce, 1964; STL, 1963] and that pictures be telemetered to earth for analysis prior to the second midcourse maneuver. This critical phase of the mission provides sufficient motivation for carrying out an appraisal of the system requirements for on-board early-flight tracking of comets. The analysis in this section leads to an estimate of the weight, power consumption and size of optical trackers required to track comets early during the flight prior to the encounter phase for purposes of spacecraft guidance.

The study considers magnitudes of a faint level at which it is difficult to distinguish a comet from a stellar background for observation times less than 100 seconds. Section A.2 summarizes relevant comet illumination data collected. Probably the most significant effect of the stellar background is that the number of stars brighter than a given magnitude increases rapidly with increasing magnitude, with the overall effect that a faint comet is lost in the background. Section A.3 reports the results of parametric studies defining threshold levels for various sizes of optical systems using two sensitive detectors to scan an angular sector of the celestial sphere. The weight estimates reported therein are extrapolations of the Orbiting Astronomical Observatory (OAO) experimental optical packages. Also, since earth-based observations have demonstrated the feasibility of using these detectors for exposure times of up to 15 minutes, it is evident that the threshold rates of the attitude control system limit the exposure times.

A.2 ILLUMINATION CONTOURS AND INTENSITY

Tracking a comet requires that the comet illumination contours and the stellar background be differentiated. A summary of pertinent details related to comet illumination contours and comet brightness is included below. The references surveyed for this data report the general characteristics of illumination contours but report little on the characteristics of the individual periodic comets selected for analysis during the Comet Mission Study. It is anticipated that photographic plates of these comets of interest could be obtained for a final consideration. These were not available during the study for an accurate densitometer analysis.

A.2.1 Isoradiance Plots

According to Bobrovnikoff [1951], illumination contours in the head of a comet follow three patterns:

1. Jets - Streams of matter emitted from the center; these may be curved or spiral streams.
2. Fans - Wide streams of matter emitted from the center.
3. Halos - Spherical distribution of matter from the head with radially diminishing intensity.

The latter pattern more closely describes the appearance of the comets under consideration. On this basis, the intensity distribtution of a comet, could be represented in the form

$$I = I_o \exp\left[\frac{-(r-p)^2}{r_e^2}\right], \qquad \text{(A-1)}$$

which neglects the dependence on heliocentric distance, probe distance and position, observed spectrum, cometary material and activity. The parameters are defined as follows:

I_o = maximum radial intensity

r = distance from comet center

p = position of comet point of symmetry

r_e = effective radius of comet

Such a distribution is gaussian and the specification of an effective radius results in 68% of the flux originating from within the enclosed area.

A.2.2 Brightness

The brightness of a comet is usually represented by an empirically justified relation of the form

$$J = \frac{J_o}{\Delta^2 r^n} , \qquad \text{(A-2)}$$

Where Δ is the earth-comet distance, r is the sun-comet distance, and n characterizes the degree of central condensation of the comet under observation. Phase with respect to the observer is neglected and comet activity is assumed not to vary widely in time. Values of n range from 2 to 6 generally, with an average of 4. Expressed in stellar magnitudes, the relation becomes

$$m = m_o + 5 \log \Delta + 2.5\, n \log r, \qquad \text{(A-3)}$$

where m_o is an absolute magnitude. Theoretically, it represents the brightness that a comet appears to exhibit at unit distance from the sun and from the earth (Δ= r = 1 A.U.). However, the light from a comet results from sunlight reflected and scattered by the nucleus and dust particles, and from light re-emitted by molecules excited to fluorescence by solar radiation. These different contributions vary with heliocentric distance and the particular apparition, and thus cannot be represented

strictly by a magnitude law as the one expressed in Equation (A-3). Nevertheless, the time-honored formula is useful.

For the comets of interest, the light curves are expected to exhibit no sporadic intensity changes. The likelihood of outbursts occurring in these periodic relatively faint comets during their approach to and passage through periheion is small. Outbursts usually occur in Mars-type comets with perihelion distances far greater than the Mars-type periodic comets considered (e.g., "old" comet Schwassman-Wachmann I, and "new" comet Burnham 1960). The angular size of a comet of various diameters as viewed from varying probe-comet distances is shown in Figure A-1. The irradiance in lumens/cm^2 for any point source within the range of positive stellar magnitudes up to $\pm 12^M$ can be read from the straight-line functions of Figure A-2.

From the scattered literature, data on the absolute brightness of the seven selected periodic comets have been tabulated in Table A-1.

TABLE A-1 Comet Absolute Magnitudes

Comet	m_o
Tuttle-Giacobini Kresak	11.7
Arend-Rigaux	12.0
Pons-Winnecke	12.5
Tempel (2)	13.0
Kopff	13.8
Bonda-Mrkos Pajdusakova	14.1
Brooks (2)	14.4

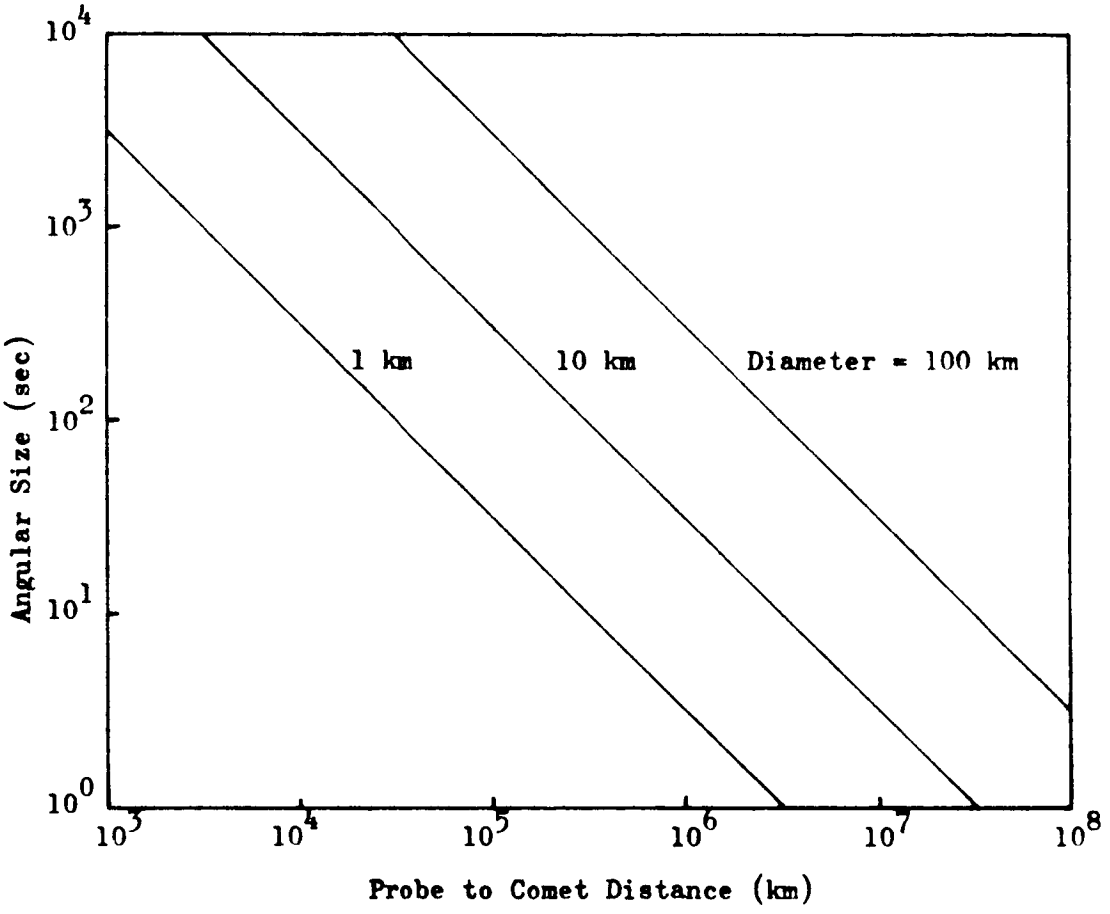

Fig. A-1 Angular Size of a Comet

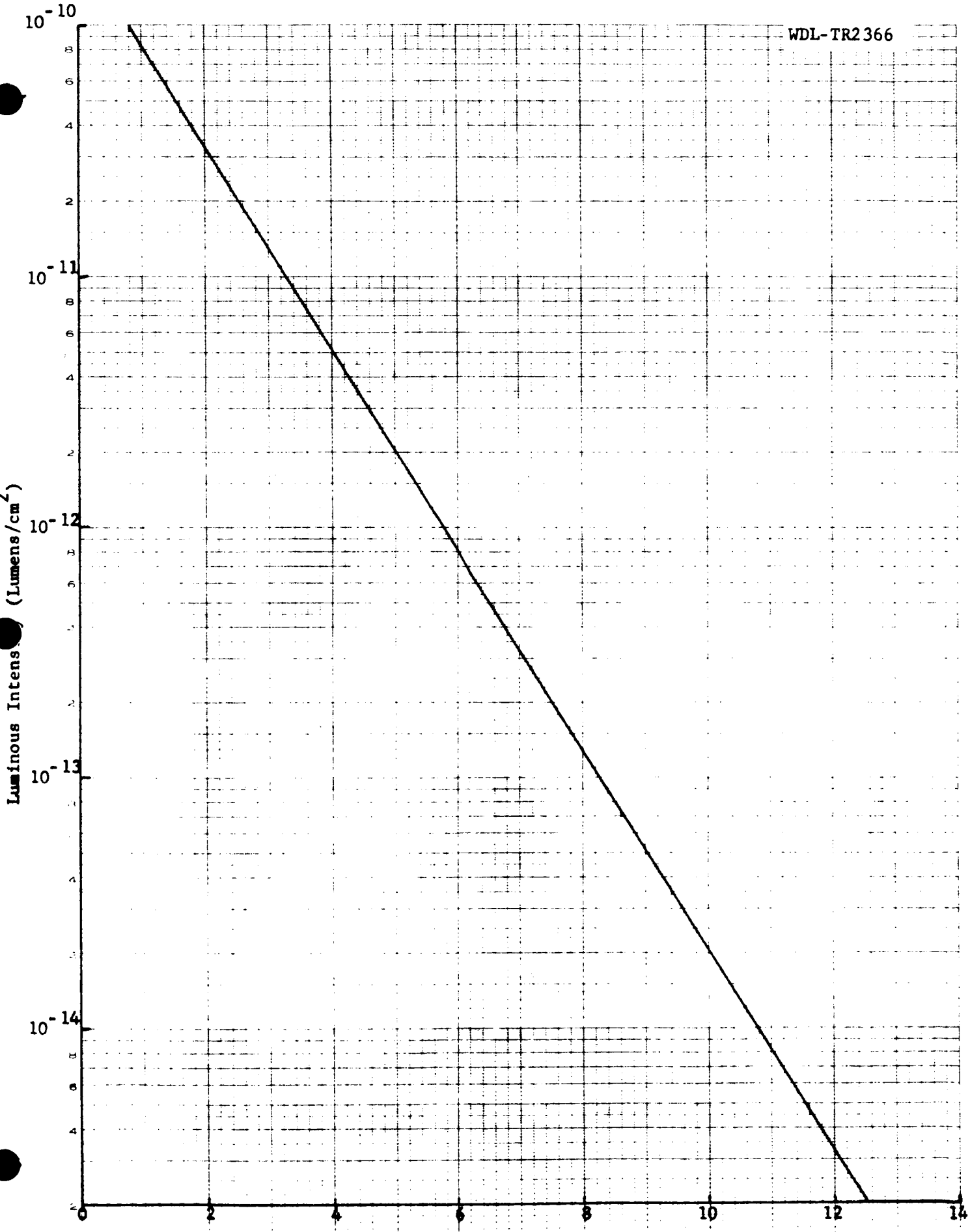

Fig. A- 2 Irradiance from a Point Source of Magnitude

The absolute magnitudes m_o tabulated are within $\pm 2^M$ accuracy; the variation depends upon the observer, his instrument and the sighting conditions during the comet's passages through perihelion when it is near its maximum brightness. An accurate value for the activity coefficient n cannot be assigned because of the same conditions. A value of 4 ± 1 appears adequate for estimating the total surface brightness of the head (nucleus plus coma). Neither the n_o nor n values apply to the comet's brightness when it is recovered as a starlike object with no coma or at best with a very fuzzy coma -- a condition characteristic of the faint periodic comets under consideration.

A.3 STELLAR BACKGROUND

The effect of the stellar background in the vicinity of the comet affects the capability of comet tracking devices in two ways. First, the presence of bright stars will saturate the scanning device (e.g., a photomultiplier); second, the increased current will generate added shot noise.

The exact effect of bright stars in the background is difficult to assess without a definitive description of the tracking scheme, the comet brightness and the probe's orbit.

A definition of the stellar background applies in all tracking or TV monitoring systems but the stellar background varies with the galactic direction of the probe-comet direction. It is well known that the average number of stars varies as a function of galactic direction and that the average brightness is highest near the galactic plane. In order to organize the large variations in this data, the maximum background has been compared to the minimum background and a representative value selected for use in the parameteric studies. It is important to realize also that the brightness of the comet compared to the number of stars of equivalent brightness in the optical field must be considered. The number of such stars increases with the tracking of the less intense comets. As

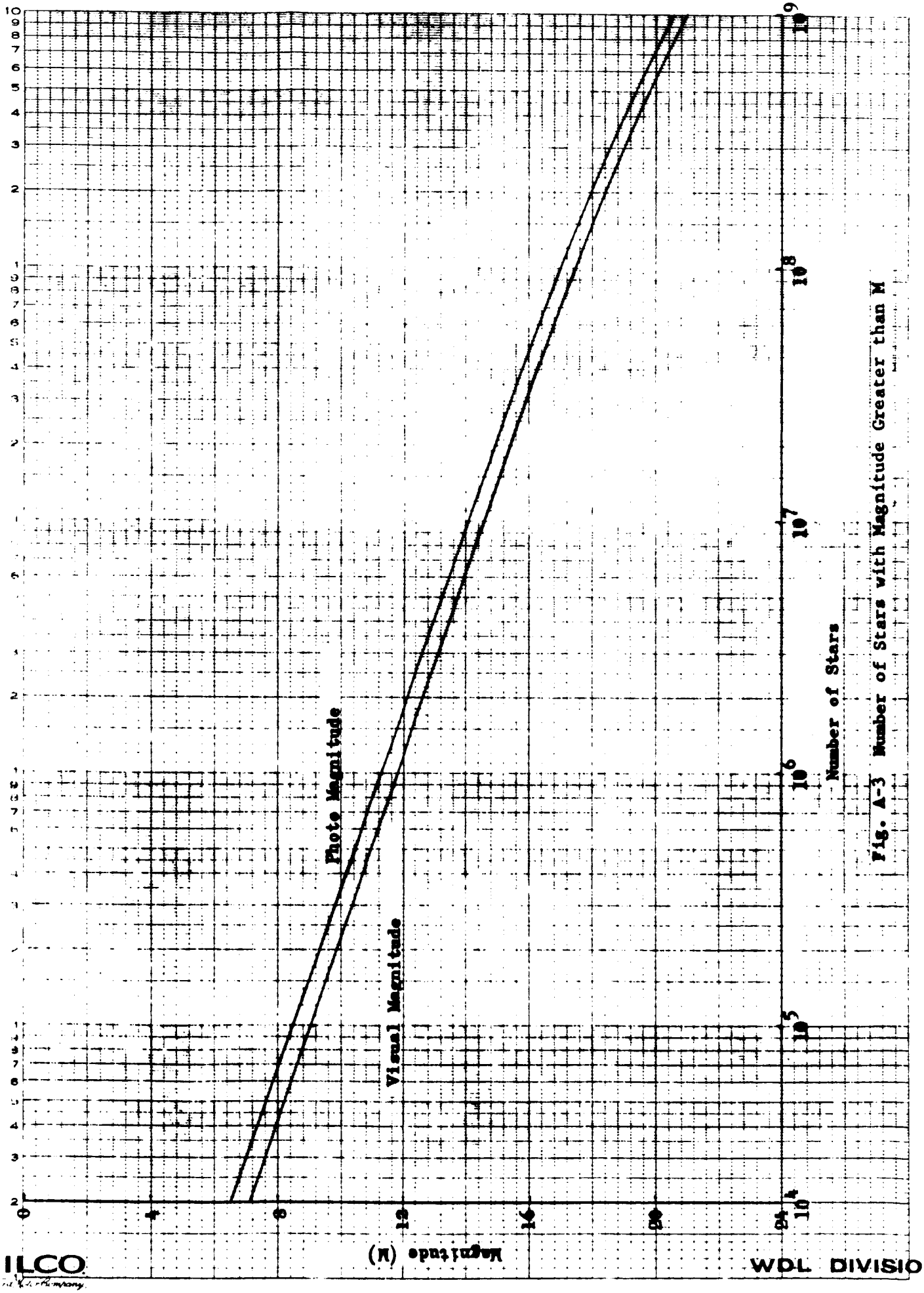

Fig. A-3 Number of Stars with Magnitude Greater than M

a result of investigations, the tracking of a 10^M comet is considered representative. However, the large number of stars which are brighter than 10^M (see Figure A-3) suggests that continuous, automatic on-board tracking is not possible.

A second consideration of the tracking background results from detector noise. The total noise out of the photomultiplier (presently considered to be the most sensitive electro-optical detector) consists of shot noise, which depends on the average current flow in the tube. The rms noise is given by

$$I_n^2 = 2e\, I_{ave} \int_0^{+\infty} G(f)\, df \qquad \text{(A-4)}$$

where

I_n = rms noise out of the tube
e = electron charge
I_{ave} = average tube current
$G(f)$ = system weighting function (bandpass)

Assuming the gain to be flat over the bandpass, Δf, the noise can be written as follows:

$$I_n^2 = 2e\, I_{ave}\, \Delta f. \qquad \text{(A-5)}$$

The average current in the tube is the sum of the tube dark current plus the average intensity of the optical image over the scanned pattern. This sum illustrates that the presence of stars in the comet background results in an increase of the noise level. If the stellar-background current level can be controlled, the average current is absolutely limited by the tube dark current which is a measure of tube performance.

The average space background is also important since the comet is masked by its presence. In the event that the system must be configured in order to insure that tracking is greater than a given probability, the field of view of the tracker can be used to control the number of and frequency of appearances of bright stars occurring in the field of view. The task of identifying a comet from the stellar background becomes progressively more difficult as the tracking of lower magnitude comets is contemplated, since the number of entries to a star catalogue increases rapidly with increasing magnitude (decreasing brightness).

The variation of sky brightness is given in Table A-2.

TABLE A-2 Sky Brightness

Sky Region	Number of Stars of Given Magnitude	Reference
Near Galactic Pole	43 stars, $m_v = 10/deg^{-2}$	[Allen; 1963]
	(mean brightness: $m_v = 5.9/deg^{-2}$)	
Entire Sky	1160 stars, $m_v = 1/deg^{-2}$	[Allen; 1963]
	580 stars, $m_{pg} = 1/deg^{-2}$	
Galactic Latitude 90°	33 stars, $m_v = 10/deg^{-2}$	
	17 stars, $m_{pg} = 10/deg^{-2}$	
Galactic Latitude 0°	397 stars, $m_v = 10/deg^{-2}$	
	184 stars, $m_{pg} = 10/deg^{-2}$	

As is apparent from entries (3) and (4) in the table, these values can vary by a factor of $\pm$ 3.5 between the galactic equator and the galactic poles or equivalently, $\pm$ 1.0^M. Evidently the variations reported here indicate the coarseness of data which complicates the problem of identifying a comet. However, a crude estimate can be given based on Cunningham's

estimate of the limiting magnitude for which star catalogues can be relied upon to provide sufficient ephemeris data when tracking is attempted in a region within $\pm 20^{o}$ of the ecliptic plane. Cunningham [1964] estimates that comprehensive entries exist for magnitudes 14; adding a $\pm 2^{M}$ uncertainty in observed magnitudes from apparition to a apparition, it appears that a 12^{M} comet represents a limiting case.

A.3.1 Stellar Photometry

The sensitivity of a detection system is based on the minimum detectable image, the spectral energy distribution of the source, the transmission and responsivity of the detector-optical system, and the observation integration time. No definition of the detection system is attempted at this time since the detection scheme is a function of the system threshold levels and the target signal level. In this section the definition of signal intensity will be carried out and the detection scheme is left for Section A.4.

The signal, i_c, from the detector can be written for a point source target as follows:

$$i_c = AG_c \int_0^{\infty} I(\lambda)\, R(\lambda)\, \tau(\lambda)\, s(\lambda)\, d \qquad \text{(A-6)}$$

where

- A = collecting aperture area
- $I(\lambda)$ = spectral irradiance of the star
- $R(\lambda)$ = spectral reflectance of the mirrors
- $\tau(\lambda)$ = transmission of the refractive elements
- $s(\lambda)$ = detector responsivity
- λ = optical wavelength

The systems presently of interest would use reflective optics having typical reflectivities of 0.95 or better over the entire optical spectrum.

These systems have no refractive elements; thus the transmission term is unity over the wavelength interval of interest. Unfortunately, the convolution indicated in Equation (A-6) cannot be carried out simply.

The quantitative measure of energy received by the detector can be predicted using conventional definitions to describe the comet and its star background. The situation considered in these studies takes advantage of the fact that the reflected energy from the comet is identical to that of the sun. The solar spectra is well approximated using a Planck black-body radiator having an equivalent temperature of 5780°K. Estimates in the literature are within 20°K of this temperature; this uncertainty need not be a source of concern since it introduces a negligible effect in the estimate of total irradiance from a comet. Stellar magnitudes are expressed according to the arbitrary scale,

$$m = -2.5 \log \frac{I}{I_o} \qquad \text{(A-7)}$$

where I is the effective irradiance and I_o is the standard irradiance. In order to define a magnitude reference, the definition of I_o must be carried out. The irradiance is given in terms of the spectral irradiance, $E(\lambda)$,

$$I = \int_o^{oo} E(\lambda)\, d \qquad \text{(A-8)}$$

Certainly the response of the detector must consider the spectral energy distribution and historically this has been done by identifying the star class. Also the detector response has been classed according to the spectral class. The result is a rather cumbersome cataloging of the response of a given class detector with a given class star and a specific set of optics. Needless to point out, the literature is filled with such tabulations, all of which are really the result of the convolution indicated by Equation (A-6) (see for example Table A-3).

Table A-3 Typical Star Catalog Special Classifications

Star	Spectral Class	M (S-4)	M(v)
α CMa	AO	- 1.60	- 1.58
α Car	FO	- 0.52	- 0.86
α Lyr	AO	+ 0.14	+ 0.14
β Ori	B8	+ 0.25	+ 0.34
α Eri	B5	+ 0.36	+ 0.60
β Cen	B1	+ 0.41	+ 0.86
α Vir	B2	+ 0.81	+ 1.21
β CMi	F5	+ 1.00	+ 0.48
α Aur	GO	+ 1.10	+ 0.21
α Cru	B1	+ 1.13	+ 1.58
α Cen	GO	+ 1.14	+ 0.06
α Aqu	A5	+ 1.15	+ 0.89
α Leo	B8	+ 1.25	+ 1.34
α Boo	KO	+ 1.37	+ 0.24
α Cyg	A2	+ 1.39	+ 1.33
α PsA	A3	+ 1.46	+ 1.29

[Russell, Dugan, and Stewart; 1955]. The system of classification seems crude; however, any system of cataloging these stars more precisely would result in a fairly extensive overhaul of existing data. Since no effort is either available or desired, the approach taken here consists of using the coarse system of classification for computing the stellar background and using the solar spectral distribution for computing the comet spectral irradiance. The detector spectral sensitivities are well documented.

A.4 OPTICAL DESIGN CONSIDERATIONS

The faint character of comets requires that the threshold levels of any tracking system be defined. The optical requirements, i.e., collecting aperture size, field of view and off-axis performance, provide the means of making weight comparisons using examples of space flight systems. In this section, the vehicle attitude control requirements will be outlined. Two sensitive electronic detectors, one using an image dissector and the other using an image orthicon will be evaluated and the trade-off data presented. Although both systems use a telescopic optical imaging device, each differs considerably in terms of vulnerability to the launch environment. The image orthicon has a comparatively delicate mechanical construction compared to the image dissector and is considerably larger.

Several other advantages result from the use of an image dissector if a sufficiently bright optical level is possible. The image dissector has an almost indefinite lifetime since it contains no hot cathode and the photocathode will tolerate large variations in temperature. Finally, the photo-multiplier section will provide a high signal level without concern over saturation and amplification linearity. Figure A-4 shows a sketch of image dissector and image orthicon phototubes. Such detectors represent the most sensitive devices presently available for the 1967-1975 time period.

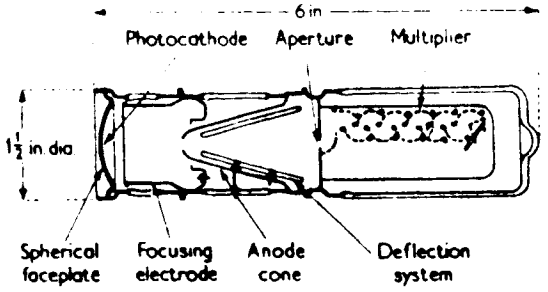

Electrostatic Image Dissector

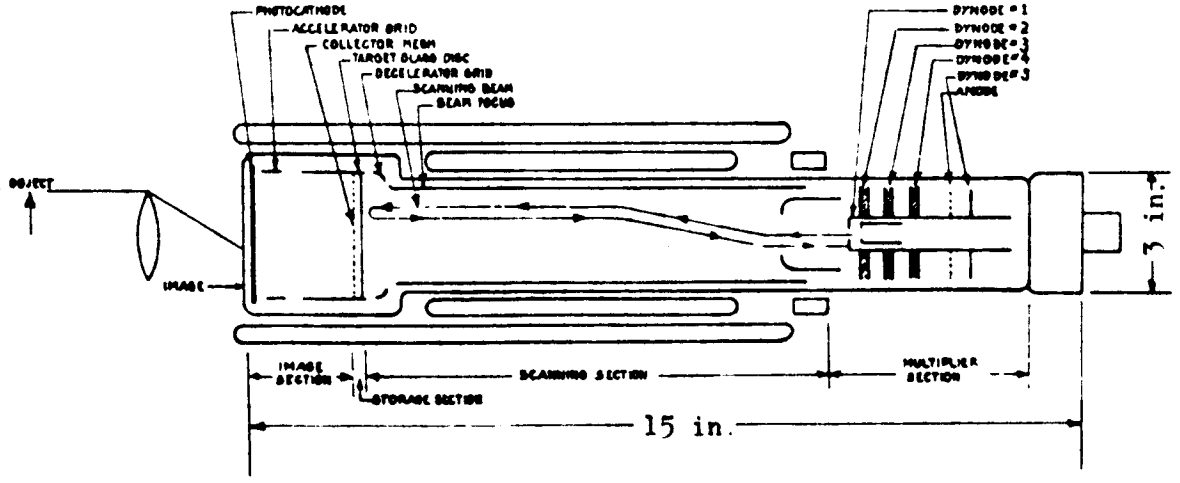

Image Orthicon Showing Deflection Coils, Focus Coil, and Internal Structure of Tube

Fig. A-4 Sketch of Image Dissector and Image Orthicon Phototubes

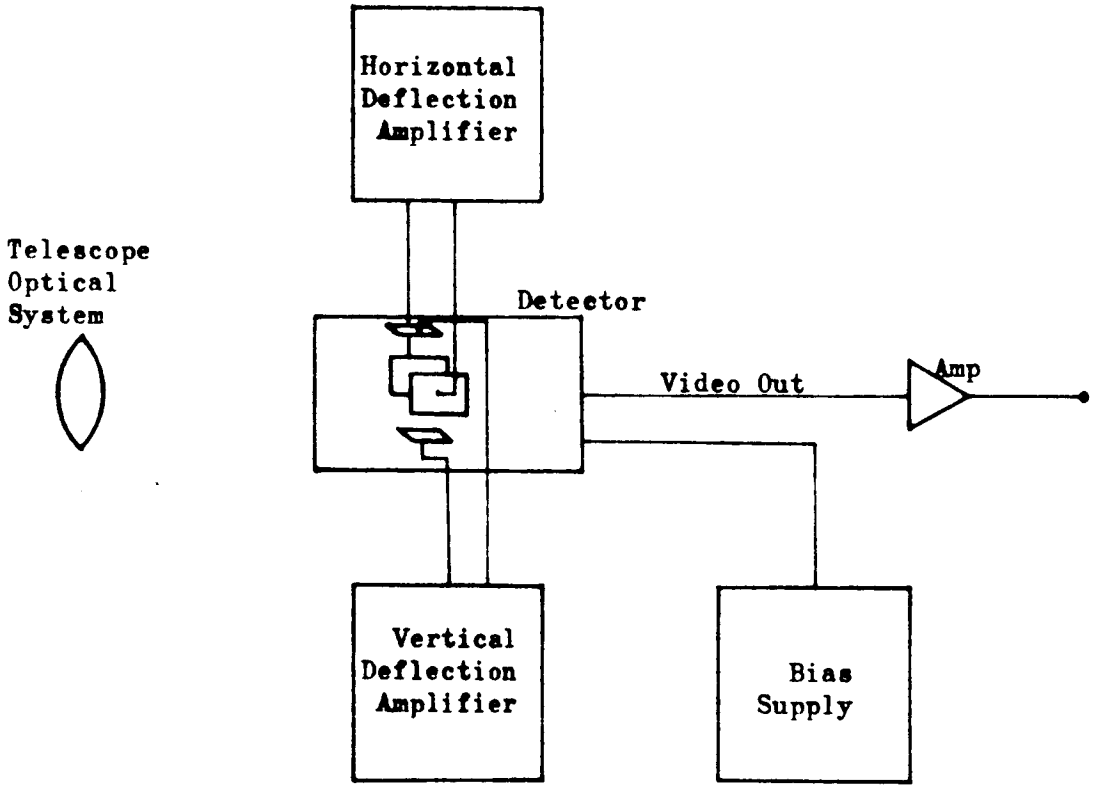

Fig. A-5 Scanning System Block Diagram

The principal limitation to this type of system involves the detection of very small amounts of radiation from on-board the spacecraft. A schematic drawing of the scanning system is presented in Figure A-5 in which the system would either interface with a data storage and telemetry network or with a tracking processor contained on board the vehicle. While the latter presently represents a system considered to be unfeasible, it is included here for the sake of completeness. On-board tracking of the comet would require that the comet be distinguishable from the stellar background and presently the only difference identified is the relative motion. The sketch below (Fig. A-6) represents a schematic of the processing network required to detect the comet motion using a radar motion indicator technique.

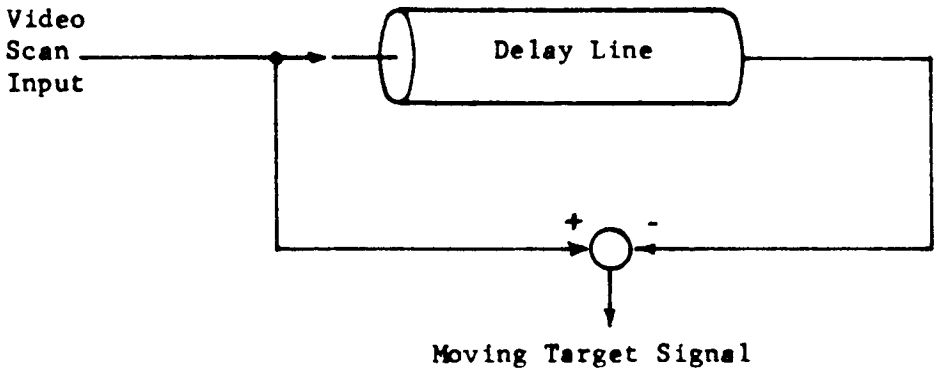

Fig. A-6 Relative Motion Indicator

A.4.1 OAO Optical Systems

The Goddard Experimental Package (GEP) has a 38-inch clear aperture, weighs approximately 750 pounds and has a usable field of ±15 seconds of arc. Project Celescope has a 12-inch clear aperture, weighs approximately 60 pounds and has a usable field of ±1.4 deg. The approximate weight of an optical system can be estimated on the basis of the size

of the collecting aperture area, assuming that the telescope weight is proportional to area. On this basis, if the 38-inch telescope weight would be 750 lbs; this is to be compared with 60 lbs. Another method of estimating weight on the basis of aperture diameter, d, would curve-fit d^n for these two weights, in which case, n = 2.2 This latter approximation shall be used as the basis for estimating the optical system weight.

A.4.2 Image Dissector Sensitivity

The image dissector developed by P. T. Farnsworth has been combined with an electron-multiplier section to form an image-dissector photomultiplier. The tube operates by scanning a photocathode on which a desired image has been placed. Each resolution element on the photocathods emits electrons in accordance with some statistical efficiency and an accelerating potential drives these toward a plate having a scanning aperture. The traverse focus and deflection fields control the trajectory of the photoelectrons such that a particular element on the photocathode can be focused on the aperture. By varying the traverse focus and deflection field either magnetically or electrically, the entire surface of the photocathode can be scanned. Since the dissector resolution can be controlled on a first-order basis by the aperture size, and since our principal interest is sensitivity, the source of noise for the detector system will be considered next. The comet will be assumed to subtend an angle less than the resolution of the detector system in the early portion of its apparation; this permits the simplifying assumption that the comet is a point source. This assumption does not apply prior to intercept when the image is considered to be an extended source; in this case the comet intensity pattern must be considered.

The intensity, L, from a point source having a stellar irradiance, E, is related to the area of the collecting aperture, $\pi d^2/4$, and the optical efficiency, ϵ, as follows:

$$L = \epsilon E \pi d^2/4 \qquad \text{(A-9)}$$

The optical efficiency can approach unity in these systems. Consequently, the signal level at the photomultiplier cathode is

$$i_c = G_c L \qquad \text{(A-10)}$$

where G_c is the photomultiplier cathode gain. Consider the stellar background of intensity, L_B, for an optical field angle, α, viewing a sky of brightness B_B, to be

$$L_B = \epsilon \pi^2 \frac{d^2}{4} \alpha^2 B_B, \qquad \text{(A-11)}$$

The average current resulting from the background, the comet under observation and the detector dark-current is

$$i_{c_{ave}} = G_c \epsilon \left(\pi \frac{d^2}{4}\right)(E + \pi\alpha^2 B_B) + i_{dark}. \qquad \text{(A-12)}$$

Assuming a uniform gain over the system band pass of Δf, the noise power is

$$i^2 = 2e\, i_{ave} \Delta f. \qquad \text{(A-13)}$$

Consequently, the signal-to-noise ratio, when observing the comet, is given by

$$S/N = \frac{G_c \epsilon (\pi d^2/4)}{\left\{2e\, \Delta f \left[G_c \epsilon (\pi d^2/4)(E + \pi\alpha^2 B_B) + i_{dark}\right]\right\}^{\frac{1}{2}}}. \qquad \text{(A-14)}$$

Certain desirable operating conditions would be accomplished by restricting α^2 to be small and using a collecting area sufficiently large to permit

i_{dark} to be dropped. Unfortunately, this would not reflect the situation for the comet magnitudes under consideration.

In the case of a video scanning device, the scanning spot of radius r_s will subtend a half-angle according to the relationship

$$\frac{\alpha}{2} = \frac{r_s}{2f} \qquad \text{(A-15)}$$

where d is the diameter of the collecting aperture and f is the system focal length. Thus, for specific systems, the measurement of S/N serves as an effective index of system merit and performance. The above analysis permits the evaluation of the slow-scan TV and the radar relative-motion-indicator.

A.4.3 Slow-Scan TV

A slow-scan TV could use a photomultiplier image dissector to scan the comet in the background field of stars and the above analysis used to determine threshold levels. One very sensitive tube for this application has been available for nearly eight years; that tube is the CBS CL-1147 developed to sense low-light levels. Tube life is long but has not been defined since the number of failures has been too sparse on which to base data.

The noise equivalent input intensity of the CL-1147 dark current is 6.7×10^{-11} lumen. By comparison, the noise due to the average sky brightness (see Table A-2) is equivalent to 43 stars of magnitude 10 per deg^2. Referring to Figure A-2, the luminous intensity for a 10^M star is 2×10^{-14} $lumen/cm^2$, so that the background brightness is

$$B_B = 3.68 \times 10^{-12} \text{ lumen/cm}^2/\text{deg}^2$$

Correspondingly, the worst case can be seen to occur near zero galactic latitude where

$$B_B = 3.68 \times 10^{-12} \text{ lumen/cm}^2/\text{deg}^2$$

Figure A-7 shows the tradeoff among the photo-intensity of the star background, the aperture size and the field angle. It is evident that the control of background level is accomplished by restricting the field angle, since the intensity of a point-source comet is not affected by the field angle.

Some physical interpretations are in order since control of the sky background has implications not obvious in the derivation of a "mean" or "worse case" sky background. Only in certain cases is it reasonable to consider that the background is virtually continuous as in the Milky Way. Normally, the star background is composed of discrete stars and the use of an average background does not apply. It is seen from Figure A-7 that for α = 10 seconds and d = 100 inches, the background noise is slightly higher than detector dark current. In order to meet this 10-second field for a scanning spot of 0.001-inch diameter, the focal length must be at least 100 inches.

Using the earlier relation in Equation (A-14) for the signal-to-noise ratio, the parameteric results of this can be plotted as a function of collecting aperture d and by using representative values for dark current, stellar background, tube gain, and band pass. These values are the following:

ϵ = 0.9

i_D/G_c = 5×10^{-10} lumen
(the equivalent input for the dark current)

B_B = 8.6×10^{-3} lumen/cm^2/deg^2

f = 15 Kc
(the frame frequency of one second being selected to

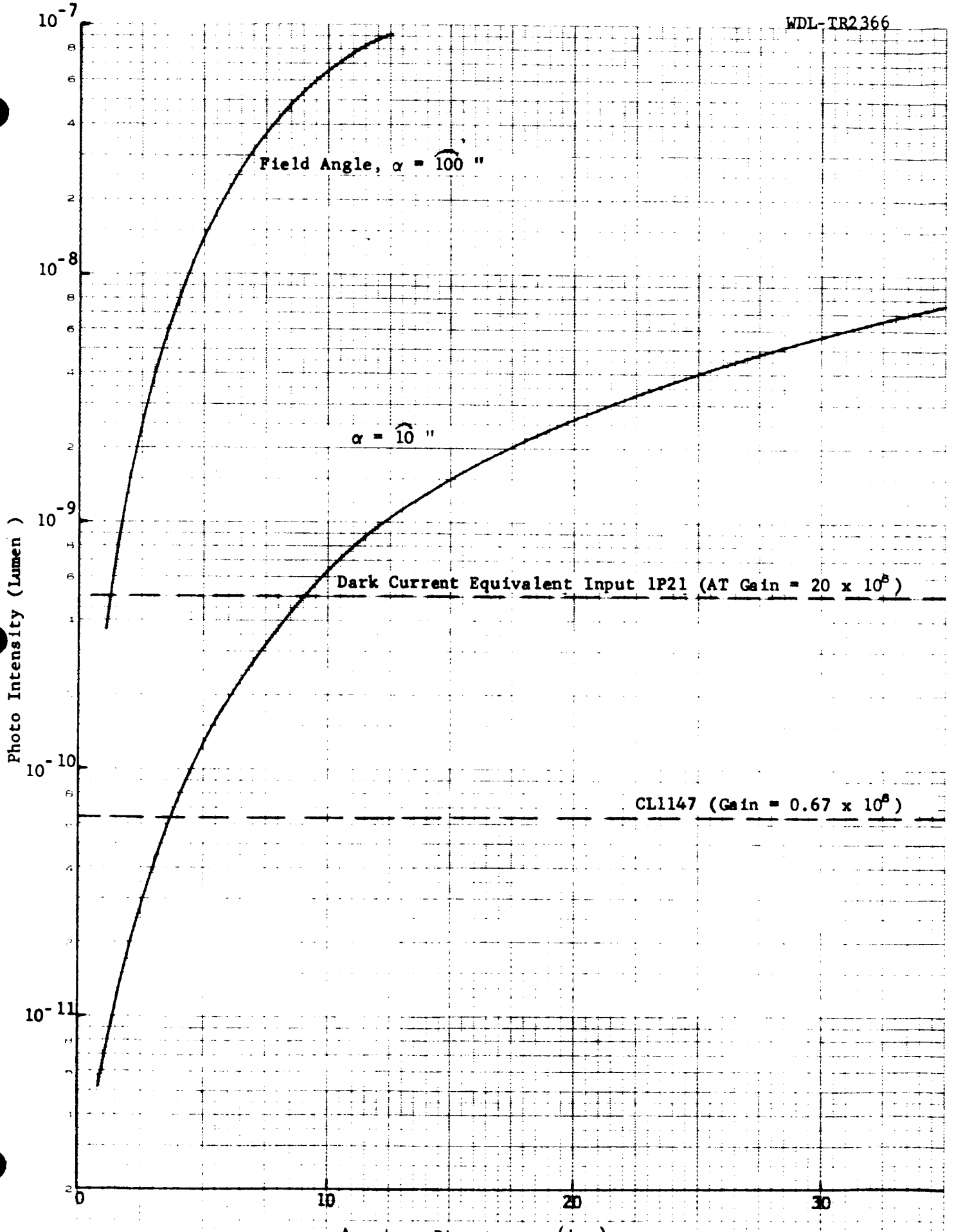

Fig. A-7 Trade-off of Optical Field with Collecting Aperture

avoid low-frequency semiconductor noise, the number of lines per frame is 100 and the time to resolve an element per line to 1/100 the line length is 0.2 millisec. corresponding to a fundamental of 5 Kc. Thus, passing the first three harmonics, the bandpass required is 5 Kc to 20 Kc.)

Note that, for a resolution of 100 elements in which the scanning spot corresponds to 10 seconds, the TV raster will cover a solid angle 1000 by 1000 sec. (15 min by 15 min). Another point to be noted is that, at a frame rate of one second, the TV readout must interface with the telemetry with a 15 Kc bandwidth. This is extremely demanding in any case, however, it may be possible to playback at a much lower rate. Also, slower scanning or a reduced raster size could be traded off here for telemetry bandwidth.

The trade-off of S/N is shown in Figure A-8 for various combinations of field angle, aperture size, and star magnitude. Since this data does not include noise from tracker electronics, the criterion of a usable S/N is somewhat arbitrary: the ratio of signal-to-rms-noise out of the phototube must be at least six. Using such a criterion, it is possible to make certain comparisions with existing optical equipment, namely the OAO - Goddard Experimental Package and the Smithsonian Observatory "Project Celescope". On this latter basis, system weights are indicated in Figure A-8.

A.4.4 Image Dissector and Video Sweep Integrator

Considering the time required to read out a single video sweep from the dectector and the relative angular motion of the tracker or TV telescope with respect to the celestial reference, it is evident that successive video sweeps can be autocorrelated or integrated to improve the target signal-to-noise. An autocorrelation technique of this type is illustrated schematically in Figure A-9. The basic circuity consists of a video adder, a delay line and a feedback loop to the video adder. The time

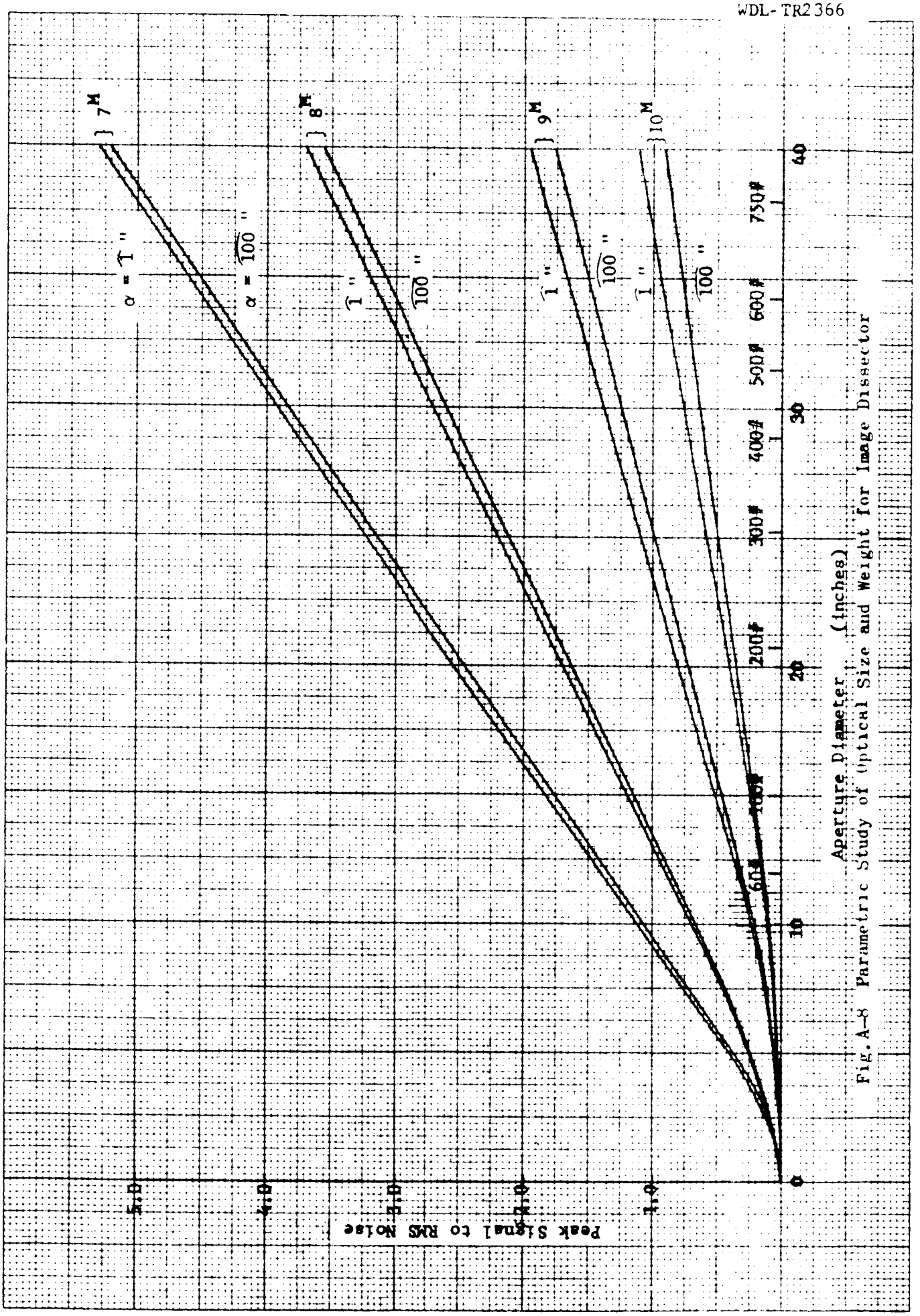

Fig. A-8 Parametric Study of Optical Size and Weight for Image Dissector

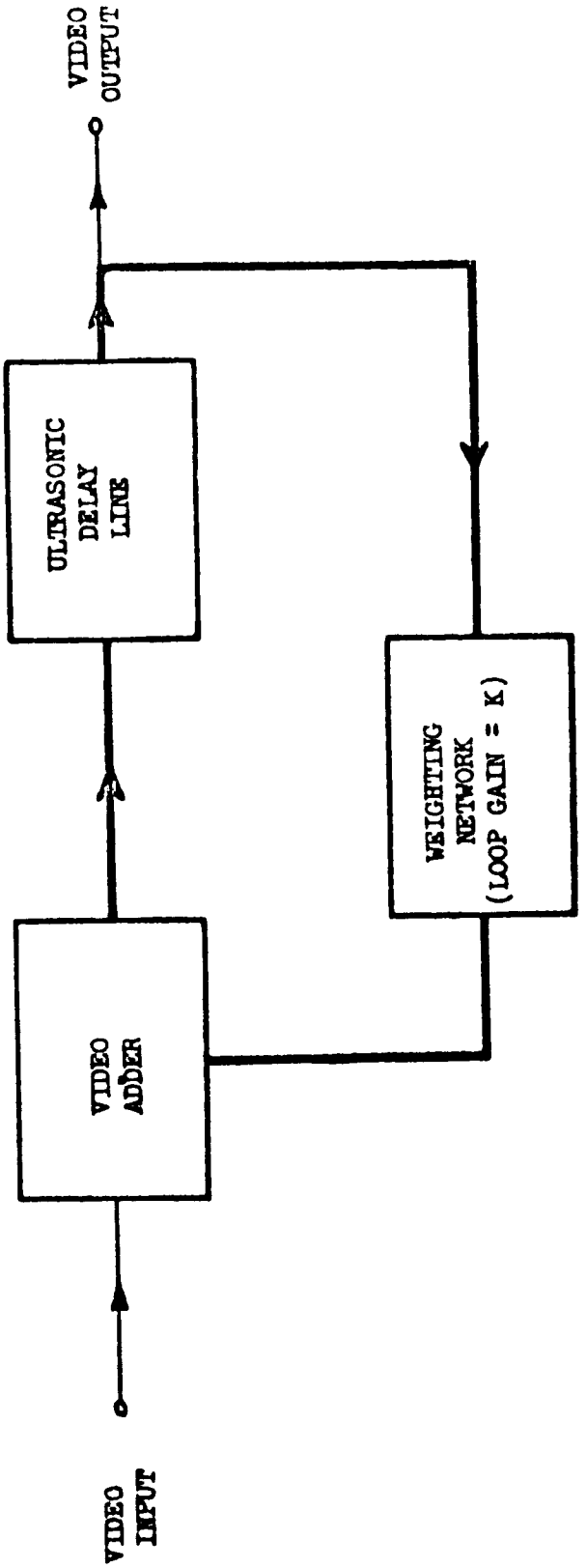

Fig. A-9 Video Sweep Integrator, Simplified Block Diagram

delay in the loop is equal to the video frame rate such that the positive feedback occurs at harmonics of the frame rate, resulting in an effective buildup of synchronous video signal and discrimination against random noise and any other uncorrelated signal. The system bandpass must be selected to retain unambiguous information storage since the bandpass of the system has images centered about harmonics of the frame rate. The bandpass characteristics for such a device is equivalent to that of a comb filter, as shown in Figure A-10. This reflects the operation of the device in that coherent signals containing energy at frequencies only at multiples of the frame rate are built up, whereas non-coherent signals are not built up. The non-coherent signals are averaged and their effect is thus reduced by the linear processing. Compared to display averaging, which averages the absolute amplitude and produces an optical display proportional to the rms noise level, the linear averaging of positive and negative noise tends to reduce the rms noise output. The sharpness of the comb filter is a function of the feedback gain and the harmonic center frequency is determined by the frame rate.

In order for the system to be stable, delay-line losses and feedback gain (which constitutes the loop gain) must be less than unity. As the loop gain approaches unity the circuit gain approaches infinity and becomes unstable; however, at a gain of 0.96 to 0.98, the system operates as a video sweep integrator. Pulse signals occurring at the frame rate will be built up according to the feedback factor in the following manner. Considering a video pulse of amplitude e_o from a star to occur at the beginning of each scan, the amplitude of the pulse in the delay line, e_d, after n frames have been stored is

$$e_d = e_o + ke_o + k^2e_o + k^3e_o \ldots k^ne_o, \qquad \text{(A-16)}$$

where k is the feedback factor.

For n approaching infinity,

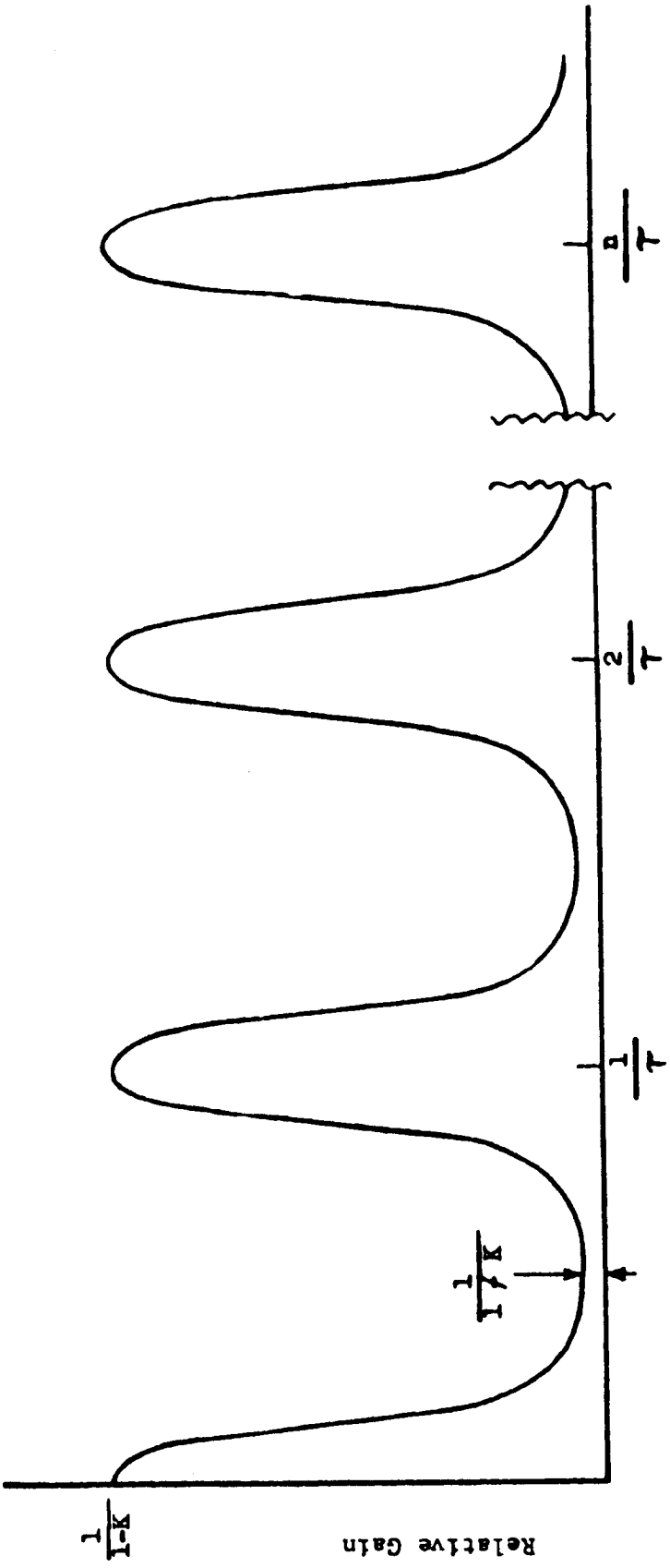

Fig. A-10 Video Sweep Integrator, Frequency Response

$$e_d = e_o (1 - k)^{-1} \qquad \text{(A-17)}$$

The noise is also summed in the same manner; the noise in the delay line is

$$e_{dn} = e_{no} + ke_{ni} \ldots k^n e_{nn} \quad . \qquad \text{(A-18)}$$

The rms noise is given by assuming the mean of the noise is zero. Then

$$\begin{aligned} \text{Var}\left[e_{dn}\right] &= E\left[e_{dn}\, e_{dn}\right] \\ &= E\left[e_{no}^2 + k^2 e_1^2 + \ldots k^{2n} e_n^2\right] \quad , \end{aligned} \qquad \text{(A-19)}$$

since each event is assumed to be independent (or, equivalently, the sweep bandwidth signal spectrum is not folded by the comb filter). The rms noise as n approaches infinity is

$$e_{dn}^2 = e_n^2 \frac{1}{(1 - k^2)^1} \qquad \text{(A-20)}$$

Figure A-11 is a plot of the signal-to-noise improvement out of the delay line for varying values of k and number of frames. Practical systems presently use loop gains of 0.96 to 0.98 with a corresponding improvement in S/N of 10 to 14.

The required collecting aperture for a system using the image dissector and the video sweep integrator is shown in Figure A-12 in which an improvement in S/N of 10 has been assumed. It is noted that the 38-inch optical telescope from the OAO-GEP is required to observe an 11th magnitude comet. The video sweep integrator weights 10 lbs., occupies a volume of 8" x 8" x 8", and consumes 30 watts of power for thermal control and amplifier operation.

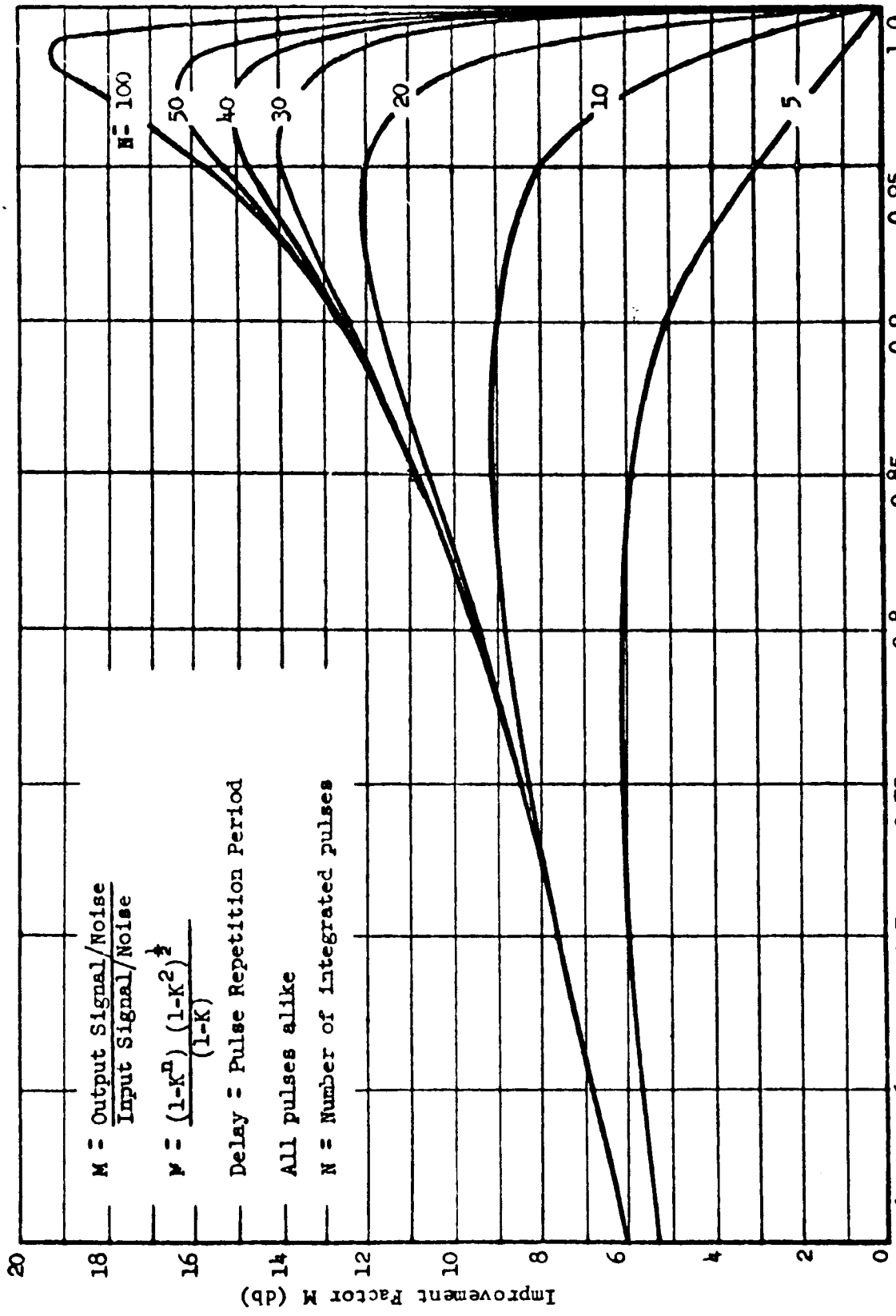

Fig. A-11 Theoretical Improvement by Video Integration

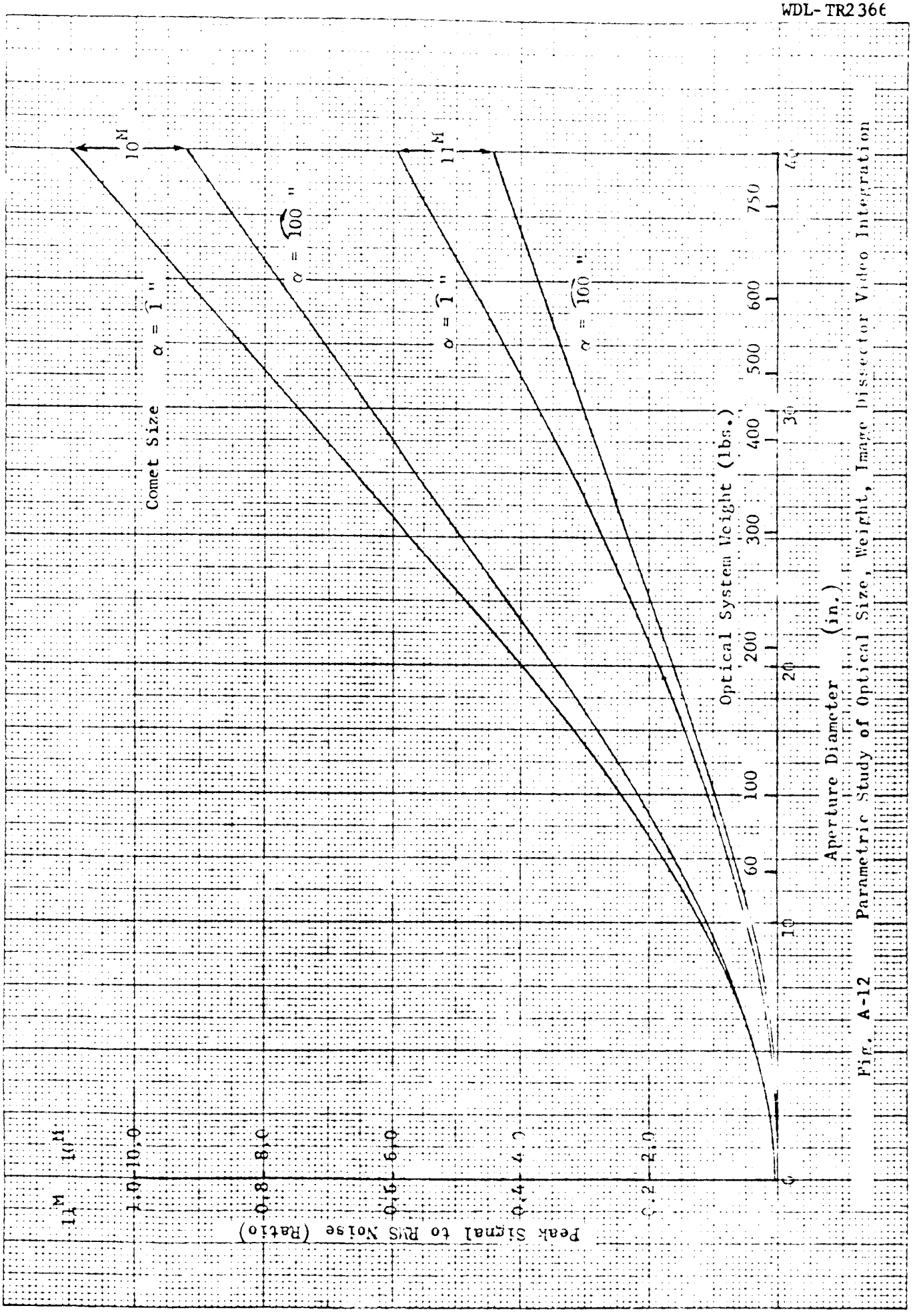

Fig. A-12 Parametric Study of Optical Size, Weight, Image Dissector Video Integration

A.4.5 Image Orthicon Sensitivity

The most sensitive device presently available for tracking and scanning using electronic means is the image orthicon. Earth-based astronomical applications for the image orthicon have demonstrated that the threshold light levels are set primarily by skylight [Powers and Aikens; 1963]. Several evaluations of image-orthicon astronomy are reported in the literature [Livingston, 1962 and Malling, 1963]. Experimental evidence indicates that this detector can provide lower thresholds and better resolution of stars than is possible with photographic emulsions. Space applications of stellar tracking have been made on the OAO-GEP but the application and threshold levels quoted in the OAO User's Handbook [Grumman, 1962] to be at a stellar magnitude of 6.37. Using longer exposures and larger optics, lower thresholds are possible. The limiting threshold in a space environment is set not by the sky background but by the limiting exposure as specified by the vehicle attitude threshold rates and the system resolution.

The scanning beam is a low-velocity electron beam originating from a thermionic cathode and accelerated by grid potentials such that the beam electron velocity near the target approaches zero. Low-energy electrons in the beam discharge the target as the beam is scanned, thereby modulating the beam current. The return beam is directed into the electron-multiplier section and the video signal level is multiplied. The electron multiplier section is the most significant source of noise in which the noise power is proportional to beam current. The beam current may be adjusted so that it covers the maximum lumination intensity of interest. Conventional television techniques are available to adjust the beam current to cover the most intense illumination element. However, a comet tracker does not require this feature since a bright star in the field will saturate the comet intensity pattern by increasing the average current. The comet signal could be swamped by the noise level in such a case.

The signal output sensitivity of the RCA image-orthicon industrial type 7198 for low light levels is linear at 60 microamps/lumen/sec.

In order to provide a linear signal for a comet uncertainty of $\pm$ 2 magnitudes (equivalent to a factor of 10), the average beam current must be adjusted to the level corresponding to the most intense comet considered. The signal from a comet having a flux level of E produces a current level of

$$i_s = \pi \frac{d^2}{4} E G_c t, \qquad \text{(A-21)}$$

where G_c is the tube sensitivity (60 μa/lumen/sec) and t is the exposure time. The rms noise, e_n, is

$$e_n^2 = 2e I_{AVE} \Delta f, \qquad \text{(A-22)}$$

where I_{AVE} is adjusted to the comet signal level. Accordingly, the peak signal-ro-rms noise ratio becomes

$$S/N = \left[\frac{\pi/4 \, d^2 E G_c t}{2 e \Delta f} \right]^{\frac{1}{2}}, \qquad \text{(A-23)}$$

where beam current noise has been neglected. The computation is valid only when a brighter star is not present for which the beam current would be adjusted to a higher level.

For a given exposure time the signal-to-noise is improved as a function of $t^{\frac{1}{2}}$. However, the limit of exposure time is set by the attitude control system rates. Using the OAO specifications that the drift rate be less than 15 seconds of arc in 50 minutes and the optical system resolution be one second, the allowable maximum exposure for avoiding skewing the image is approximately three minutes (200 seconds). Earth-based exposures of 100 seconds have been reported and will be used in the

analysis. Figure A-13 is a parametric study of the aperture requirements for various stellar magnitudes. The data will be obtained by first clearing the photocathode by scanning with a high beam current to uniformly discharge the target, then allowing the photocathode to be exposed without target readout for 100 seconds. At the end of this time, the target is scanned at a rate compatible with the 15 Kc bandwidth used in the photomultiplier detector system.

The sensitive image orthicon photosurface must be protected from viewing bright stars for extended periods of time to prevent, burning the tube face. Further considerations are beyond the scope of this feasibility investigation.

A.5 SUMMARY

The Comet Mission Study has investigated the need to determine the capability of tracking a comet from on-board the spacecraft prior to the terminal phase of the mission as a prerequisite to executing an accurate second midcourse maneuver. The objective of this section has been to provide a means of estimating the weight and size of an optical system required to track the comet. The scope of the early-flight comet tracking study includes the definition of comet brightness models and the star background. Included is an evaluation of two sensitive photo-detectors, an image dissector and an image orthicon, and an extrapolation of comet-tracking optical system weights based on optical systems used in space flight experiments. The image dissector is less sensitive for this application; however, it is inherently more rugged than the image orthicon. The optical systems used for this comparison are the OAO-GEP and Celescope systems since the weight of these systems are comparable to the total payload capability of a comet probe.

The definition of a comet model confirms the assumption that the comet will subtend an angle less than 10 seconds of arc and may be considered

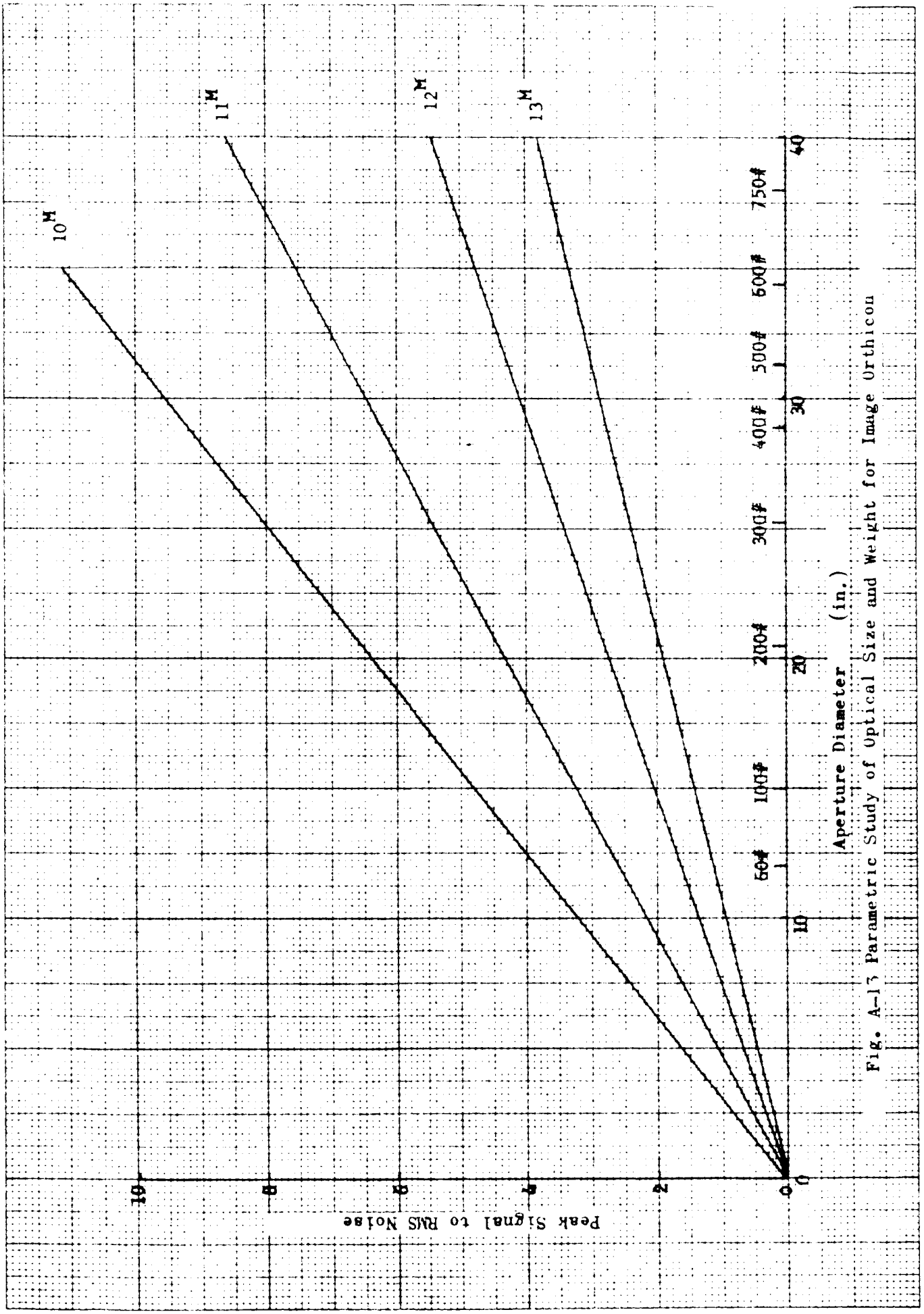

Fig. A-13 Parametric Study of Optical Size and Weight for Image Orthicon

as a point source during early flight. The models reported here indicate that the brightness of a comet during the early portion of its apparition is too low for on-board tracking. The threshold levels of available detectors, the stellar background and the low relative velocity of the comet against the stellar background prohibit any completely automatic on-board tracking during early flight.

The possibility of using a slow-scan TV system appears possible if large optical systems and telemetry requirements can be accommodated. Considering the most sensitive system using an image orthicon and a 100-second exposure time, the weight of an optical system require to observe a 10^{th} magnitude comet is 180 lbs (360 lbs for an 11^{th} magnitude comet). Threshold levels have been defined on the basis of the ratio of peak signal-to-rms-noise level. A level of 6 has been selected as the criterion for observing a signal in the presence of background random noise. TV resolution limits the accuracy to which the position can be determined with respect to a known stellar background pattern. The use of a 0.5° optical field would be practical for an optical system of this size; would be easy to orient using standard attitude control system components, and would have sufficient resolution to observe the comet position to 10 or 20 seconds of arc.

However, the large weight of the optical system requires a major redesign of the Mariner spacecraft structure. Furthermore, pointing of the optical system requires either maneuvering the spacecraft or accurately pointing a gimbal system, both of which require redesigning the spacecraft structure and changing the attitude control and thermal control subsystem. Probably the most demanding of these redesigns involves the thermal control necessary to maintain optical alignment and to eliminate thermal stress in the optical materials.

The data presented in Figure A-13 show the weight trade-off for the most sensitive system.

APPENDIX B

RESULTS OF ANALOG SIMULATION

B.1 STABILIZATION SYSTEM EVALUATION

The objectives of these studies have been to determine the capability of the solar vanes to acquire from relatively high angular rates (10^{-4} rad/sec), and the effect of flexible booms on the stabilization system's stability and acquisition time. The block diagram representing the long-term stabilization control system is shown in Figure B-1. The transfer functions shown in the blocks are simulated by an analog computer, the interconnection of each function-simulation is the total analog of the control system.

The simulation of the vehicle and flexible member dynamics is considered first. The following equations are implied in Figure B-1:

$$\theta_B = \frac{T_{Dist} + T_c - T_F}{J_B s^2} \qquad \text{(B-1)}$$

$$T_F = (\theta_B - \theta_{FM})(K + Ds) \qquad \text{(B-2)}$$

$$\theta_{FM} = \frac{T_F}{J_F s^2} \qquad \text{(B-3)}$$

where

θ_B = vehicle body angular position

θ_{FM} = flexible member angular position

T_C = control torque

T_S = solar control torque

T_{Dist} = disturbing torque(s) or de-stabilizing torques resulting from solar pressure

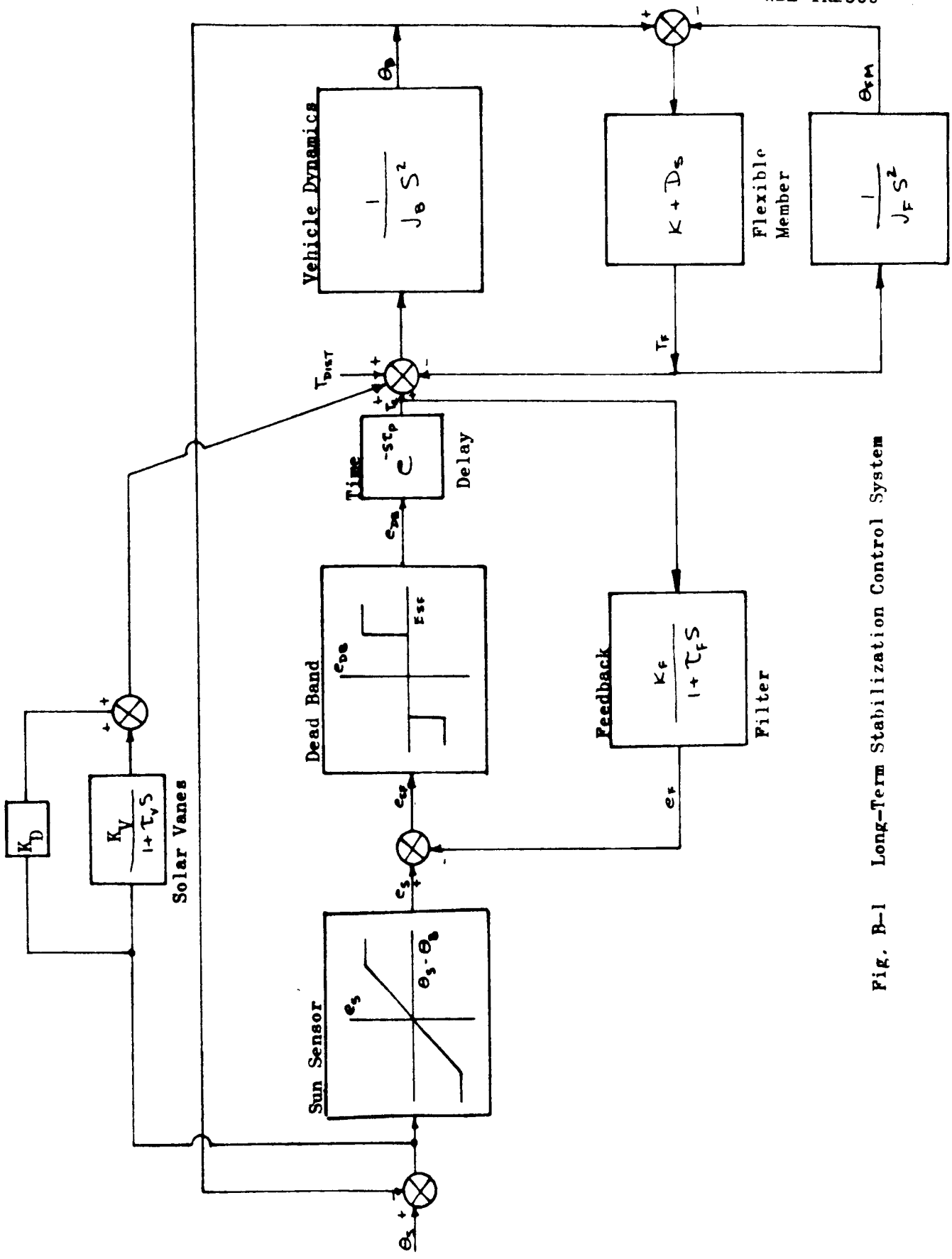

Fig. B-1 Long-Term Stabilization Control System

T_F = torque due to oscillations of flexible member

J_B = inertia of vehicle body

J_F = inertia of the flexible member

K = spring constant of the flexible member

D = damping of the flexible member

Converting from operator notation to time-dependent variables yields the following simultaneous differential equations:

$$\ddot{\theta}_B = \frac{1}{J_B}\left[T_C + T_D + T_S - K(\theta_B - \theta_{FM}) - D(\dot{\theta}_B - \dot{\theta}_{FM})\right] \qquad \text{(B-4)}$$

and,

$$\ddot{\theta}_{FM} = \frac{1}{J_F}\left[-K(\theta_{FM} - \theta_B) - D(\dot{\theta}_{FM} - \dot{\theta}_B)\right] \qquad \text{(B-5)}$$

Machine-time, T, is defined as T = t/1000 (i.e., the simulation runs at 1000 - times real-time). Hence,

$$\dot{\theta} = \frac{d\theta}{dt} = \frac{d\theta}{d(1000T)} = 10^{-3}\,\frac{d\theta}{dT} \equiv 10^{-3}\,\bar{\theta} \qquad \text{and,}$$

$$\ddot{\theta} = \frac{d^2\theta}{dt^2} = \frac{d^2\theta}{d(1000T)^2} = 10^{-6}\,\frac{d^2\theta}{dT^2} = 10^{-6}\,\bar{\bar{\theta}}$$

The time-scaled equations for T = t/p are,

$$\ddot{\theta}_B = \frac{1}{J_B}\left[P^2(T_c + T_D + T_S) + P^2k(\theta_B - \theta_F) - P\,D(\dot{\theta}_B - \dot{\theta}_F)\right] \qquad \text{(B-6)}$$

$$\ddot{\theta}_F = \frac{1}{J_F}\left[p^2\,K(\theta_B - \theta_F) - p\,D(\dot{\theta}_F - \dot{\theta}_B)\right] \qquad \text{(B-7)}$$

The following nominal values for system parameters are assumed:

Solar Vanes

$K_s = 9.26 \times 10^{-6}$ ft lb/rad

$K_v = 3.6 \times 10^{-6}$ ft lb/rad

$\tau_v = 2430$ sec

} based on values reported by Acord and Nicklaus (1964)

Flexible Members

$J_F = 1$ slug-ft^2

$J_B = 50$ for pitch and yaw; 30 for roll

$\omega_0 = \sqrt{\frac{K}{J_F}} = 0.03$ rad/sec

$D/J_F = 10^{-5}$ sec^{-1}

$p = 10^3$ sec/sec

for the analog computer simulation shown in Figure B-2.

The generation of the sun sensor error signal, e_s, is based on the relationship,

$$e_s = K_s(\theta_s - \theta_B) \text{ for } |\theta_s - \theta_B| \leq 10^\circ \qquad \text{(B-8)}$$

$$e_s = 10K_s \text{ for } |\theta_s - \theta_B| > 10^\circ \qquad \text{(B-9)}$$

The nominal value of the parameter K_s is 1 Volt/$_{\text{Deg.}}$ Based on this value, amplifier 30 output was limited to the deadband limit in milliradians.

The simulation of derived rate used amplifier 17 to produce a desired level of minimum impulse in conjunction with the control torques picked up by relays K02 and K03. The actual simulation of the scaled parameters

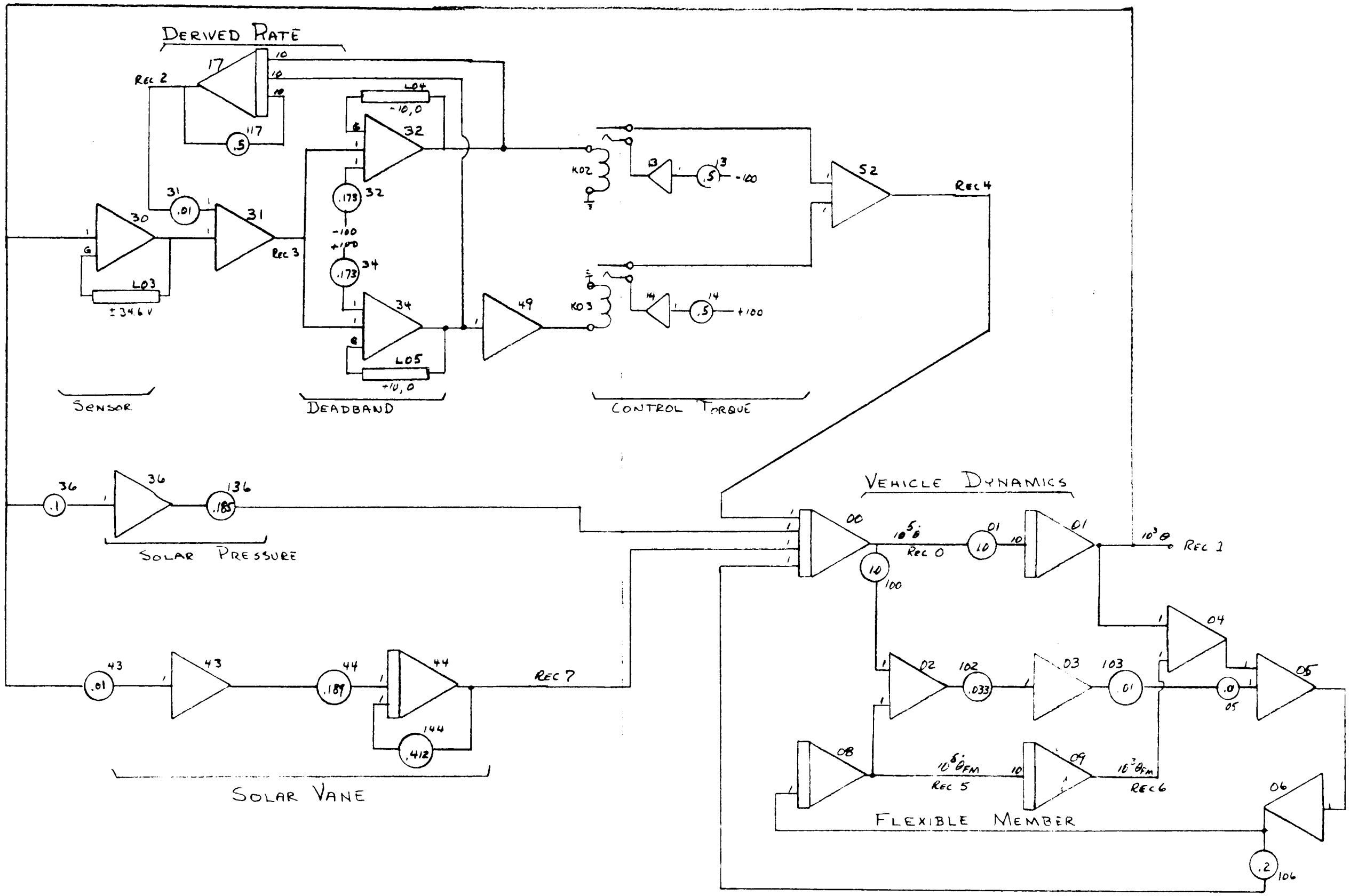

Fig. B-2 Analog Computer Connection Diagram

was beyond the capability of the analog computer. Since the objective of the simulation was to determine the settling time required to acquire the solar pressure system, an equivalent impulse was programmed. The simulation of a one-pound engine having a minimum on time of 10 milliseconds would produce total impulse bit of 0.006 pound sec which if mounted with a 2.5 level arm would result in a velocity increment of

$$\frac{0.006 \times 2.5}{30} = 5 \times 10^{-4} \text{ rad/sec}$$

about the roll axis. The angular rate about the pitch and yaw axis is somewhat less so that this simulation was arbitrarily selected at 10^{-4} radians/sec for the study. The problem scale for this parameter is 10^5 volts = 1 radian/sec so that 10^{-4} rad/sec is equivalent to 10 volts at the output of integrator 00. This is accomplished by applying 50 volts for 200 millisec.

Simulation of the deadband used two biased amplifiers 32, 34, and 35 to drive relays K02 and K03; the deadband corresponded to ± 17.3 volts, or one degree scaled.

The effect of solar torque was simulated using amplifiers 36 and 43 and 44. Note that the solar vane actuator must be a positive feedback.

The transfer function for the solar vane is

$$\frac{T_s}{\theta_s} = \frac{K_v}{1 + \tau_v s} = \frac{3.9 \times 10^{-6}}{(1 + 2430s)} \qquad \text{(B-10)}$$

and time scaling this becomes

$$= \frac{p^2 K_v}{1 + \tau_v S/P} \qquad \text{(B-11)}$$

The computer scales this to angular acceleration, α, by the use of 1 volt = 10^3 radians and 1 volt = 10^3 rad/sec^2, so that the transfer equation is

$$\frac{e_\alpha}{e_\theta} = \frac{K_\alpha}{K_\theta} \; P^2 J_B \; \frac{K_v}{(1 + \tau_v S/P)} \qquad \text{(B-12)}$$

and for $K_\alpha = K_\theta = 10^3$, $P = 10^3$ $K_v = 3.9 \times 10^{-6}$, $J = 50$ we have

$$\frac{0.0780}{(1 + 2.43S)}$$

for the solar vane. On a similar basis the gain for the stabilizing solar torques is given by

$$\frac{K_\alpha}{K_\theta} \; \frac{P^2 K_s}{J_B} = 0.1855 \qquad \text{(B-13)}$$

for $K_\alpha = K_\theta = 10^3$, $P = 10^3$ $K_s = 9.28 \times 10^{-6}$ and $J_B = 50$.

B.2 SIMULATION STUDIES

The purpose of this simulation is to demonstrate the ability of the solar vanes to acquire and stabilize with respect to the sun from large angular rates (10^{-4} rad/sec). The simulation has shown the effects of a flexible member on this acquisition.

While it is desirable to detail a stabilization system using a micro-thruster for roll stabilization, this could not be done within the limits for this program.

The study results have shown the single axis operation using an xy-plotter to show phase plane (θ, $\dot{\theta}$) characteristics and using a strip chart

recorder to record $-\dot{\theta}_B$, θ_B, derived rate, actuator drive, control torque, $\dot{\theta}_F$, $-\dot{\theta}_F$, solar torque.

The basis for presuming that acquisition can be carried out is made assuming that the undamped solar pressure must cause the vehicle to miss the deadband limit ± 1.0° on the first trajectory. The equations of motion for the undamped system, considering that only the solar stabilizing torque acts, are:

$$J\ddot{\theta} = K_s\theta \tag{B-14}$$

and assuming constant total energy

$$\frac{J\dot{\theta}^2}{2} + \frac{K_s\theta^2}{2} = \text{constant} \tag{B-15}$$

then the maximum angular excursion (θ_{max}) from the null point for a given initial condition, $\dot{\theta}_o$, would be determined from the solution to the above equations, which is

$$\theta_{max} = \dot{\theta}_o\sqrt{\frac{J}{K_s}} \tag{B-16}$$

$$= \dot{\theta}_o\sqrt{\frac{50}{9.28 \times 10^{-6}}} = 2.32 \times 10^3\ \dot{\theta}_o .$$

The use of a one degree deadband would result in a velocity on axis of 0.534×10^{-4} rad/sec. Or conversely a 10^{-4} rad/sec rate would require a deadband of 0.232 rad or approximately 13.4° in order to avoid actuating the thrusters and inducing a high rate. Naturally the damping effect will improve this slightly, however, the simulation of this showed the overall significance of this to be negligable. Therefore, the deadband must be widened either permanently or temporarily in order to acquire the solar vanes from higher rates.

Figure B-3 is a typical example of a simulation run in which the isolated effects are shown for (a) deadband operation with control torques only, (b) including the torques from the flexible member and (c) solar torques only and (d) a combined simulation. Figure B-4 is the strip chart recording for this run. The deadband width was chosen wide enough to allow acquisition.

Figure B-5 and B-6 are a rerun using a 5 degree deadband and a minimum impulse of 3×10^{-5} rad/sec.

The simulation results indicate that acquisition of the solar vane system requires that the deadband be widened. It is also certain that once a sufficiently low rate has occurred the solar vane will acquire. Acquisition in this process is not predictable and the time required for this to happen is likely to be long. Needless to say the latter condition is not a recommended technique.

Root Locus

The effect of adding flexible members to the solar vane stabilization subsystem was investigated by means of the root locus for the system. The open loop transfer equation for the stabilization system small angle equivalent is

$$\frac{(K_v+K_d)\left(1+\frac{K_D}{K_D+K_v}\right)\tau_v s)\ (J_F s^2+Ds+K)}{(1+\tau_v s)\ JS^2\qquad \left[J_F S^2+D\left(1+\frac{J_F}{J}\right)S+K\left(1+\frac{J_F}{J_J}\right)\right]} \qquad \text{(B-17)}$$

Substituting the parameters given earlier this becomes

$$\frac{1.132 \times 10^{-7}\ (3.98 \times 10^{3}\ S + 1)(S^2 + 10^{-5}S + 9.0009)}{S^2(2.43 \times 10^{3}\ S + 1)(S^2 + 1.02 \times 10^{-5}S + 0.000918)} . \qquad \text{(B-18)}$$

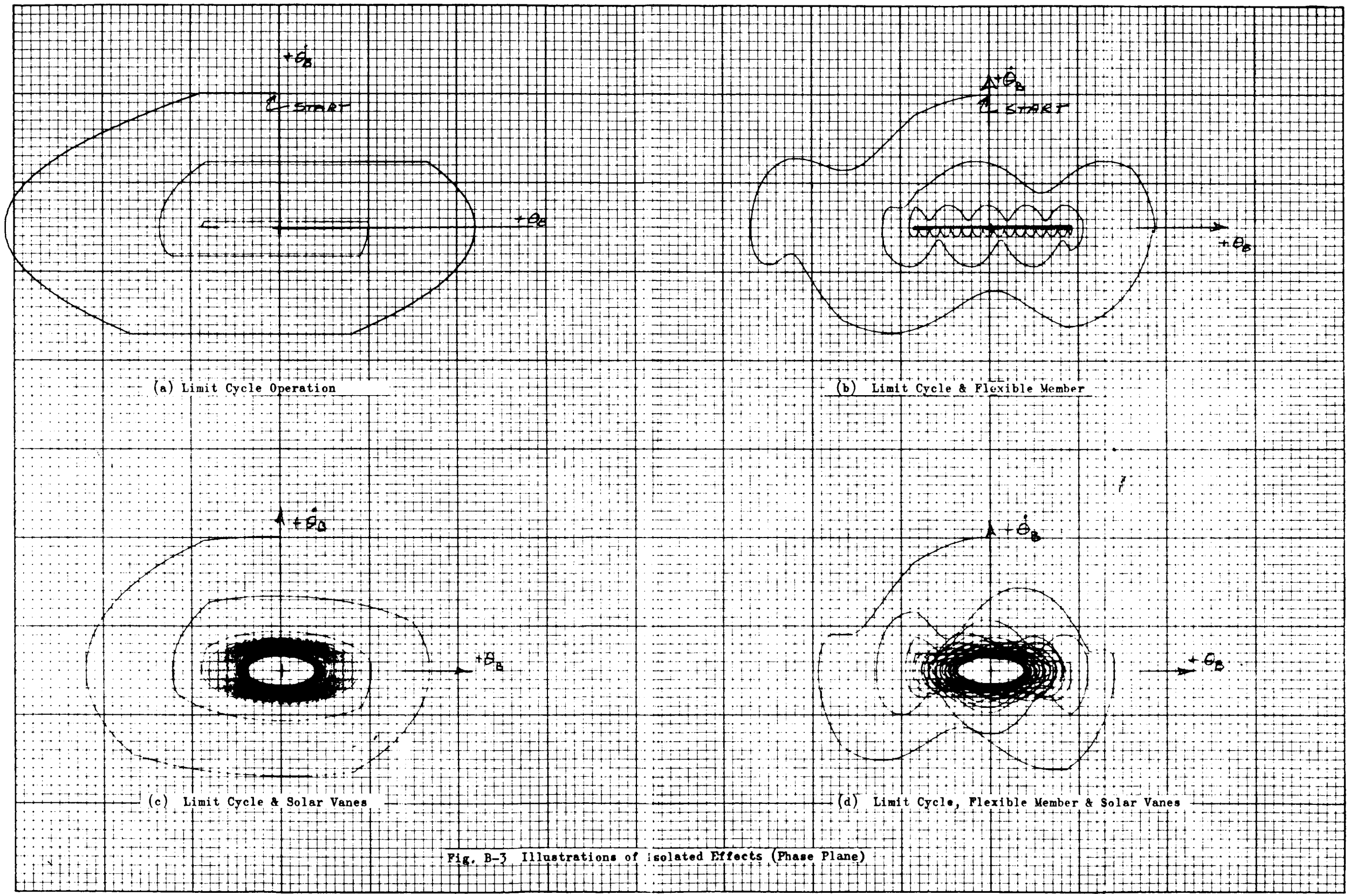

Fig. B-3 Illustrations of Isolated Effects (Phase Plane)

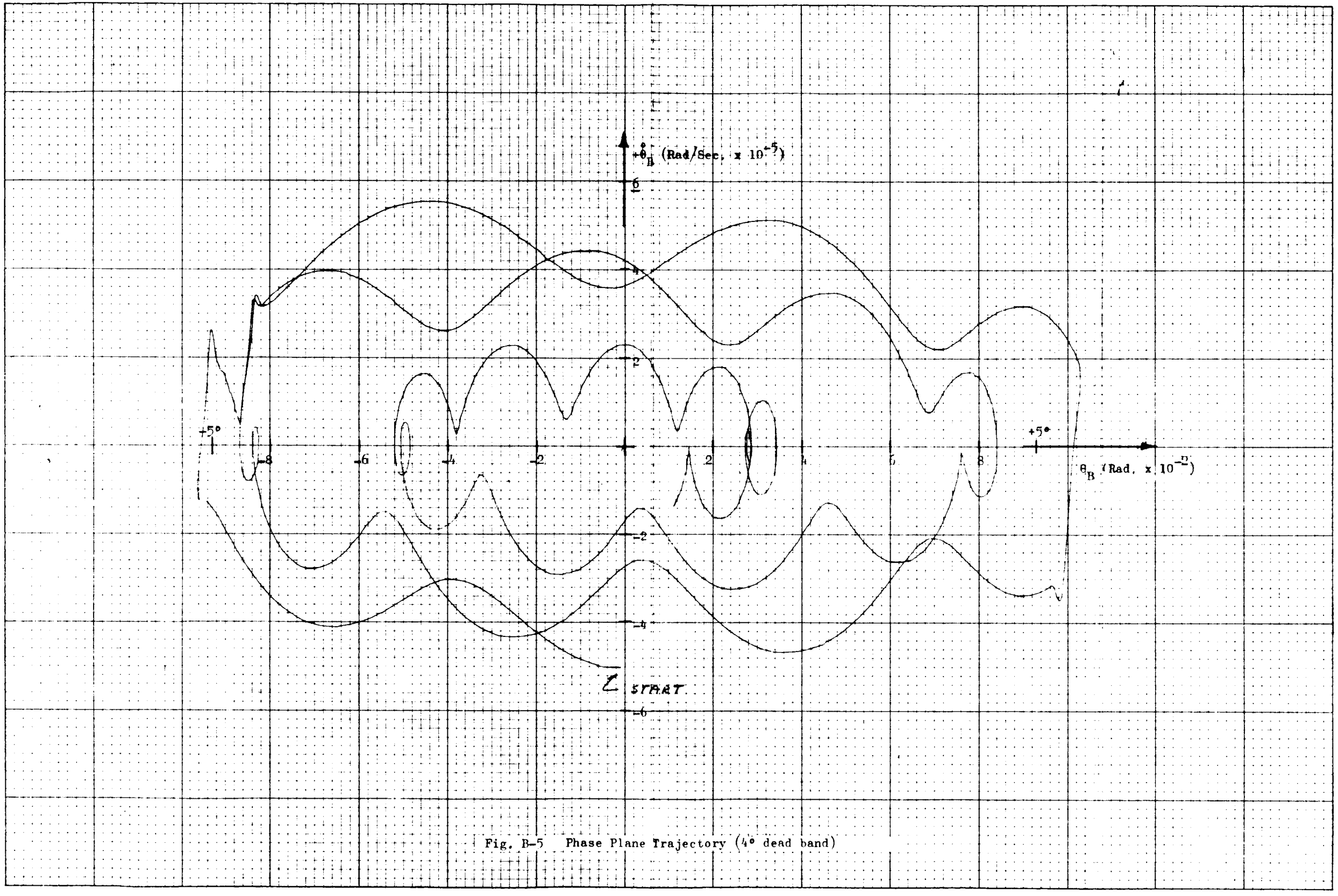

Fig. B-5 Phase Plane Trajectory (4° dead band)

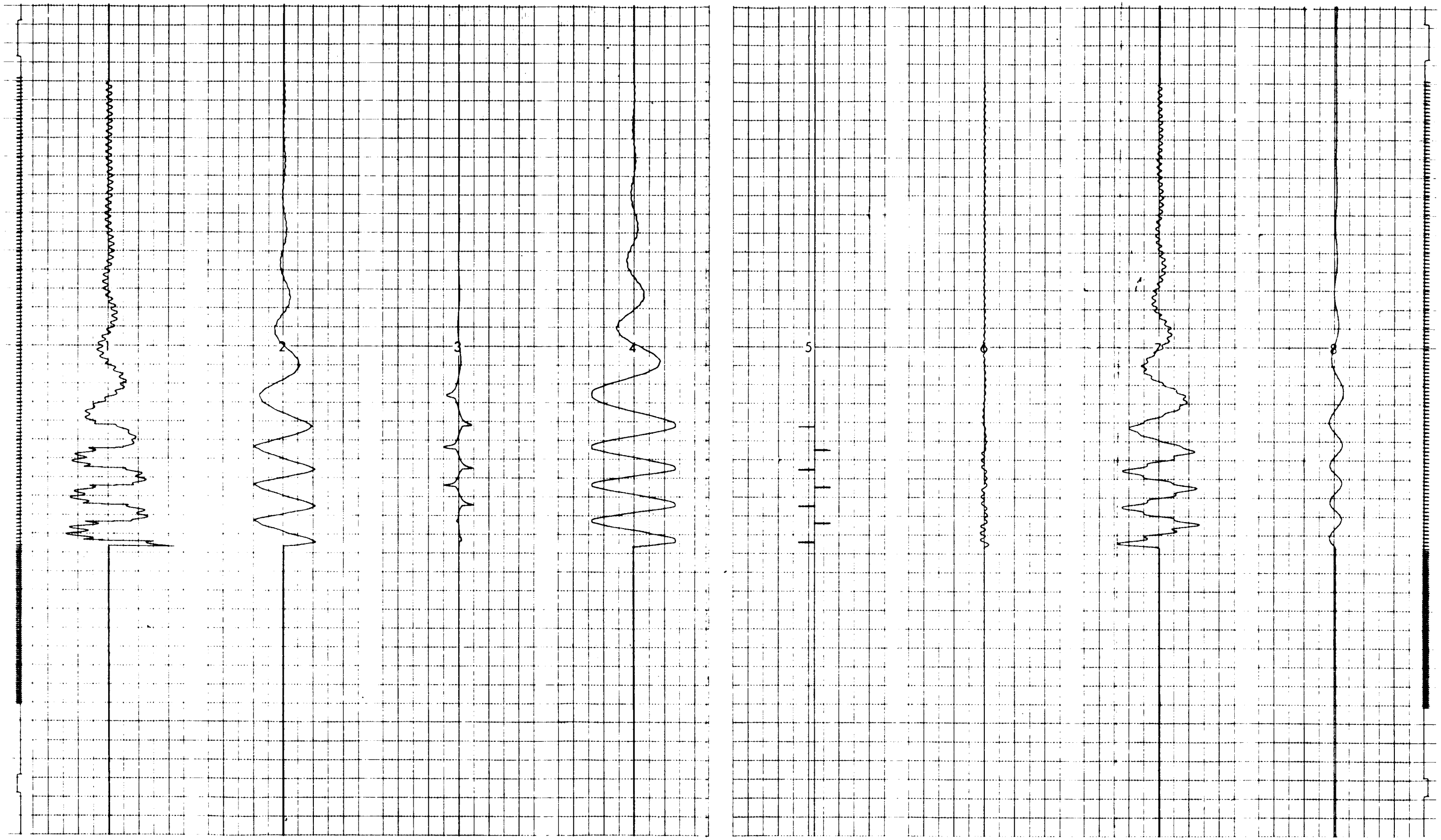

Fig. B-6. Acquisition From 5×10^{-5} Rad/Sec Using 4-Degree Deadband

Considering Equation (B-18) it is evident that the relationship of K_v and K_D is a key to system stability, in fact it is readily observed that for

$$\frac{K_D + K_v}{K_D} < 1$$

or

$K_D + K_v < K_D$; the system is unstable.

So $K_v < 0$ which is the case for which the solar vane must constitute positive feedback in order to retain system stability. Furthermore it is also evident that $K_D + K_v > 0$ and then $K_D > -K_v$ for stability. All of these conditions are evident from the root locus plot of Equation (B-7).

Figure B-7 is a plot of the root locus for that system in which the gain of the solar vane has been varied according to the values indicated in that figure. The flexible member resonance was varied to determine effect on system stability.

B.3 SUMMARY

As a result of these investigations it is clear that:

1. The solar vane can be used to remove the deadband rates for the high minimum impulse system. The effect of using the higher deadband rate for coarse stabilization is to lengthen the time required for acquisition. As an alternative, acquisition of the solar vane can be accomplished by the widening of the deadband.

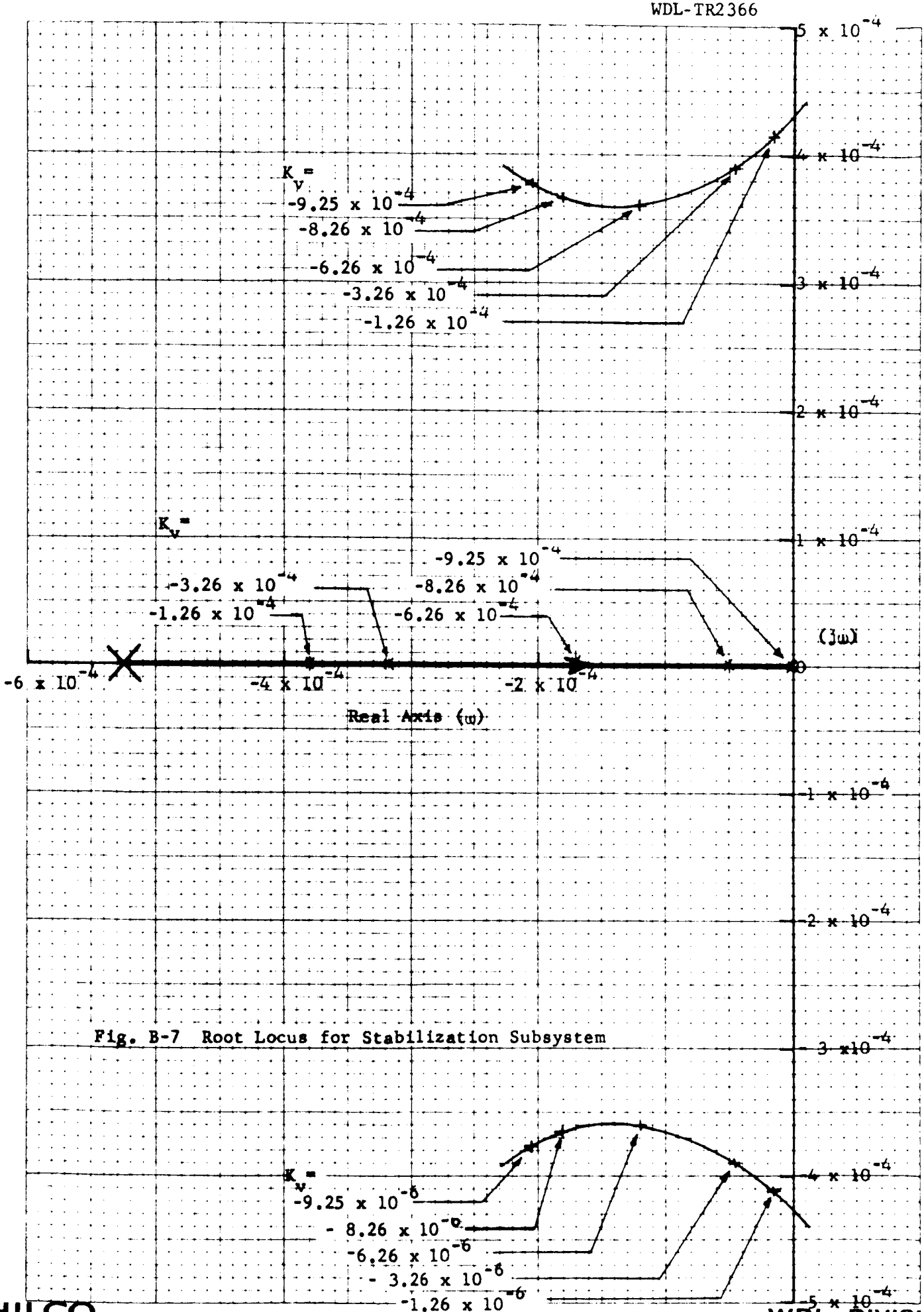

Fig. B-7 Root Locus for Stabilization Subsystem

2. Flexible members having resonance above the solar vane time constant are acceptable. Roughly speaking, the resonance should be above 412×10^{-3} rad/sec for a solar vane time constant of 2430 seconds.